Mechanical Modeling of Microtubules in Living Cells

by

MingZhao Jin

A thesis submitted in partial fulfillment of the requirements for the degree of

Doctor of Philosophy

Department of Mechanical Engineering
University of Alberta

Abstract

Three important mechanical behaviors of microtubules *in vivo*, i.e., buckling, vibration and splitting are investigated with especial focus on their relevance to biological functions of microtubules. To study the vibration and buckling of a microtubule, we model a microtubule as an elastic beam and surrounding three dimensionally distributed biopolymers as springs by using finite element method. Our model predicts that the buckling and vibration of microtubule are highly localized within several microns. As a result the critical buckling force and the lowest vibration frequency are insensitive to the total length of microtubule. The localized buckling and vibration predicted by the present model agree with a number of experimental observations which cannot be well explained by the existing elastic foundation model. Compared with predictions from the existing elastic foundation model, some key parameters (e.g., critical buckling force, buckling wave length, vibration frequency and vibration wave length) obtained from the present model are also in better agreement with experiments. In addition to our finite element results, several empirical equations, which are unavailable from the existing elastic foundation model, are provided to calculate these key parameters in terms of mechanical and geometrical properties of microtubule and surrounding biopolymer.

To investigate splitting of a microtubule into splayed protofilaments, we model protofilaments as individual elastic beams in parallel and laterally assembled to form a microtubule. Our analytical model shows that an axial compressive force could

induce splitting of a microtubule shorter than 450 nm even if it is protected by a “cap” consisted of strongly bonded GTP dimers at the end. For a longer microtubule, the axial compressive force might cause overall buckling prior to splitting. On the other hand, after the strong “cap” at the end of microtubule is lost (not necessarily due to compressive force), a molecular ring coupled to the frayed end of microtubule could provide a pulling force with splitting propagation of microtubule to move chromosome during mitosis. Our model predicts that the splitting of microtubule will spontaneously propagate with splitting length around 15 ~ 18 nm, which is comparable with the frayed end in microtubule of 10 ~ 30 nm observed in experiments. By using the predicted splitting length, we estimate the theoretical upper limit of pulling force as 7 ~ 24 pN, which is close to the upper bound of the experimentally measured pulling force 0.5 ~ 5 pN with reasonable accuracy.

In summary, our numerical simulations and analytical models offer plausible explanations to some important experiments of microtubules *in vivo* which have not been well explained by existing models. It is hoped that the present study could bring some new insights to the understanding of interacting between mechanics and biology of microtubule and spark further research interest in mechanical modeling of microtubules.

Preface

The main body of this thesis is composed by four published/unpublished journal papers. See below for details.

Chapter 2 of this thesis has been published as “Jin, M.Z., Ru, C.Q., 2013. Localized buckling of a microtubule surrounded by randomly distributed cross linkers, Physical Review E 88, 012701.” I proposed the topic and was responsible for numerical simulations and paper writing. Dr. Ru C.Q. is the supervisory author who checked results and revised the manuscript.

Chapter 3 of this thesis has been published as “Jin, M.Z. & Ru, C.Q. 2014. Localized Vibration of a Microtubule Surrounded by Randomly Distributed Cross Linkers, Journal of biomechanical engineering, 136, 071002.” I proposed the topic and was responsible for numerical simulations and paper writing. Dr. Ru C.Q. is the supervisory author who checked results and revised the manuscript.

Chapter 4 of this thesis has been published as “Jin, M.Z., Ru, C.Q., 2012. Compressed microtubules: Splitting or buckling, Journal of Applied Physics 111, 604701.” Dr. Ru C.Q. and I selected this topic together through discussion and I was responsible for math derivation, results analysis and writing manuscript. Dr. Ru C.Q. is the supervisory author who checked results and revised the manuscript.

Chapter 5 of this thesis is expected to be my first sole author paper and will be submitted soon.

Acknowledgements

I gratefully thank my supervisor Dr. Chongqing Ru for his guidance, support, and encouragement during my Ph. D study. His vast knowledge and skill in solid mechanics greatly helped me in solving technical problems; however the most important thing he passed on me is his expertise to identify important and solvable problems in research. His help to me is beyond academia. Since very beginning of PhD study, he gave me many advices about future plan after graduation. He also kept trying to offer me a multilingual/culture environment in office to improve my communication and sociability. He is always ready to help me in preparing reference letters and paper works for my immigration, APEGA membership, scholarship applications and job hunting. I highly appreciate all his efforts in last four years.

I would also like to thank Dr. Cagri Ayranci and Dr. Tian Tang as my supervisory committee members for valuable suggestions and discussion in my research. Dr. Walied Moussa, Dr. Chongqing Ru, Dr. Peter Schiavone and Dr. Tian Tang who offered me interesting courses are also greatly acknowledged. Very special thanks go to Dr. Peter Schiavone and Dr. Tian Tang for their reference in Alberta Innovates industry r&D program application, which is now granted to support my research in another area.

I also want to express my gratitude to all office and technical staff in Mechanical Engineering Department of University of Alberta, my research would be possible without their everyday work. Financial supports from NSERC and Alberta Innovates are also greatly acknowledged.

Table of content

List of figures

Figure 2.8 Localzed buckling wavelength λ_L given by the present numerical model compared with the wave length calculated from the empirical equation (2-8).

Figure 2.9 Different buckling cases of microtubules in *vivo/vitro*: the free-standing microtubule buckling with clamped-free (a) or clamped-clamped (b) end conditions observed in *vitro* (Kikumoto et al., 2006, Elbaum et al., 1996); the localized buckling with clamped-free (c) and doubly clamped (d) end conditions, which are similar to the observation in *vivo* (Brangwynne et al., 2006, Mandato and Bement, 2003, Gupton et al., 2002)

Figure 3.1 Finite element models: (a) equivalent elastic foundation model; (b) presently developed randomly distributed 3D cross linker model.

Figure 3.2 Three lowest transverse (mode number=7, 11, 15) and longitudinal (mode number=1, 2, 3) vibration frequencies predicted by Eqs. (3-1) and (3-2) are in good agreement with simulations given by the present equivalent 2D elastic foundation model shown in Figure 3.1 (a). Simply-supported end conditions are applied for all cases.

Figure 3.3 Illustration of vibration modes (A, B and C) from the randomly distributed 3D cross linker model. The deflection patterns of these three typical cases are localized. The vibration mode with longer deflected length is associated with higher vibration frequency.

Figure 3.4 Vibration frequencies (from the lowest) of a microtubule with length of 50 μm, k of 39 pN/nm and L_d of 25 nm predicted by the randomly distributed 3D cross linker model. All transverse vibration modes with lower frequencies shown here are localized.

Figure 3.5 The frequencies of transverse vibration are distributed more densely for longer microtubules, where microtubule length varies from 240 L_d to 2800 L_d. Here the localized critical frequency marked by the dashed line is obtained by the mean value of the lowest 10 very close frequencies, above which densely distributed frequencies of localized modes are identified.

Figure 3.6 The deflected length d (through which the deflection is larger than 5% of

the maximum deflection) versus vibration frequencies obtained from four tests with the same L_d of 25 and k of 39 pN/nm but different random angles assigned to cross linkers. Each data point is obtained by the mean value of 10 frequencies and associated deflected lengths. The data point with lowest frequency and shortest wave length indicates the critical frequency f_L and the associated wave length λ_L of localized mode.

Figure 3.7 The total deflected length d versus vibration frequencies obtained from our randomly distributed 3D cross linker model for microtubules of length (L) of 5000, 6000, 8000 and 10000 nm (with k of 39 pN/nm and L_d of 25 nm). All frequencies of localized modes are lower than the lower-bound minimum frequency $f_{\min}$ of 448 MHz given by Eq. (3-2), and beyond $f_{\min}$ the deflection spreads through the whole microtubule and vibration modes are no longer localized.

Figure 3.8 The dependency of the critical frequency f_L (a) and the associated wave length λ_L (b) of localized vibration on L_d and k. The lower-bound minimum frequency $f_{\min}$ given by Eq. (3-2) is always higher than the critical frequency f_L of localized modes given by the present model.

Figure 3.9 Comparison between the critical frequency f_L predicted by empirical formula (3-5) and numerical simulation with variable k (a) and L_d (b).

Figure 3.10 Comparison between the wave length λ_L predicted by empirical formula (3-6) and numerical simulation results with variable k (a) and L_d (b). The formula (3-6) is valid only when the predicted λ_L is longer than $13L_d$.

Figure 3.11 Effect of the bending rigidity EI on the critical frequency f^* (a) and the associated wave length λ^* (b) of localized vibration.

Figure 3.12 Effect of ρA on the critical frequency f^* of localized vibration.

Figure 4.1 Three possible failure modes of a microtubule under axial compression with the minus end anchored in centrosomes (Howard and Hyman, 2003): (a) splitting at the middle, (b) splitting at the plus end, and (c) buckling as a column.

zone with r_0 / w_0 =0.1 and 1.

Figure 5.6 For non-monotonic potential with r_0 / w_0 =0.05 and r_1 / w_0 =0.3: (a) the range of $w_0 R / L_D^2$ to provide non-negative pulling force during spontaneous splitting propagation versus U_M / U_C . (b) Normalized maximum pulling force $F_{p\max} / U_C$ during spontaneous splitting propagation versus U_M / U_C.

Nomenclature

A	cross section area of microtubule
A_{p}	cross section area of protofilament
b	width of protofilament
E	Young's modulus of microtubule
E_c	modulus of two dimensional elastic foundation
EI	bending rigidity of microtubule
EI_{p}	bending rigidity of protofilament
f_{A}	longitudinal vibration frequency of microtubule in elastic foundation
F_{cr}	critical buckling force
f_{T}	transverse vibration frequency of microtubule in elastic foundation
$f_{\min}$	minimum transverse vibration frequency of microtubule in elastic foundation
F_{L}	localized critical buckling force
F_p	pulling force stimulated by splaying of a individual protofilament
h	thickness of protofilament
I_{p}	second inertia moment of cross section of protofilament
k	spring constant of biopolymer (cross linker)
k_0	reference value of spring constant of biopolymer (cross linker)
L	total length of microtubule
L_d	spacing between cross linkers for microtubule vibration analysis
L_{d}	spacing between cross linkers for microtubule buckling analysis
L_D	splitting length of microtubule
L_m	length of a dimer
L_0	reference value of spacing between biopolymers (cross linkers)

m	number of GTP layers
r_0	maximum adhesive separation of cohesive zone
r_1	maximum repulsive separation of cohesive zone
R	radius of natural curvature of a protofilament with GDP dimers
U	potential energy of cohesive zone at the splitting end of microtubule
U_C	bending strain energy stored in straight protofilament per unit length
U_{D1}	elastic strain energy of a unbuckled protofilament with GDP dimers
U_{D2}	elastic strain energy of a buckled protofilament with GDP dimers
U_{T1}	elastic strain energy of a unbuckled protofilament with GTP dimers
U_{T2}	elastic strain energy of a buckled protofilament with GTP dimers
U_M	energy increase at initial stage of cohesive zone per unit length of protofilament
U_P	energy drop at post stage of cohesive zone per unit length of protofilament
w	deflection of protofilament
w_0	maximum deflection of protofilament
x	coordinate along microtubule axis
ΔU	energy difference before and after buckling of a protofilament
α	percentage of GDP dimers in a microtubule
ε	compressive strain applied along microtubule axis
ε_{cr}	critical axial strain for buckling of a protofilament
ε_{crm}	critical axial strain for buckling of a microtubule
ε_{cr1}	critical axial strain for buckling of a protofilament with doubly clamped boundary condition
ε_{cr2}	critical axial strain for buckling of a protofilament with clamped-free boundary condition

λ	wave length of periodic buckling
λ_{L}	wave length of localized buckling
λ_{T}	transverse vibration wave length of microtubule in elastic foundation
ρ	density of microtubule
γ_{D}	adhesion energy between GDP dimers
γ_{T}	adhesion energy between GTP dimers
Π_D	elastic strain energy of a protofilament within splitting length
Π_C	total energy of cohesive zone
Π_0	sum of elastic energy and cohesive zone energy before splitting propagation
Π_1	sum of elastic energy and cohesive zone energy after splitting propagation

1. Introduction

1.1. What is microtubule

1.1.1. Composition and structure

Microtubule is one of most important cytoskeletal elements in eukaryotic cells (Boal, 2002). A microtubule has a tube like structure and is composed of Alpha/Beta tubulin heterodimers (called “dimers”). These dimers are helically assembled to form a microtubule with outer diameter about 24 nm and length varying from hundreds of nanometers to tens of microns. Because the inter-dimer adhesion along the axis of microtubule is much stronger than the inter-dimer in circumferential direction (VanBuren et al., 2002, VanBuren et al., 2005), a microtubules is also considered to be composed of 13/14 protofilaments in parallel with the microtubule axis. A protofilament is a single chain biopolymer polymerized by assembling of dimers end to end. For an illustration of microtubule composition and structure, see Figure 1.1.

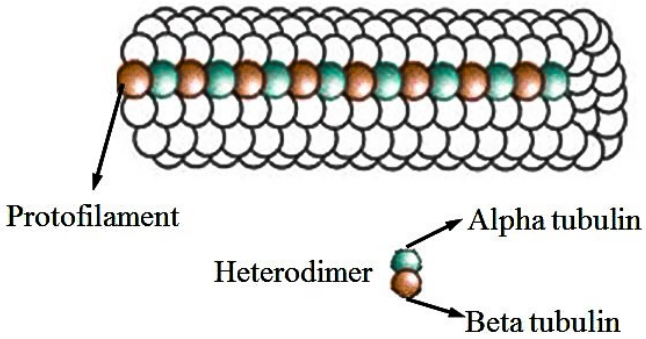

Figure 1.1 Composition and structure of a microtubule.

1.1.2. Functions of microtubule in biological cell

Microtubules serve as: (a) key components of cell’s skeleton, (b) engines to move chromosome during cell division and (c) rails for cellular materials transportation. As the key component of cell’s skeleton, a microtubule anchors one end in the centrosome which located at the center of cell with another end toward the membrane of cell. In this manner, microtubules maintain geometrical shape of cell with bending rigidity about 3-4 orders magnitude higher than other biopolymers in cell (Subra, 2007). Other biopolymers laterally support microtubules to prevent microtubule with

very high ratio of length to diameter from mechanical failure such as buckling or bending.

Serving as engines to move chromosome during cell division, microtubules take advantage of its polymeric properties. Actually, microtubules are firstly organized to form the mitotic spindle with two ends connected to chromosomes via kinetochores. Then depolymerization (shrinking) of microtubules generates a pulling force via Dam1 ring to position duplicated chromosomes to two poles of newly formed daughter cells, see Figure 1.2 (Inoué and Salmon, 1995). Thus chromosomes positioning is well controlled by switching between polymerization and depolymerization of microtubule, a process named "dynamic instability" (Mitchison and Kirschner, 1984). A microtubule is initially polymerized by GTP dimers (each dimer formed by an alpha and a beta tubulin monometers carries two GTP molecules). It has been now widely recognized that a "cap" at the end of microtubule, composed of a few layers of strongly bonded GTP dimers, is essential to prevent microtubules from depolymerization. Strongly attached stable GTP dimers will be hydrolyzed to unstable GDP dimers after being added to the tip of microtubule. GTP dimers are straight and considered to be stable because its shape is compatible with cylinder shape of microtubule, while the GDP dimers are naturally curved thus not stable within microtubules. According to existing literatures (Mitchison and Kirschner, 1984, Hyman et al., 1992), the loss of "cap" was considered as a result of hydrolysis of stable GTP dimers to unstable GDP dimers.

Another important function of microtubules is rails for cellular materials transportation. Motor proteins can move along a microtubule as trains travelling along a railway. The energy for motor protein moving is provided by ATP hydrolysis. For example, Kinesin as one typical microtubule motor protein can move toward plus end of the microtubule, while Dynein, another type of motor protein, commonly moves toward the negative end of microtubule (Kelly, 1990). Many types of cargo proteins bound and transported by motor proteins are playing vital roles in numerous organelle activities (Hirokawa, 1998). The movement of motor proteins might introduce significant mechanical transverse disturbance to microtubules.

1.2. Why is microtubule mechanics important

Biological functions of microtubule are largely based on microtubule mechanics. As

the strongest component of the cell skeleton, sometimes microtubules are curved and appear buckled under compressive loads. It is important to study how much force a single microtubule can bear without being buckled and what its mechanical failure modes look like (Brangwynne et al., 2006). Some experiments found that mechanical interaction between some biopolymers and microtubules is related to high mobility and metastasis of cancer cells (Guck et al., 2005, Ochalek et al., 1988, Korb et al., 2004). Also, because of microtubule's key role in maintaining the shape of cell, mechanical vibration of microtubule directly coordinates the movement and shape variance of cells (Tounsi et al., 2010, Allen et al., 2008). As a result, mechanical vibration of microtubule is related to electrodynamic activities of cells (Cifra et al., 2010, Pokorný, 2004), which are important in cancer cell identification (Pokorný et al., 2011, Daneshmand, 2012).

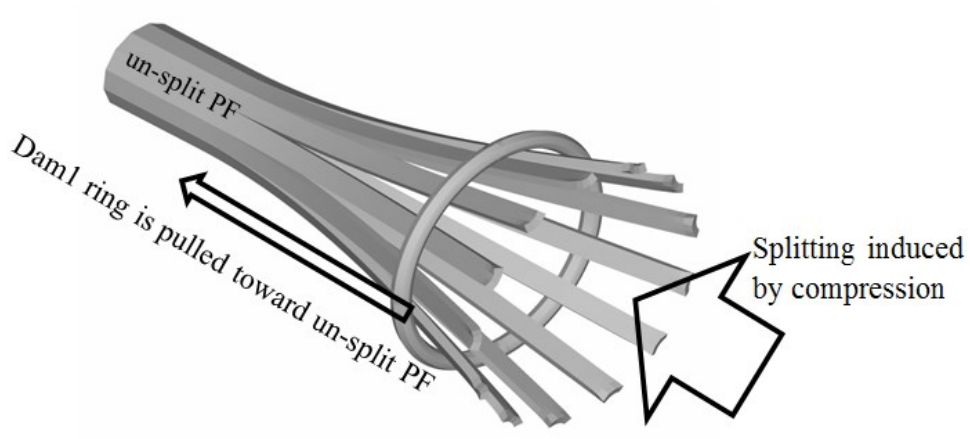

Figure 1.2 Illustration of (a) microtubule splitting induced by axial compression and (b) pulling force generated by splitting acting on Dam1 ring (note: the figure is only for illustration and the two phenomena do not necessarily occur simultaneously and the size of Dam1 ring, microtubule and protofilament, short for PF in figure, are not in scale).

When a microtubule serves as an engine to move chromosome, it is now well recognized that the kinetics energy required for moving chromosome comes from strain energy previously stored in protofilaments within microtubule (Westermann et al., 2006). Analysis of this process greatly relies on understanding of mechanical behavior of microtubules. Protofilaments can be modeled as naturally curved beams but being bent straight to fit into the tube-like shape of a straight microtubule. After the strong constraint at the end of a microtubule is lost, outward bending of

protofilaments could pulling Dam1 ring and generate pulling force to move chromosome, see Figure 1.2. During this process, mechanical strength of microtubule is relevant for cell division because chromosome positioning could fail due to buckling and bending of microtubules (Faivre-Moskalenko and Dogterom, 2002). On another hand, applied external force might also affect polymeric behaviors of microtubule. For example, under tensile force, the depolymerization of microtubule can be suppressed (Akiyoshi et al., 2010). In addition, mechanical vibration of a microtubule could be stimulated by an external force engendered in mitosis and transverse disturbances caused by the moving of motor proteins along the microtubule (Rai et al., 2013).

1.3. Microtubule mechanics models review

As presented in last section, buckling, vibration and splitting are three most relevant mechanical behaviors of a microtubule to perform its biological functions in a living cell. For buckling and vibration, a microtubule was commonly modeled as a continuous elastic structure, e. g., an elastic beam or elastic shell. The free-standing elastic beam and shell models without surrounding biopolymers (named "cross linkers" in this thesis) are used to predict experimentally observed mechanical buckling and vibration behaviors of microtubule *in vitro* (Pokorný, 2004, Sirenko et al., 1996, Tounsi et al., 2010, Wang et al., 2006, Xiang and Liew, 2012, Kurachi et al., 1995). However the free-standing beam and shell models failed to explain some mechanical behavior of microtubules in biological cells. For example, it is observed that microtubule can bear a compressive force much higher than the theoretical critical buckling force of a free-standing elastic beam (Li, 2008). The high buckling force was attributed to surrounding cross linkers, which were modeled as a homogenous elastic foundation in the existing literature for both buckling (Brangwynne et al., 2006, Jiang and Zhang, 2008, Brodland and Gordon, 1990, Ugural and Fenster, 2003) and vibration (Shen, 2011, Ghavanloo et al., 2010, Zeverdejani and Beni, 2013). Despite the merits of the elastic foundation model as compared to the free-standing beam models in exploring microtubule buckling and vibration *in vivo*, the elastic foundation model still suffer from three major draw backs when compared with experimental observations:

First, for microtubule buckling, the elastic foundation model predicts a uniform

multiwave buckling mode when a microtubule is under an axial compressive force higher than the critical buckling force (Li, 2008, Mehrbod and Mofrad, 2011, Jiang and Zhang, 2008). However microtubule *in vivo* often exhibits a failure pattern refereed as "localized buckling" in which the magnitude of deflection quickly decays from the site where the compressive force is applied (Brangwynne et al., 2006, Mandato and Bement, 2003, Gupton et al., 2002).

Secondly, for microtubule vibration, the elastic foundation model predicts that the lowest natural frequencies depend on microtubule length and the associated vibration modes are characterized by long wavelength spreading through the entire microtubule. This feature is in direct contradiction with experimental observation that vibration modes of microtubule *in vivo* are highly localized at certain locations of microtubule (Marrari et al., 2003, Mandato and Bement, 2003).

Third, the relationship between the elastic foundation modulus (a key parameter of the elastic foundation model) and properties of three dimensionally distributed cross-linkers remains a problem to be addressed (Jiang and Zhang, 2008, Wang et al., 2009, Gao and An, 2010, Li, 2008, Mehrbod and Mofrad, 2011). The approach widely adopted by the existing elastic foundation models to determine the elastic foundation modulus is essentially under a two dimensional assumption of in-plane vibration or buckling (Ugural and Fenster, 2003), which is inappropriate for three dimensionally distributed cross-linkers. Actually some studies have already suggested that it is over idealized to model the random distributed cross linkers as a homogenous elastic medium (Mehrbod and Mofrad, 2011).

Microtubule splitting was also extensively studied in the literature. In this case a microtubule cannot be modeled as an indivisible shell or beam because splitting or depolymerization eventually leads to microtubule disassembling. Instead, protofilaments or dimer were modeled as basic units assembled together to compose a microtubule (Akiyoshi et al., 2010, Franck et al., 2007, Jánosi et al., 2002, Molodtsov et al., 2005a, Vichare et al., 2013, Dogterom et al., 2005, Westermann et al., 2006, Inoué and Salmon, 1995). The interaction between protofilaments or dimers was commonly governed by an assumed potential energy function (e. g., Lennard-Jones or Morse potentials), which may have different forms in various models suggested by different researchers (Hunyadi and Jánosi, 2007, Molodtsov et al., 2005a, Molodtsov et al., 2005b, Jiang et al., 2002). Because the natural curvature of naturally bent

protofilament is a key driving force to cause splitting of a microtubule, it plays a key role in splitting of microtubules. Two key questions for microtubule splitting are how splitting occurs with loss of the strongly constrained "cap" at the tip of a microtubule, and 2) how microtubule splitting provides pulling force to move chromosome.

To answer the first question, extensive researches have been done on biochemical effects due to hydrolysis of tubulin dimers and activities of microtubule associated proteins (Mitchison and Kirschner, 1984, Hyman et al., 1992, Vitre et al., 2008, Ji and Feng, 2011, Höög et al., 2011). However destruction of strongly constrained "cap" might also be induced by a compressive force applied from the membrane of microtubule. Similar phenomena have been observed in fiber-composites or carbon nanotube ropes (Chai et al., 1981, Kachanov, 1988, Ru, 2004) but not yet been investigated for microtubules.

For the second question, some studies discussed the mechanism of force generation by microtubule splitting from biological aspects (Grill and Hyman, 2005, Dogterom et al., 2005, Kimura and Kimura, 2011, Jánosi et al., 2002), and most researches showed that mechanical modelling of microtubule and protofilaments is crucial to quantitatively predict the pulling force provided by microtubule splitting. Vichare et al., developed an analytical model to calculate the pulling force of a splitting microtubule with given splitting length, however whether such force can be generated continuously associated with spontaneous splitting of microtubule is not yet verified (Vichare et al., 2013). Some numerical simulations were conducted with adhesion between protofilaments based on an assumed potential energy (Molodtsov et al., 2005b, Molodtsov et al., 2005a). Due to intrinsic limitations of numerical simulation techniques, this model rendered a less clear picture for us to physically understand how splitting and force generation could occur simultaneously and cooperatively in depolymerization of microtubule. Generally speaking, most of existing studies have focused on calculating the force produced by microtubule splitting while little attention has been paid to determining the range of splitting length which makes spontaneous splitting propagation possible.

1.4. Objectives and outline

Mechanical modelling of a microtubule is of great importance to study biomechanical

and biophysical behaviors of microtubules, cytoskeleton and biological cell. As presented in section 1.3, many previous mechanics models were successfully employed to predict some important mechanical responses of microtubules. Compared with the existing research works, two major objectives of the present thesis are:

a) Develop more realistic mechanics models to demonstrate some key experimentally observed buckling and vibration behaviors of microtubule *in vivo*, which are relevant for microtubules' biological functions but cannot be well explained by existing models.

b) Enhance the understanding of interaction between mechanical and biological behaviors of microtubule splitting by exploring the effect of some mechanical factors which have been ignored by the existing models for microtubule splitting.

Specifically, the present thesis is organized as follows:

1) In chapter 2 and 3, two numerical micro-mechanics models are developed to simulate microtubule buckling and vibration respectively. Our new models are more "realistic" than the existing free-standing elastic beam model and the elastic foundation model in the description of mechanical interfacing between microtubules and surrounding cross linkers in living cells. The comparison with some known experimental observations show that our new models could better explain some key features of microtubule buckling and vibration in living cells, which cannot be explained by the existing models.

2) In chapter 4, a micro-mechanics model is proposed to investigate splitting of a microtubule caused by an axial compression force, see Figure 1.2. Different than the common opinion in the existing literature which always explains splitting of microtubule as a consequence of the loss of cap at the tip of a microtubule due to biochemical reaction. The proposed new model shows that a mechanical compressive force could cause splitting of a microtubule even without the loss of its cap.

3) In chapter 5, the micro-mechanics model developed in chapter 4 is modified and refined by introducing a cohesive zone at the tip of a splitting microtubule, which could better model the interaction between protofilaments. The new model is employed to study the pulling force generated by microtubule splitting, see

Figure 1.2, and a criterion is derived for spontaneous propagation of microtubule splitting. Our new model predicts a range of splitting length for spontaneous splitting of microtubule, on which the maximum pulling force is estimated.

4) In chapter 6, major conclusions of the present thesis are summarized and a few further research topics are suggested.

2. Localized buckling of microtubule

2.1. Introduction

The microtubule is one of the most important cytoskeletal elements in eukaryotic cells (Boal, 2002). Although mechanical behaviors of microtubules *in vitro* were well predicted by elastic column model, microtubules *in vivo* (typically tens of microns in length) can bear much higher compressive force than that in *vitro*. The increase of critical buckling force is attributed to surrounding cross-linkers, which are often modeled as a continuous and homogenous elastic foundation (Brangwynne et al., 2006, Jiang and Zhang, 2008, Brodland and Gordon, 1990). As a result of the lateral elastic constraint, the multiwave buckling mode charactzerized by uniform short buckling waves with smaller deflection is energically favorable over the singlewave buckling mode predicted by the free-standing elastic column model. With such an elastic-foundation model, the critical compressive force and associated wavelength of buckling modes can be calculated by the conventional method of elastic buckling (Ugural and Fenster, 2003). In particular, the predicted critical force and wavelength are insensitive to the length of microtubules and the end conditions.

Despite the success of the elastic-foundation model in explaining higher critical buckling force, this model suffers several limitations. First, the relationship between the elastic foundation modulus and the properties of discrete cross-linkers remains a problem to be addressed (Jiang and Zhang, 2008, Wang et al., 2009, Gao and An, 2010, Li, 2008, Mehrbod and Mofrad, 2011). Actually, the commonly used approach to determine the elastic foundation modulus is under the assumption of in-plane two dimensional (2D) buckling (Ugural and Fenster, 2003), which is inappropriate for the three dimensional (3D) microtubule-cross linker system. More importantly, refereed to as “localized buckling” by some authors (Brangwynne et al., 2006), microtubule buckling *in vivo* exhibits a localized buckling mode in which the magnitude of deflection quickly decays from the site where the compressive force is applied. Similar localized buckling modes are observed in other experiments (Mandato and Bement, 2003, Gupton et al., 2002). The observed localized buckling is inconsistent with the uniform multiwave buckling mode predicted by the elastic foundation model (Li, 2008, Mehrbod and Mofrad, 2011, Jiang and Zhang, 2008). In addition, the possible effect of end conditions (e. g., free or clamped), which may lead to different buckling wavelength and critical force, cannot be captured by the elastic foundation

model. In view of the fact that the critical force for observed localized buckling could be much lower than that given by the elastic foundation model based on the uniform multiwave buckling mode, this discrepancy deserves a further study. To this end, it is crucial to examine the role of discrete cross linkers in *vivo,* which are laterally attached to microtubules and distributed randomly in both longitudinal and circumferential directions (Boal, 2002). Furthermore, as suggested by the "tensegrity" model (Wang et al., 2001, Canadas et al., 2002), the cross linkers have negligible bending rigidity and cannot bear compressive force, a feature which cannot be well modeled by the existing elastic foundation model.

In the present study, a micromechanics numerical model is developed to simulate buckling behavior of microtubules based on measured properties and observed morphology of microtubules and cross linkers. The proposed numerical model is validated by comparing its predictions with the elastic foundation model for simple 2D in-plane buckling of a microtubule supported by continuously distributed linear springs. The validated model is then employed to investigate 3D buckling behaviors of the microtubule-cross linker system. Based on our numerical simulations, two empirical relations are proposed for the critical force and wavelength of localized buckling of microtubules. As will be shown, the localized buckling of microtubules predicted by the present model is in reasonable agreement with some recent experimental data.

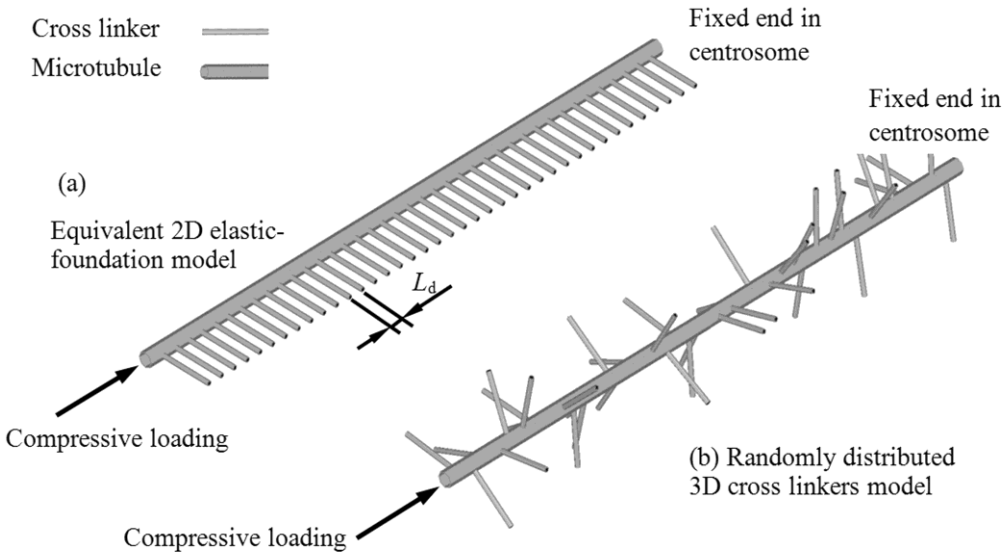

Figure 2.1 The present numerical models: (a) equivalent 2D elastic foundation model; (b) randomly distributed 3D cross linkers model.

2.2. Numerical models

The microtubule-cross linker system, studied in the present thesis, is composed of a microtubule surrounded by cross linkers randomly distributed along longitudinal direction, see Figure 2.1. The microtubule is modeled as an elastic hollow cylinder column, while the modeling of cross linkers is illustrated in following two sections. The two key parameters of the cross-linkers are the spring constant k and the spacing of cross linkers L_d, whose values will be given based on available experimental data. Buckling of microtubules is stimulated by imposing compressive axial displacement at one end of the microtubule with the other end clamped. Some details of using finite element method for the buckling of microtubule can be found in Appendix A.

2.2.1. Microtubule modeling

The microtubule is modeled as a hollow cylinder column with outer diameter of 24 nm and thickness of 1.86 nm (Mehrbod and Mofrad, 2011, Jin and Ru, 2012). The geometry of cross section and the Young's modulus E of 1 GPa (Li et al., 2006) give the bending rigidity EI of 9.034×10^{-24} Nm^2, which is within the range of the measured values of several experiments (Hawkins et al., 2010). The length of microtubule L in the present study is between 300 nm, which is almost the minimum length of microtubules in experiments (Howard, 2001), and a few tens of microns. As our major concern is the localized mode or uniform multiwave buckling mode with shorter wavelength (typically, around 1-3 micron), the length dependency of bending rigidity (Pampaloni et al., 2006) is not included in the present thesis. Thus, the 3D Timoshenko shear deformable beam elements are used to mesh the microtubule. The microtubule is always clamped in one end as it is anchored in centrosome in living cells (Howard, 2001, Boal, 2002). Another end of the microtubule is subjected to a compressive load under different types of end conditions (e. g., free or clamped) (Boal, 2002). To initiate buckling of the microtubule, an extremely small perturbation force is applied at the end in the direction perpendicular to the microtubule. Our simulations show that the magnitude of the small perturbation force is irrelevant to simulation results.

2.2.2. Cross linkers modelling

All cross linkers are modeled as linear springs with one end permanently attached to the microtubule and the other end fixed in all degrees of freedom. The spring constant k of cross linkers (of length 45 nm) used here, 39 pN/nm, is taken from (Peter and

Mofrad, 2012). As the spring constant k may change for different types of cross linkers, a wider range of the spring constant (which may depend on length of cross linkers) is also considered in the present work. On the other hand, the spacing L_d ranging from 25 nm to 300 nm (Peter and Mofrad, 2012, Svitkina et al., 1996) will be considered. The 3D elastic linear spring elements are used to mesh the cross linkers. Two numerical models, characterized by different distributions and constitutive laws of cross linkers, are illustrated below, and referred to as the equivalent elastic-foundation model and the randomly distributed 3D cross linker model respectively.

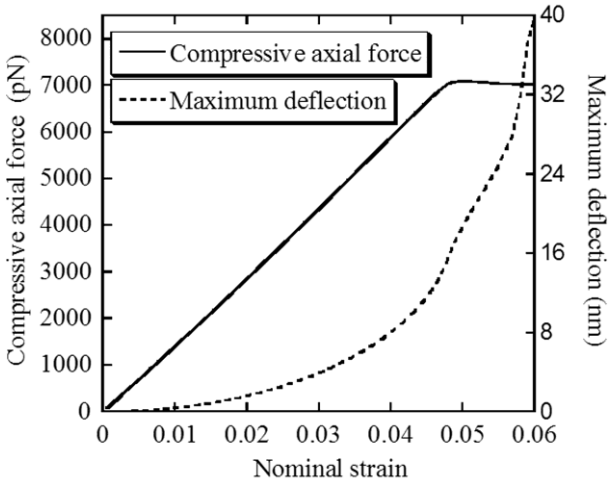

Figure 2.2 A typical relation between the compressive axial force or the maximum deflection and the nominal axial strain given by the present model.

To demonstrate the efficiency of the present numerical model, first we shall apply it to the simple 2D in-plane uniform multiwave buckling and compare its results with the elastic foundation model. For the 2D in-plane buckling of a microtubule supported by a continuum elastic foundation, the wave length and critical buckling force are given by (Brodland and Gordon, 1990)

$$\lambda=2\pi\left(\frac{EI}{E_c}\right)^{\frac{1}{4}} \tag{2-1}$$

and

$$F_{cr}=2\sqrt{E_c EI}=8\pi^2\frac{EI}{\lambda^2} \tag{2-2}$$

where EI is the bending rigidity of the microtubule and E_c is the elastic foundation modulus. The elastic foundation modulus E_c in the 2D condition is directly proportional to the spring constant k and inversely proportional to the spacing L_d of uniformly distributed linear springs (Ugural and Fenster, 2003) as

$$E_c = \frac{k}{L_d} \tag{2-3}$$

This formula (2-3) is commonly used provided that L_d is much smaller than the wave length.

To compare the present numerical model with the elastic foundation model, a 2D numerical model is shown in Figure 2.1 (a), where all cross linkers are aligned in the same plane and perpendicular to the microtubule. All out-of-plane displacements and rotations are not allowed. In addition, as assumed in the elastic foundation model, all cross linkers in the equivalent elastic foundation model shown in Figure 2.1(a) are capable of bearing both compressive and tensile forces (Wang et al., 2001, Canadas et al., 2002).

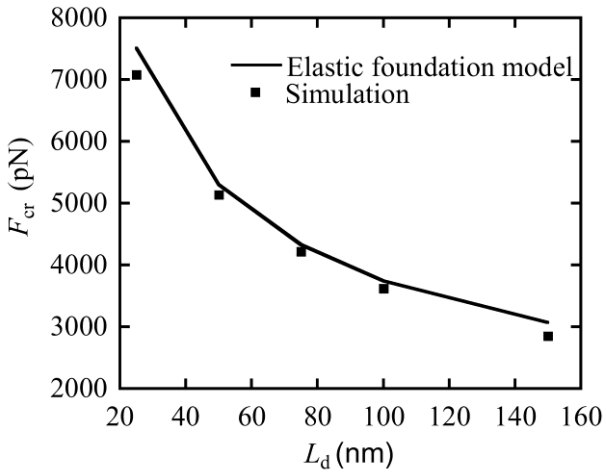

Figure 2.3 Critical buckling forces F_{cr} predicted by the present equivalent elastic foundation model compared with the elastic foundation formulas Eqs. (2-1) and (2-2) with k=39 pN/nm.

The major goal of the present study is buckling behaviors of a microtubule surrounded by 3D randomly distributed discrete cross linkers. The morphological details of the cross linkers are modeled based on experimental observations. All cross linkers are attached to the microtubule in random directions assigned by the uniform

distribution rule, see Figure 2.1 (b). The cross linkers are modeled as linear springs with negligible bending rigidity (Mehrbod and Mofrad, 2011, Bathe et al., 2008), thus they can bear axial tension but are vulnerable to any axial compression. To realize this, the load increments are sufficiently small, and every spring element is verified after each load increment and will be permanently removed if the axial force becomes compressive (Actually, if a small non-zero threshold value of compressive force, such as 1-2 pN, is used, our results remain essentially unchanged. Therefore we have simply set the threshold value as zero). Different from the equivalent elastic foundation model (where out-of-plane displacements and rotations are not allowed), the 3D buckling behaviors are modeled by allowing buckling deflections in all directions.

2.2.3. Model verification by comparison with a classical model

First let us consider the classic 2D uniform multiwave buckling mode which evenly spreads over the entire microtubule (Ugural and Fenster, 2003). In this case, the results given by the present equivalent elastic foundation model are compared with the classical elastic foundation model.

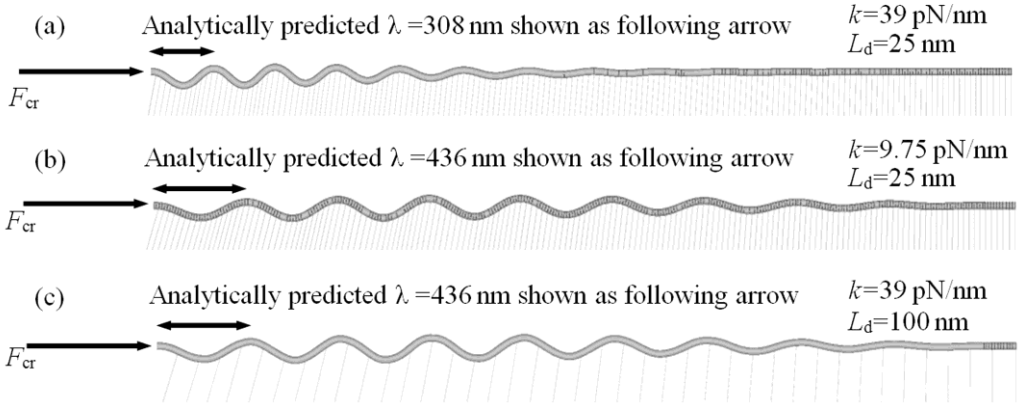

Figure 2.4 2D in-plane multiwave buckling modes (buckled grey color beam) given by the present equivalent elastic foundation model compared with the wave lengths given by the classical elastic foundation model Eq. (2-1) (black arrows).

First compared are the critical buckling forces predicted by the present numerical model and the classical formula Eq. (2-2). From the present numerical model, a curve of the axial compressive force versus the nominal axial strain is plotted in Figure 2.2, with k =39 pN/nm and L_d =25 nm. It is seen from Figure 2.2 that the axial compressive force linearly increases with the nominal axial strain until a plateau is

reached. Also included in Figure 2.2 is the maximum deflection of the microtubule, which upturns remarkably as the plateau is approached. Therefore the critical buckling force F_{cr} from our numerical simulations is defined as the axial compressive force on the plateau. It is seen from Figure 2.2 that after the critical force is reached, the axial compressive strain increases quickly without significant change in the axial force (for example, the axial force changes only by less than 5% as the axial strain doubles). It is seen from Figure 2.3 that the critical buckling force F_{cr} given by the present numerical model is in good agreement with the Eq (2-2). In particular, consistent with the elastic foundation model, the critical buckling force and wave length simulated by the present numerical model is also found to be insensitive to the microtubule length.

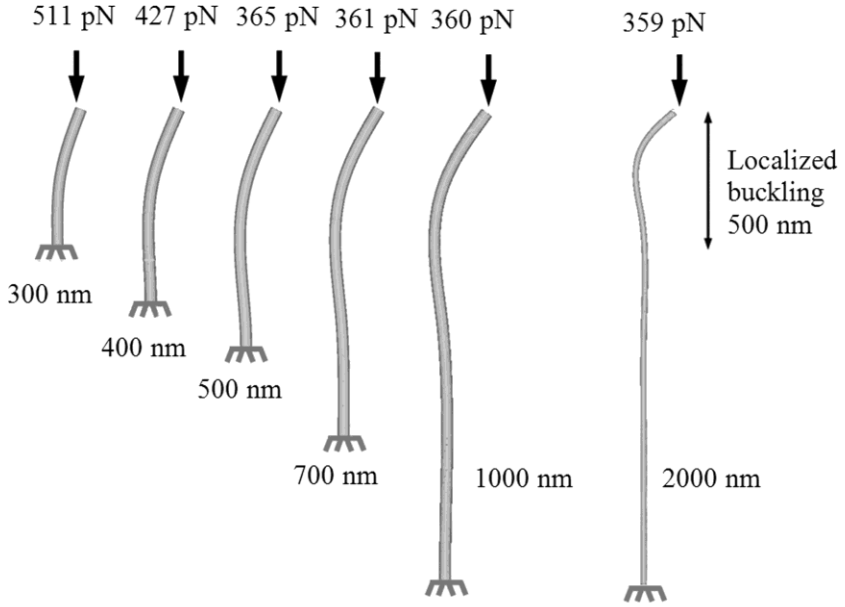

Figure 2.5 Buckling of a microtubule given by the present randomly distributed 3D cross linkers model with spring constant k=39 pN/nm and spacing L_d=50 nm. The buckling wave length and critical buckling force are essentially length independent as the length of microtubule is much longer than the buckling wave length.

Three buckling modes given by our numerical models are shown in the Figure 2.4, with a good comparison to the classical wavelength formulas Eqs. (2-1) and (2-3). In Figure 2.4 (a), the shorter wavelength is associated with the highest spring constant k =39 pN/nm and the shortest spacing L_d =25 nm. In particular, our numerical results confirm that the buckling predicted by the 2D equivalent elastic foundation model is

characterized by the uniform multiwave mode rather than localized mode, and the predicted wave length is insensitive to the length of microtubule.

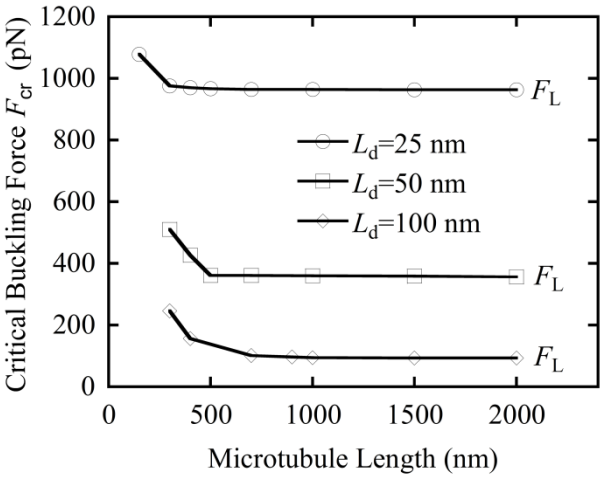

Figure 2.6 The critical forces F_{cr} quickly converges to a constants (defined as the localized buckling force F_L) as the microtubule length exceeds a critical length (the latter is around 500 nm when L_d =50 nm). This critical length increases with increasing spacing of cross linkers L_d.

2.3. Results and discussion

2.3.1. Features of localized buckling

Now let us investigate 3D buckling behaviors of the microtubule-cross linker system using the randomly distributed 3D cross linkers model. It is seen from Figure 2.5 that a remarkable feature of the buckling behavior given by our 3D cross linkers model is that the buckling mode is highly localized near the end, which bears great similarity with the microtubule buckling observed in *vivo* by Brangwynne et al. (2006) and refereed as "localized buckling". Although the localized buckling mode obtained in our simulations is actually 3D in nature, the out-of plane helical deflection is much smaller than the in-plane deflection. Here it should be noted that the localized buckling mode predicted by the present static 3D cross linkers model is significantly different from those reported in some previous studies, say the localized mode caused by the wave of compressive force propagating from one end at which localized buckling mode is initiated (Ranjith and Kumar, 2002), or the localized mode as a result of the large deflection post-buckling of a compressed column on a 2D elastic foundation (Hunt et al., 1993, Lee and Waas, 1996) which has the uniform multiwave

mode as its linearized buckling mode. Different than these mentioned works, the localized mode obtained by the present model is static in nature and not a result of post-buckling developed from an initial uniform multiwave buckling mode.

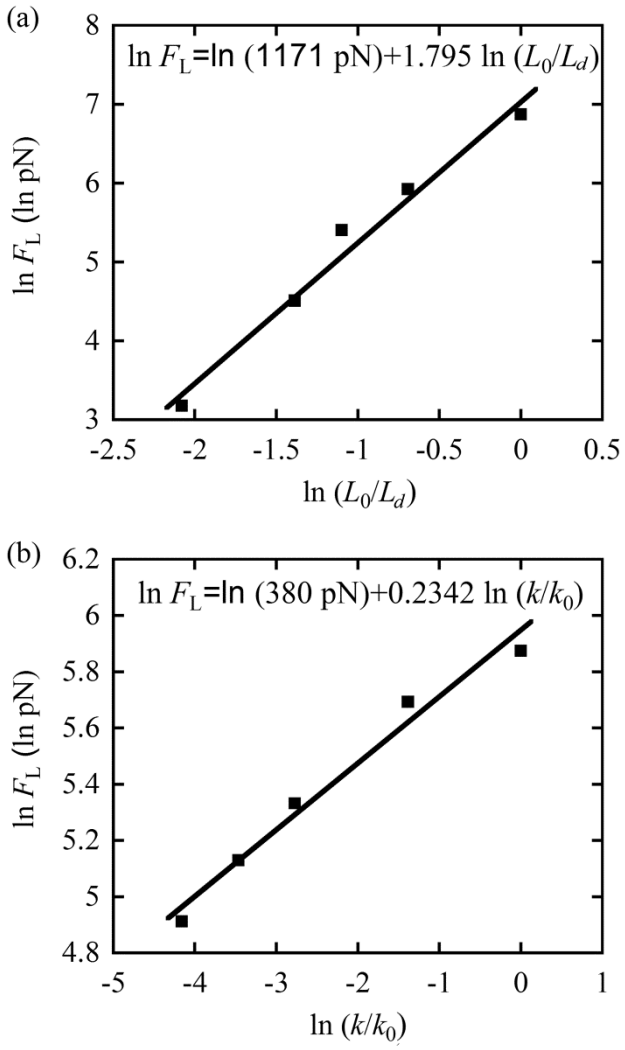

Figure 2.7 Determination of the p and q in the proposed empirical equations (5) by linearly fitting simulation results of localized buckling.

What is shown in Figure 2.6 is the dependence of the critical buckling force F_{cr} on the microtubule length. Although the critical buckling force F_{cr} changes considerably with length for extremely short microtubules (say, F_{cr} decreases from 511 pN to 365 pN as the length of microtubule increase from 300 nm to 500 nm), the critical force F_{cr} becomes length-independent when the microtubule length exceeds a critical value (say, larger than 500 nm). For example, for a microtubule of 2000 nm in length, the critical force F_{cr} for localized buckling is around 360 pN (which is almost the same as

the critical force 365 pN for a microtubule of 500 nm in length), and the localized buckling wavelength is about 500 nm (almost the same as the localized buckling wavelengths of much shorter microtubules). In Figure 2.6, it can be seen how the buckling force F_{cr} quickly converges to a constant, defined as the localized critical buckling force F_L, when the length of microtubule exceeds a critical value (say, 500 nm for k =39 pN/nm and L_d =50 nm). Indeed, the critical force F_L for localized buckling and the associated wavelength λ_L become essentially length-independent when the microtubule length exceeds a critical value.

The spring constant k and spacing L_d of cross linkers influence the predicted critical force F_L and wave length λ_L of localized buckling, as well as the critical length of microtubules beyond which F_L and λ_L become essentially length-independent. For example, our numerical results show that as spacing L_d changes from 25 nm to 100 nm with k =39 pN/nm, the critical length of microtubules, beyond which F_L and λ_L keep essentially constant, increases with the increasing spacing L_d. Additionally, as expected, our simulations show that higher critical force F_L and shorter wave length λ_L are achieved with larger spring constant of cross linkers, as to be detailed in section 2.3.2.

2.3.2. Empirical relations for localized buckling

The localized buckling is characterized by the two key parameters, the localized buckling wave length λ_L and the critical force F_L for localized buckling. In what follows, based on our numerical simulations, two empirical relations will be given for the dependency of the two key parameters on the spring constant k and the spacing L_d of cross linkers.

In view of the classical formula (2-1), we seek for an empirical relation for the localized buckling wave length of the following form

$$\lambda_L = 2\pi\left(\frac{EI}{Q}\right)^{\frac{1}{4}}\left(\frac{k_0}{k}\right)^{\frac{p}{4}}\left(\frac{L_d}{L_0}\right)^{\frac{q}{4}} \tag{2-4}$$

where Q, p and q will be determined to fit numerical data (Q has the unit of Pa, while p and q are dimensionless). The reference spacing L_0 is 25 nm (which is probably the shortest cross linker spacing, say with the length of GTP/GDP dimers of

8.1 nm, see ref. (Hunyadi et al., 2007)), and the reference spring constant of cross linkers k_0 is 39 pN/nm (Peter and Mofrad, 2012). In view of the classical formula (2-2), we also seek for an empirical relation for the critical force for localized buckling of the following form:

$$F_{\mathrm{L}}=\frac{B\pi^2}{4}\frac{EI}{\lambda_{\mathrm{L}}^2}=\frac{B}{16}\sqrt{EIA}\left(\frac{k}{k_0}\right)^{\frac{p}{2}}\left(\frac{L_0}{L_{\mathrm{d}}}\right)^{\frac{q}{2}} \tag{2-5}$$

where B is a dimensionless constant. To determine p and q based on our numerical simulations, we rewrite Eq. (2-5) as

$$\ln F_{\mathrm{L}}=\ln\left(\frac{B}{16}\sqrt{EIA}\left(\frac{L_0}{L_{\mathrm{d}}}\right)^{\frac{q}{2}}\right)+\frac{p}{2}\ln\left(\frac{k}{k_0}\right) \tag{2-6}$$

and

$$\ln F_{\mathrm{L}}=\ln\left(\frac{B}{16}\sqrt{EIA}\left(\frac{k}{k_0}\right)^{\frac{p}{2}}\right)+\frac{q}{2}\ln\left(\frac{L_0}{L_{\mathrm{d}}}\right) \tag{2-7}$$

In Eqs (2-6) and (2-7), the $p/2$ and $q/2$ are the slopes of the curves of $\ln F_{\mathrm{L}}$ versus $\ln(k/k_0)$ and $\ln(L_0/L_{\mathrm{d}})$, respectively. The simulation results with different combinations of k and L_{d} are linearly fitted in Figure 2.7 (a) and (b), which gives q and p as 3.6 and 0.47, respectively. With the values of q, p known, the value of Q is linearly fitted in Eq. (2-4) as 1.4 MPa based on the the wavelengths given by our simulations. With all of these values obtained, the constant B is obtained as 5.3 from Figure 2.7 (a) and Eq. (2-6). Finally two empirical relations for the critical force and the associated wave length for localized buckling are given as

$$\lambda_{\mathrm{L}}=2\pi\left(\frac{EI}{1.4\ \mathrm{MPa}}\right)^{\frac{1}{4}}\left(\frac{k_0}{k}\right)^{0.12}\left(\frac{L_{\mathrm{d}}}{L_0}\right)^{0.90} \tag{2-8}$$

and

$$F_{\mathrm{L}}=1.3\pi^2\frac{EI}{\lambda_{\mathrm{L}}^2} \tag{2-9}$$

Since p and q are determined using the data of critical force F_{L} given by Eq. (2-5), the predicted wave length λ_{L} from Eq. (2-8) is further compared with the data

obtained directly from simulations. Again, a good agreement is achieved for $k = k_0$, $k_0/4$, $k_0/16$, $k_0/32$ and $k_0/64$, as shown in Figure 2.8. Validity of the proposed relations (2-8) and (2-9) are also verified for different values of bending rigidities *EI*. For example, in a series of experiments by Felgner et al., the bending rigidity of microtubule was measured as low as 3.8×10^{-24} Nm^2 (Felgner et al., 1997). With the bending rigidity *EI* of 3.8×10^{-24} Nm^2 and the other parameters adopted in Figure 2.5, the critical buckling force given by the empirical formula Eq. (2-9) is 218 pN, which is reasonably close to 234 pN obtained by direct numerical simulations with *EI*=3.8×10^{-24} Nm^2. The two empirical relations (2-8) and (2-9) are expected to be useful within a reasonable range of the spring constant (from $k_0/64$ to k_0) and the spacing (from 25 nm to 300 nm) of cross linkers and under the condition that the localized buckling wave length λ_L is at least 10 times longer than the spacing L_d.

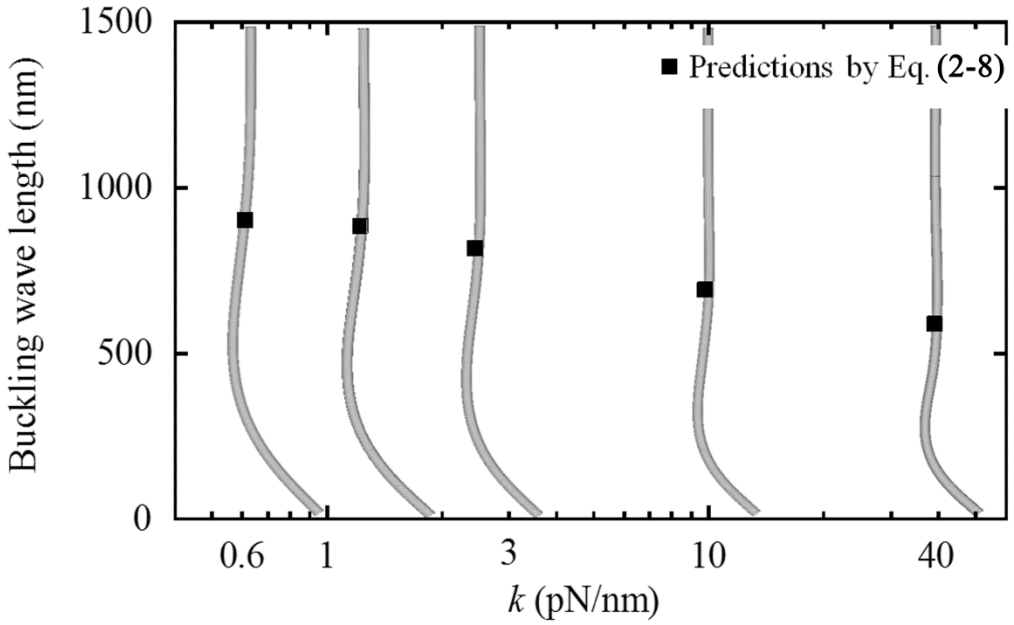

Figure 2.8 Localzed buckling wavelength λ_L given by the present numerical model compared with the wave length calculated from the empirical equation (2-8).

The proposed empirical formulas (2-8) and (2-9), obtained by fitting with our numerical data, are significantly different than 2D elastic foundation formulas (2-1) and (2-2). For example, the critical force for localized buckling predicted by Eq. (2-9) is about 1/6 of the buckling force predicted by the elastic foundation model (2-2) based on the same buckling wave length, which indicates that the critical buckling force of localized buckling is much lower than that predicted by the elastic foundation

model based on in-plane uniform multiwave buckling mode. In addition, although both our empirical formulas (2-8) and (2-9) and 2D elastic foundation formulas (2-1) and (2-2) predict that the critical buckling force increases with the spring constant k and decreases with the spacing L_d, the dependence of critical buckling force on the spring constant k decreases from the power index of 0.5 in the 2D model to 0.22 in our 3D model, and the dependence of critical buckling force on the spacing L_d increases from the power index of 0.5 in 2D model to 1.8 in our 3D model.

2.3.3. Comparison with experiments

Let us now compare the results of localized buckling given by the present model with some known experimental measurements, as well as the elastic foundation model and the free-standing elastic column model. In what follows, the microtubules in all cases are of a common length of $5\,\mu m$, which guarantees that the wave lengths of the localized buckling mode and the uniform multiwave buckling mode are much shorter than the length of the microtubule.

The buckling modes given by three models, shown in Figure 2.9, are significantly different. The buckling of a free-standing microtubule under the free or clamped end condition is illustrated in Figure 2.9 (a) and (b) respectively. With L_d =100 nm and k =39 pN/nm, the localized buckling given by the present model under free or clamped end condition is shown in Figure 2.9 (c) and (d) respectively. Finally, the buckling mode and critical buckling force of the uniform multiwave buckling given by the equivalent elastic foundation model (described in section 2.2.1) is presented in Figure 2.9 (e) with the same L_d and k as adopted in Figure 2.9 (c) and (d). All predicted buckling behaviors are compared with experimental observations (Brangwynne et al., 2006, Mandato and Bement, 2003, Gupton et al., 2002) shown in Figure 2.9 (f).

The localized buckling modes given by the present model in Figure 2.9 (c) and (d) with two different end conditions bear a resemblance to the observed microtubule buckling mode *in vivo* shown in Figure 2.9 (f) (Brangwynne et al., 2006, Mandato and Bement, 2003, Gupton et al., 2002). Although the actual end conditions of the microtubules *in vivo* (Brangwynne et al., 2006, Mandato and Bement, 2003, Gupton et al., 2002) are different, all observed buckling modes are localized in nature, which are consistent with our simulations shown in Figure 2.9 (c) and (d) but cannot be explained by the 2D elastic foundation model. On the other hand, the single-wave

buckling mode given by the free-standing microtubule model is only comparable with *in vitro* experiments (Kikumoto et al., 2006, Elbaum et al., 1996) but fail to predict the buckling behaviors of microtubules surrounded by cross linkers in living cells.

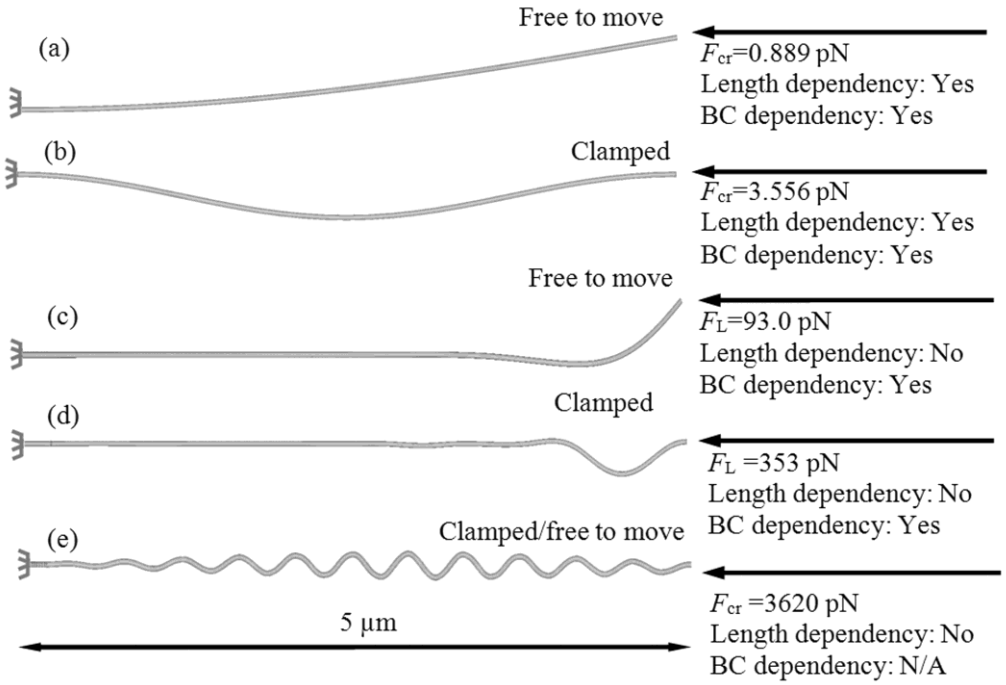

Figure 2.9 Different buckling cases of microtubules in *vivo/vitro*: the free-standing microtubule buckling with clamped-free (a) or clamped-clamped (b) end conditions observed in *vitro* (Kikumoto et al., 2006, Elbaum et al., 1996); the localized buckling with clamped-free (c) and doubly clamped (d) end conditions, which are similar to the observation in *vivo* (Brangwynne et al., 2006, Mandato and Bement, 2003, Gupton et al., 2002).

Also, the present model can effectively predict the critical force for localized buckling and the associated buckling wavelength. For example, with L_d =100 nm and k =39 pN/nm (Peter and Mofrad, 2012, Svitkina et al., 1996), the localized buckling wave length and critical force given by the present numerical model under a free end condition in Figure 2.9 (c) are about 1.2 μm and 93 pN, respectively, similar results of 1.10 μm and 97.3 pN can be obtained from the empirical Eqs. (2-8) and (2-9). With a doubly clamped end condition in Figure 2.9 (d), the localized buckling wave length and critical force given by the present model are about 1 μm and 353 pN respectively. The two predicted wavelengths agree reasonably with the observed

wavelength around 1-2 μm shown in Figure 2.9 (f). With slightly different spring constant and spacing of cross linkers, the predicted buckling wave lengths still fall into the range of experimental measurements, say 1-3 μm (Brangwynne et al., 2006, Gupton et al., 2002, Mandato and Bement, 2003). For example, the longer buckling wavelength, 3 μm, can be obtained by the present model with the spacing of 300 nm (Griffith and Pollard, 1978). In addition, the critical forces for localized buckling predicted by the present model, 93.0 pN or 353 pN, are also in reasonable agreement with the well-recognized concept that the critical buckling force of microtubules in *vivo* would be around 100 pN (Gittes et al., 1993, Li, 2008, Brangwynne et al., 2006).

Clearly, if the free-standing column model or the elastic foundation model is adopted with the above data of spring constants and spacing of cross linkers, the predicted critical buckling force and wave length are different from experimental measurements by almost one order of magnitude. For example, the critical buckling forces predicted by the free-standing column model are only 0.889 pN and 3.556 pN for a free or clamped end. On the other hand, if the elastic foundation model is adopted with the foundation modulus given by Eq. (2-3), with the same data of cross linkers as those used in Figure 2.9 (c) and (d), the predicted buckling wave length, about 400 nm, is much shorter than measured buckling wave length. Actually, in order to predict the measured buckling wave length of 2-3 μm with the bending rigidity of microtubules adopted in the literature (Li et al., 2006), i.e. 20×10^{-24} Nm^2 and L_d=100 nm, the elastic foundation model requires a spring constant of cross linkers k as low as 0.078 pN/nm, which is much lower than the spring constant of most types of protein polymers attached to microtubules (e. g., the actin filaments, 1 μm in length, have the spring constant of 44 pN/nm (Howard, 2001), and TAU, which links microtubules to form bundles, has the spring constant of 39 pN/nm (Peter and Mofrad, 2012)), and is almost one order of magnitude lower than the lower limit of measured lower limit of Kinesin (i. e., 0.65 pN/nm -1.7 pN/nm) (Carter and Cross, 2005), a key motor protein attached to microtubules for cellular transportations. Therefore, although the elastic foundation model could also give the measured buckling wave length, the assumed elastic foundation modulus (Li, 2008, Jiang and Zhang, 2008, Wang et al., 2009) cannot be obtained through Eq. (2-3) from the known data of cross linkers reported in literature (Peter and Mofrad, 2012, Svitkina et al., 1996, Griffith and Pollard, 1978). Thus it seems reasonable to conclude that, as compared with the elastic foundation

model, the present discrete cross linkers model can better explain the observed wavelength and critical force of localized buckling of microtubules in living cells.

Physically, for a number of reasons, we also believe that the present 3D discrete numerical model can better capture realistic conditions for microtubules in living cells as compared with the 2D elastic foundation model. First, the cross linkers in living cells are discrete and 3D in nature, which cannot be appropriately described by the 2D continuum elastic foundation model. Second, the geometrical nonlinearity, which is included in the present numerical model, cannot be easily carried out by the classic linear buckling analysis. Third, the cross linkers cannot be idealized as a linear elastic foundation because they cannot bear compressive force due to very low bending rigidity, a feature captured in the present 3D discrete numerical model.

2.4. Conclusions

A numerical micro-mechanics model is proposed to investigate axially compressed buckling of a microtubule surrounded by randomly distributed discrete cross linkers. The localized buckling behavior observed *in vivo* (Brangwynne et al., 2006, Mandato and Bement, 2003, Gupton et al., 2002), which cannot be predicted by the existing models, is well explained by the present numerical model. Based on our numerical simulations, two empirical relations are proposed to calculate the critical force and associated wave length of localized buckling. For typical cross linkers of the spacing of 50-300 nm and the spring constant of 39 pN/nm as reported in literatures (Peter and Mofrad, 2012, Svitkina et al., 1996, Griffith and Pollard, 1978), the present model predicts that microtubules could buckle under an axial compressive force of about 14-340 pN with a localized buckling mode of wavelength of 0.6-2.9 microns, in reasonable agreement with a few recent experiments (Gittes et al., 1993, Li, 2008, Brangwynne et al., 2006).

3. Localized vibration of microtubule

3.1. Introduction

Microtubules are highly dynamic bio-polymers involved in many cellular functions such as mitosis, intracellular transport and adhesion of eukaryotic cells (Boal, 2002). Mechanical behaviors of microtubule, e. g., buckling, bending, and vibration, are of relevance to cell biology (Stamenović and Coughlin, 1999, Molodtsov et al., 2005a). For example, vibration of microtubule could be stimulated by actomyosin powered cortical flow (Mandato and Bement, 2003, Lee et al., 2001) and external force engendered in mitosis (Rai et al., 2013). On the other hand, vibration of microtubule could play a key role in the bio-functioning of cells. For instance, vibration of microtubules directly coordinates the movement and shape variance of cells (Tounsi et al., 2010, Allen et al., 2008), vibration of microtubule might be related to the electrodynamic activities of cells as it has been shown that mechanical vibration of microtubule is coupled with its electrical oscillation (Pokorný, 2004), and the electrodynamic activities of cells are important features to distinguish cancer cells from health cells in the cancer diagnosis (Daneshmand, 2012). In addition, microtubules are used as templates for nanofabrication, which requires the knowledge of vibration of microtubules (Behrens et al., 2004).

To enhance the understanding of the microtubule dynamics, there had been a number of studies in recent years dealing with the mechanical vibration of microtubules. By modelling microtubules as an elastic shells interacting with fluids, frequencies and the energy to excite microtubule vibration were estimated (Pokorný, 2004, Sirenko et al., 1996). It is verified that continuum elastic models are capable to study microtubule vibration. To better characterize mechanical behaviors of microtubule, some elaborate beam (Tounsi et al., 2010) and shell (Wang et al., 2006) models were proposed to address the effects of orthotropic mechanical properties, transverse shear, length-dependent flexural rigidity and large deflection of microtubule. Microtubule vibration was also studied by elastic lattice model (Portet et al., 2005) and atomistic-continuum models (Xiang and Liew, 2012), which gave comparable results with the continuum elastic models.

Despite the success of the above-mentioned models in the understanding of dynamic behaviors of microtubule, they still suffer several drawbacks especially in modeling

transvers vibration of microtubule *in vivo*. Many of existing mechanics models ignored the influence of surrounding cytoplasm (Xiang and Liew, 2012, Wang et al., 2006). Although some models considered the effect of surrounding cytoplasm (Shen, 2011, Ghavanloo et al., 2010, Zeverdejani and Beni, 2013), the cytoplasm is often over-idealized as a homogenous elastic foundation, which is not capable of catching discrete features of cross linkers attached to the microtubule. Actually some studies already suggested that the random distributed cross linkers cannot be well modelled as a homogenous elastic medium (Mehrbod and Mofrad, 2011). More importantly, as will be shown later, vibration of microtubule predicted by modelling the surroundings as a homogenous elastic foundation has two features: (a) natural frequencies are strongly dependent on microtubule length and end conditions; (b) the predicted vibration modes spread through the entire microtubule. These two features are in direct contradiction with some experimental observations which indicated that vibration modes (Marrari et al., 2003, Mandato and Bement, 2003) and buckling modes (Jin and Ru, 2013, Brangwynne et al., 2006) *in vivo* are highly localized.

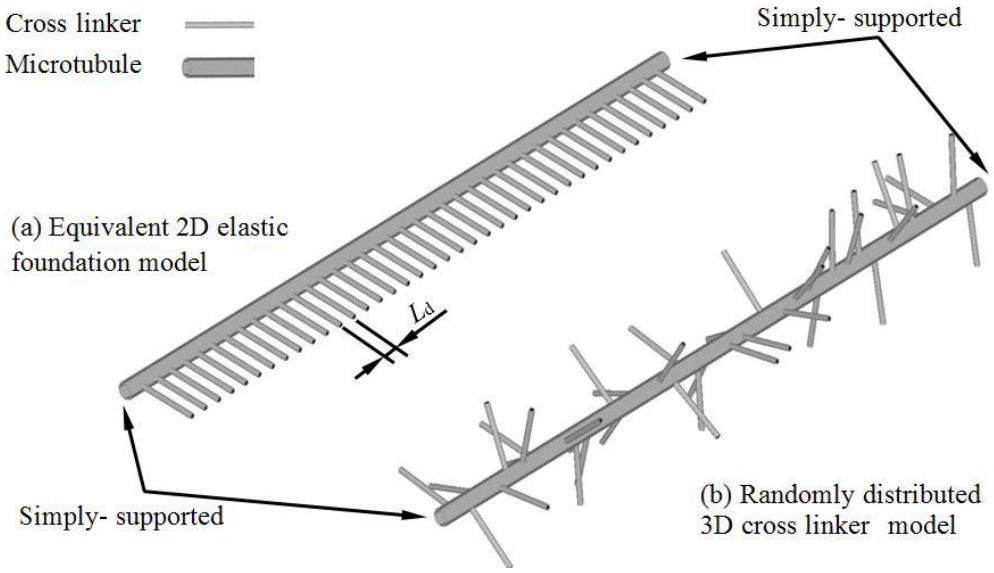

Figure 3.1 Finite element models: (a) equivalent elastic foundation model; (b) presently developed randomly distributed 3D cross linker model.

In the present study, finite element method is employed to simulate vibration behavior of microtubules based on measured properties and observed morphology of microtubule and cross linker. The proposed numerical model is firstly verified by comparing its predictions with the widely used elastic foundation model for a simple

case in which the microtubule are supported by linear springs uniformly distributed in a 2D plane. The verified model is then modified to investigate vibration behaviors of a microtubule surround by 3D randomly distributed cross linkers. Based on our numerical simulation results, some empirical relations are proposed to estimate the (lowest) critical frequency of localized vibration and the associated wave length. As will be shown, the localized vibration of microtubules predicted by the present model is comparable with some recent experimental observations.

3.2. Numerical models

3.2.1. Modelling

The microtubule is modeled as a hollow cylinder column with outer diameter of 24 nm and thickness of 1.86 nm (Mehrbod and Mofrad, 2011, Jin and Ru, 2012). The geometry of cross section and the Young's modulus E of 1 GPa (Li et al., 2006, Enemark et al., 2008) give the bending rigidity EI of 9.034×10^{-24} Nm^2, which falls into the range of the measured values of several experiments (Hawkins et al., 2010, Kikumoto et al., 2006). The Poisson ratio of the beam is assumed as 0.3 and shear modulus is 0.38 GPa. The density of microtubule is taken as ρ=1.47 g/cm^3 (Tounsi et al., 2010), which gives ρA of 2.06×10^{-12} kg/m, where A is the cross section area of microtubule. The assumed length of microtubule L is in the range from several microns to a few tens of microns (Alberts et al., 1994). The 3D Timoshenko shear deformable beam elements are used to mesh the microtubule. We only modeled one microtubule in present study thus the contact between adjacent microtubules is not considered, which might also important for microtubule dynamics. We applies the simply supported boundary condition on two ends of microtubule, which has been adopted in some previous studies of microtubule vibration as an elastic beam (Tounsi et al., 2010). Actually because the localized vibration modes are distributed through the whole microtubule, most localized vibration modes concerned in this study lies at segments far away from the end. These localized vibration modes (>95%) are not subjected to the end condition applied.

We developed two numerical models which are distinguished by the manners of cross linker distribution. To study vibration and buckling of microtubule interacting with surroundings, linear elastic foundation model was commonly used in previous studies.

In this model, microtubule is subjected to a reactive force proportional to the magnitude deflection. Mechanically, it is equivalent to that the microtubule is attached by linear springs of equal interval in the same direction and the microtubule is only allowed to deflect within the plane which the springs are distributed (Shen, 2011, Ghavanloo et al., 2010, Zeverdejani and Beni, 2013, Brangwynne et al., 2006). In the first model, all cross linkers are perpendicular to the microtubule and aligned in the same 2D plane, and all out-of-plane displacements and rotations of both cross linkers and microtubule are not allowed. We named this model as "equivalent 2D elastic foundation model" because it is consistent with all assumptions made in the classic elastic foundation model, see Figure 3.1 (a) for the detailed illustration.

In the second model (named "randomly distributed 3D cross linker model"), we consider the role of randomly distributed 3D cross linkers based on the morphological details of the cross linkers observed *in vivo*. In this model, all cross linkers are attached to the microtubule in random directions assigned by the uniform distribution rule. Different from the equivalent 2D elastic foundation model where out-of-plane displacements and rotations are not allowed, 3D deflections in all directions are allowed in the randomly distributed 3D cross linker model. The details of randomly distributed 3D cross linker model are shown in Figure 3.1 (b).

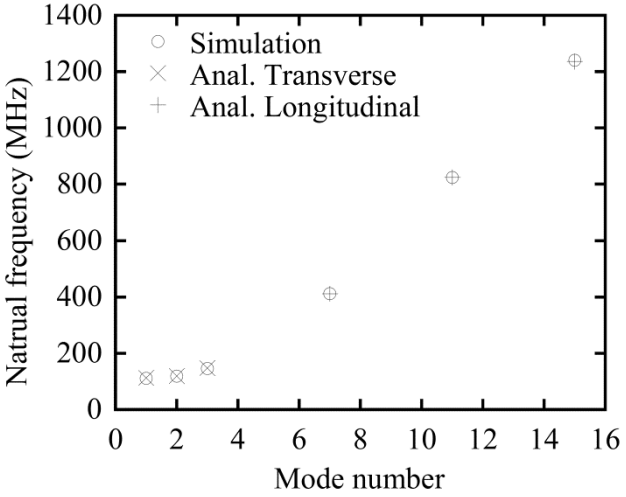

Figure 3.2 Three lowest transverse (mode number=7, 11, 15) and longitudinal (mode number=1, 2, 3) vibration frequencies predicted by Eqs. (3-1) and (3-2) are in good agreement with simulations given by the present equivalent 2D elastic foundation model shown in Figure 3.1 (a). Simply-supported end conditions are applied for all cases.

Despite different distribution morphologies, all cross linkers are modeled as linear springs with one end permanently attached to the microtubule and another end fixed in all degrees of freedom. As the spring constant k and spacing L_d may change for different types of cross linkers, in the present study, we shall consider the spring constant k of cross linkers ranging from 1pN/nm to 39 pN/nm and the spacing L_d ranging from 25 nm to 100 nm (Peter and Mofrad, 2012, Svitkina et al., 1996). For convenience, a basic case is defined by the spring constant $k = k_0$=39 pN/nm and the spacing $L_d = L_0$=25 nm, based on a few previous studies (Peter and Mofrad, 2012, Svitkina et al., 1996, Jin and Ru, 2013). Although some microtubule associated proteins cannot bear compressive force due to the negligible bending rigidity (Wang et al., 2001), such non-linear property cannot be included as a result of performing linear eigenvalue analysis in present study. Some details of using finite element method for the vibration of microtubule can be found in Appendix B.

3.2.2. Model verification by comparison with a classical model

The longitudinal vibration (displacement along the microtubule axis) frequency f_{A} and 2D in-plane transverse vibration (deflection perpendicular to the microtubule axis) frequency f_{T} can be calculated by the following formulas based on the elastic foundation model (Timoshenko et al., 1974)

$$f_{\mathrm{A}} = \frac{n}{2}\sqrt{\frac{E}{L^2\rho}} \qquad (n = 1,2,3...) \tag{3-1}$$

and

$$f_{\mathrm{T}} = \frac{1}{2\pi}\sqrt{\frac{k/L_d + EI\left(\pi/\lambda_{\mathrm{T}}\right)^4}{A\rho}} \geq f_{\min} = \frac{1}{2\pi}\sqrt{\frac{k/L_d}{A\rho}} \qquad \left(\lambda_{\mathrm{T}} = \frac{L}{n} \quad n=1,2,3...\right) \tag{3-2}$$

where all parameters are defined in sections 2.1 and 2.2, and n is the mode number. Here, our major interest is transverse vibration and the frequency f_{T} given by (3-2). It is seen from (3-2) that the frequency f_{T} monotonically decreases with the wave length λ_{T} , which implies that the minimum f_{T} is reached at n=1 when λ_{T} is equal to the microtubule length L. It is also noted from Eq. (3-2) that all transverse vibration frequencies of microtubules of variable length predicted by the classic elastic foundation model are bounded from below by the lower-bound minimum classic

frequency $f_{\min}$, which is determined by the cross linker parameters k and L_d but independent to microtubule length.

To verify our finite element model, the present equivalent 2D elastic foundation model is compared with the classic formulas Eqs. (3-1) and (3-2). Here the microtubule of length of 1000 nm, spring constant k of $k_0/8$ and spacing L_d of $2L_0$ of cross linker is taken as an example. The standard modal analysis (also called linear-eigenvalue analysis) of finite element method is performed, see Appendix B. The natural vibration frequencies and natural mode shapes are obtained from the generalized equation of motion in matrix form. From the comparison shown in Figure 3.2, we can see that the predictions given by the present finite element model agree very well with the classic formulas. In addition, the transverse vibration mode of the lowest frequency given by our simulation in this special 2D case spreads through the whole microtubule, perfectly consistent with the classic elastic foundation model.

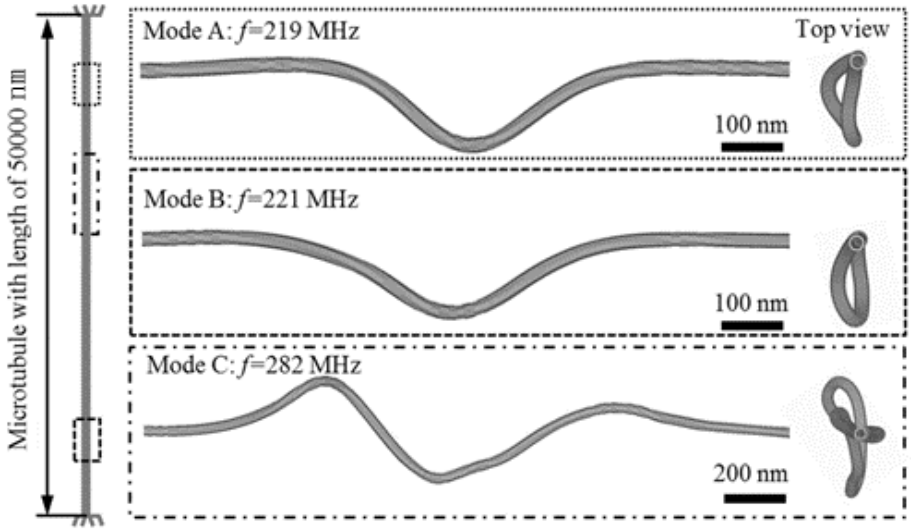

Figure 3.3 Illustration of vibration modes (A, B and C) from the randomly distributed 3D cross linker model. The deflection patterns of these three typical cases are localized. The vibration mode with longer deflected length is associated with higher vibration frequency.

3.3. Results and discussion

3.3.1. Features of localized vibration

Now let us study 3D vibration behavior by using the randomly distributed 3D cross

linker model described in Figure 3.1 (b). In Figure 3.3, firstly, we showed three typical localized vibration modes A, B and C with microtubule length of 50000 nm, $k=k_0$ and $L_d=L_0$, given by the present randomly distributed 3D cross linker model. Our simulation shows that the three modes with different natural frequencies can be stimulated in three locations of microtubule, respectively.

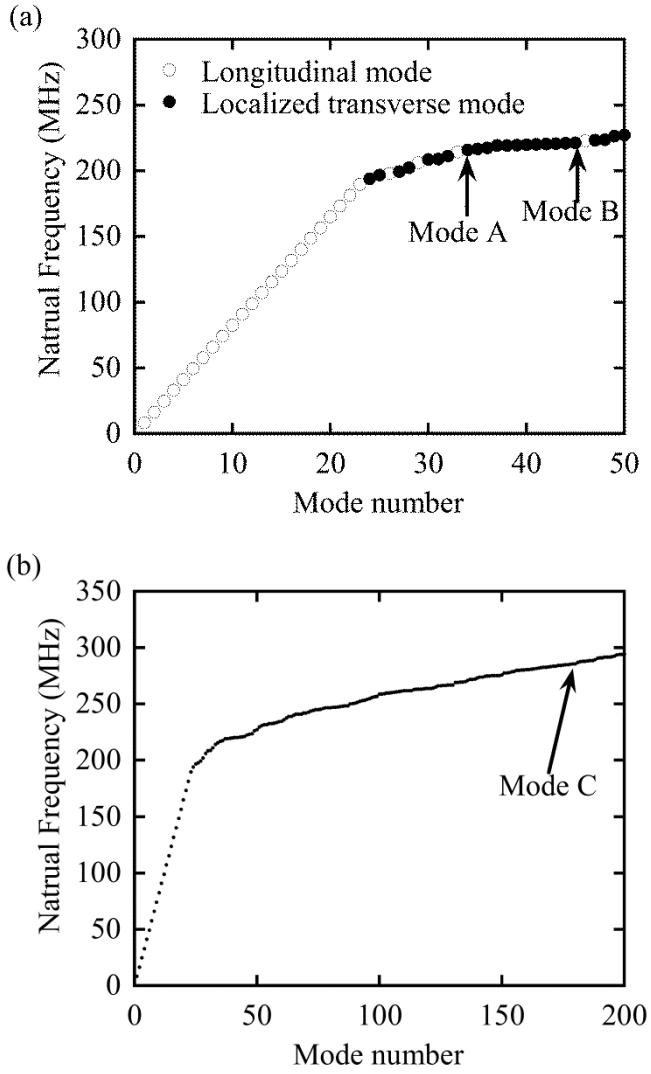

Figure 3.4 Vibration frequencies (from the lowest) of a microtubule with length of 50 μm, k of 39 pN/nm and L_d of 25 nm predicted by the randomly distributed 3D cross linker model. All transverse vibration modes with lower frequencies shown here are localized.

The lowest 50 and 200 vibration frequencies are shown in Figure 3.4 (a) and Figure 3.4 (b), respectively. All transverse vibration modes with the lowest frequencies are highly localized, in direct contradiction to the elastic foundation model which predicts

that the lowest frequency of transverse vibration is associated with a single-wave mode spreading through the entire microtubule. It is also noticed that the deflected length d (through which deflection is larger than 5% of the maximum deflection) increases with the associated frequency. In particular, the localized mode C with two waves has much longer deflected length than the localized modes A and B which have only one wave. This feature of localized vibration is different than the classic elastic foundation model which predicts that the wave length decreases with increasing frequency.

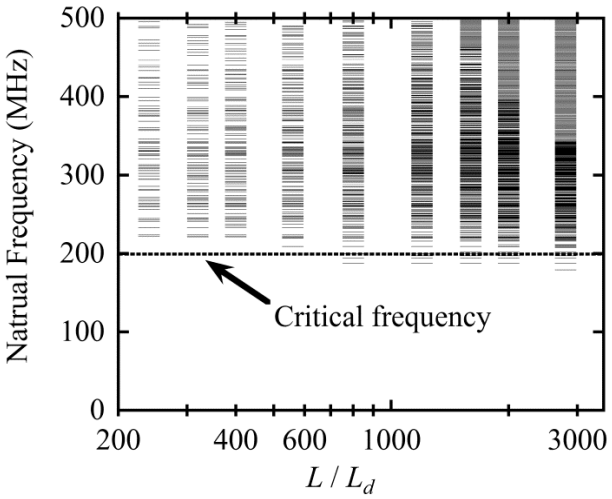

Figure 3.5 The frequencies of transverse vibration are distributed more densely for longer microtubules, where microtubule length varies from 240 L_d to 2800 L_d. Here the localized critical frequency marked by the dashed line is obtained by the mean value of the lowest 10 very close frequencies, above which densely distributed frequencies of localized modes are identified.

Within a given frequency range, more vibration modes with different frequencies can be stimulated in a longer microtubule than in a shorter microtubule, as shown in Figure 3.5, which is consistent with the concept that vibration spectrum of an infinite beam is continuous while vibration spectrum of a finite beam is discrete. It is seen from Eq. (3-2) that all frequencies obtained from the classic elastic foundation model for any microtubule length are bounded from below by the minimum classic frequency $f_{\min}$. Our simulations confirm that all frequencies of localized modes for microtubules of different length are also bounded from below. This lowest bound only slightly decreases with the increase of microtubule length (L) and converges to a non-

zero positive value, which is 200 MHz for present case with k of 39 pN/nm and L_d of 25 nm, as the ratio of L/L_d approaches and exceeds 2000. The lowest bound of localized frequencies is thus insensitive to the microtubule length and can be well estimated by using the present model with L=2000 L_d.

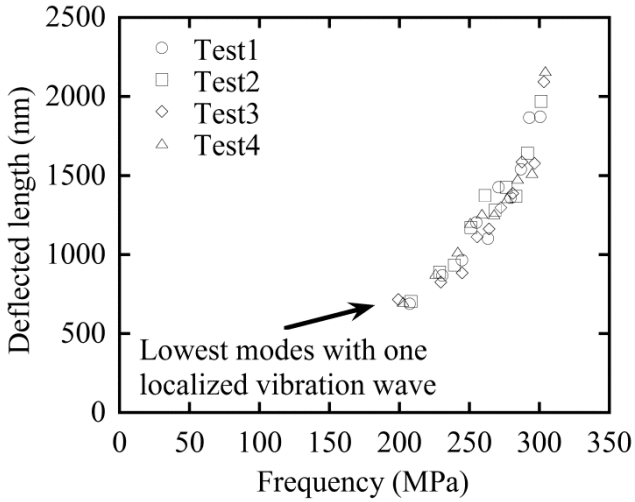

Figure 3.6 The deflected length d (through which the deflection is larger than 5% of the maximum deflection) versus vibration frequencies obtained from four tests with the same L_d of 25 and k of 39 pN/nm but different random angles assigned to cross linkers. Each data point is obtained by the mean value of 10 frequencies and associated deflected lengths. The data point with lowest frequency and shortest wave length indicates the critical frequency f_L and the associated wave length λ_L of localized mode.

Here, we defined the lowest bound (critical) frequency f_L of localized vibration as the mean value of lowest 10 very close frequencies, above which very densely distributed frequencies of localized modes are identified. In our simulations for a microtubule of length L=2000 L_d, the localized modes of the lowest 10 frequencies always have only one wave, thus it is reasonable to define the averaged deflected length d of these 10 modes as the localized wave length λ_L. The reason for defining the critical frequency and wave length based on the 10 lowest frequencies and associated wave lengths is to minimize the influence of randomness of the cross linker distribution. On using the averaged value, simulations with the same L_d and k but different random directions of cross linkers give almost the same critical frequency and associated wave length, as shown in Figure 3.6 in which four tests with the same

L_d of 25 nm and k of 39 pN/nm but different random directions of cross linkers are compared. Actually, it is showed in Figure 3.7 that all frequencies of localized vibration are roughly bounded from above by the minimum classic frequency $f_{\min}$ given in Eq. (3-2) based on the classic elastic foundation model. In other words, the minimum classic frequency $f_{\min}$ offers an upper bound for all localized frequencies predicted by the present model. All vibration modes with frequencies above $f_{\min}$ show the deflection which spreads through the entire microtubule and thus are no longer localized.

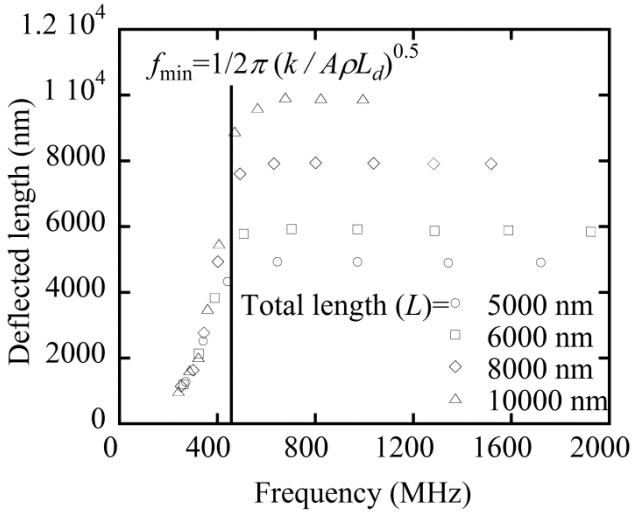

Figure 3.7 The total deflected length d versus vibration frequencies obtained from our randomly distributed 3D cross linker model for microtubules of length (L) of 5000, 6000, 8000 and 10000 nm (with k of 39 pN/nm and L_d of 25 nm). All frequencies of localized modes are lower than the lower-bound minimum frequency $f_{\min}$ of 448 MHz given by Eq. (3-2), and beyond $f_{\min}$ the deflection spreads through the whole microtubule and vibration modes are no longer localized.

The localized vibration is characterized by the (lowest) critical frequency f_L, the associated wave length λ_L, and an upper limit frequency $f_{\min}$. These three parameters are mainly determined by the cross linker parameters k and L_d. The dependency of f_L and λ_L on the cross linker parameters k and L_d is shown in Figure 3.8 for a number of different combinations of k and L_d but the same values of EI and ρA. The minimum classic $f_{\min}$ shown in Figure 3.8 (a) is approximately the upper bound for all frequencies of localized modes, which is also the lower-bound minimum classic

frequencies for all microtubules of arbitrary length given by Eq. (3-2) based on the classic elastic foundation model. As expected, $f_{\min}$, as the upper bounds for localized

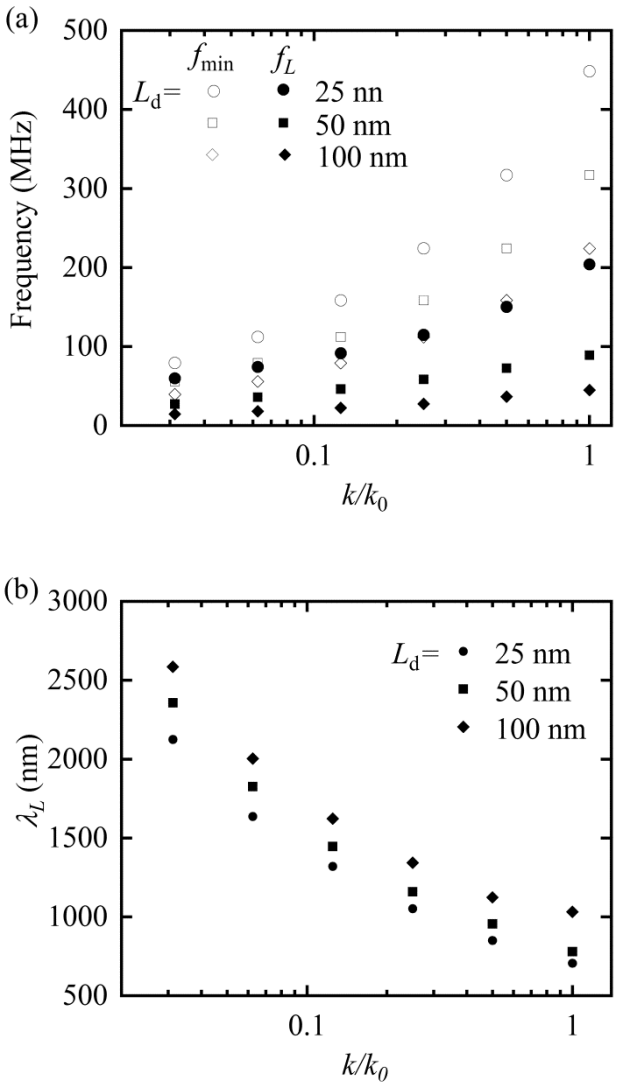

Figure 3.8 The dependency of the critical frequency f_L (a) and the associated wave length λ_L (b) of localized vibration on L_d and k. The lower-bound minimum frequency $f_{\min}$ given by Eq. (3-2) is always higher than the critical frequency f_L of localized modes given by the present model.

frequencies, are much higher than the lowest critical frequencies f_L of localized vibration. In Figure 3.8 (a), critical frequency f_L increases with increasing spring constant k or decreasing L_d, because higher frequencies are usually stimulated with higher stiffness. On the other hand, because the deflection of localized vibration is constrained by surrounding cross linkers, the wave length tends to be shorter with higher spring constant k and more densely distributed cross linkers defined by shorter

L_d, see Figure 3.8 (b).

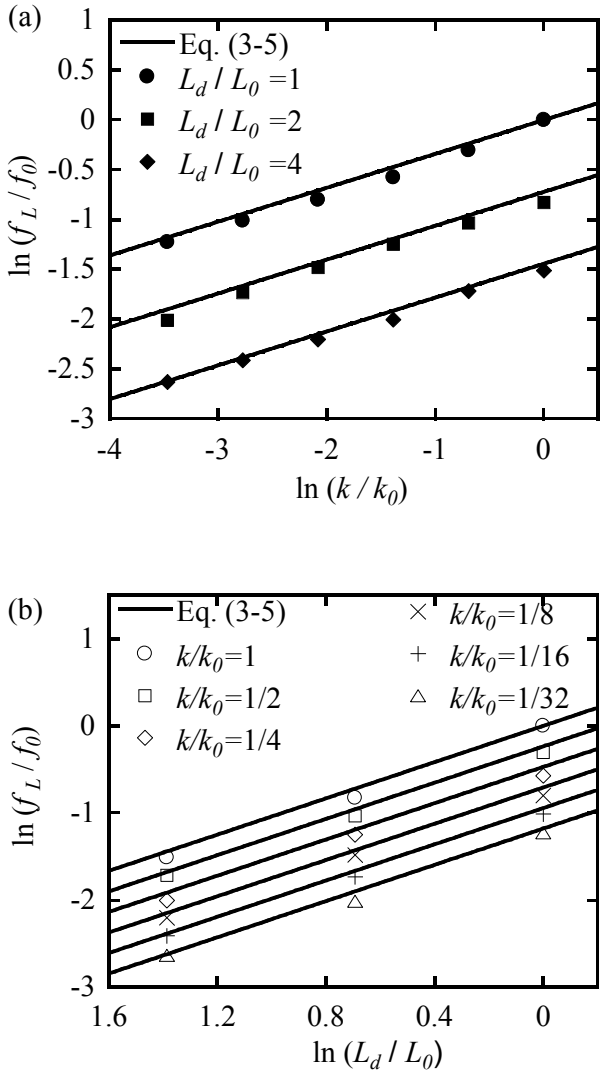

Figure 3.9 Comparison between the critical frequency f_L predicted by empirical formula (3-5) and numerical simulation with variable k (a) and L_d (b).

3.3.2. Empirical relations for localized vibration

In what follows, based on our numerical simulations, some empirical relations will be offered for the dependency of the critical frequency f_L and the associated wavelength λ_L on the spring constant k and the spacing L_d of cross linkers. Firstly we define the case used in Figure 3.3 - Figure 3.6 as a basic case with $L_d = L_0$= 25 nm, k= k_0=39 pN/nm and L=2000 L_d. The obtained critical frequency and wave length of localized

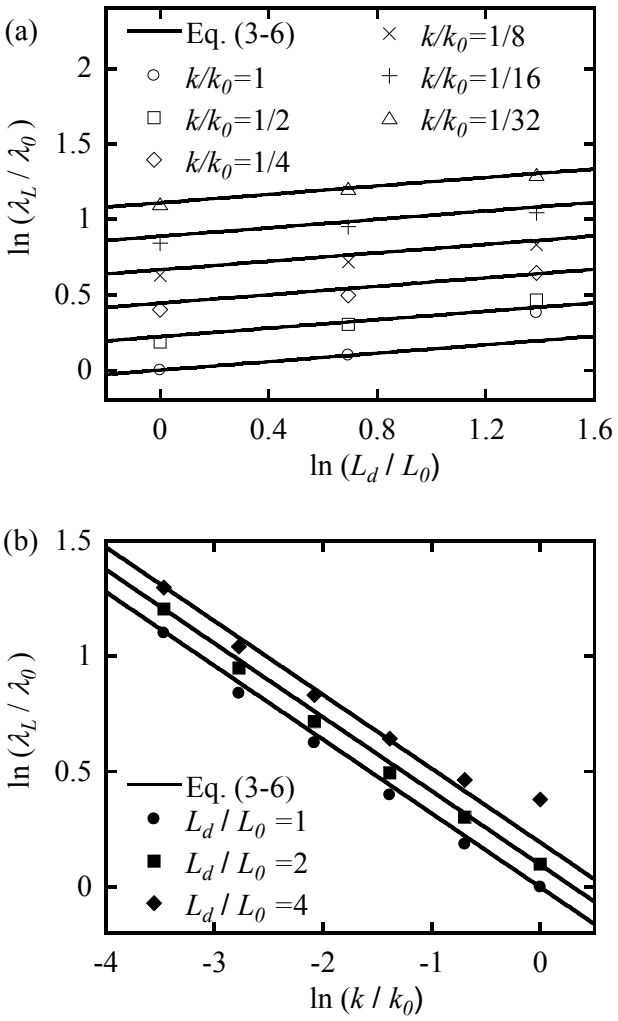

Figure 3.10 Comparison between the wave length λ_L predicted by empirical formula (3-6) and numerical simulation results with variable k (a) and L_d (b). The formula (3-6) is valid only when the predicted λ_L is longer than $13L_d$.

vibration for the basic case are defined as f_0 and λ_0 , which are 204 MHz and 706 nm respectively. Let us assume that the dependency of critical frequency and wave length on arbitrary L_d and k takes the forms of

$$\ln\left(\frac{f_L}{f_0}\right) = a\ln\left(\frac{L_d}{L_0}\right) + b\ln\left(\frac{k_0}{k}\right) \tag{3-3}$$

and

$$\ln\left(\frac{\lambda_L}{\lambda_0}\right) = c\ln\left(\frac{L_d}{L_0}\right) + d\ln\left(\frac{k_0}{k}\right) \tag{3-4}$$

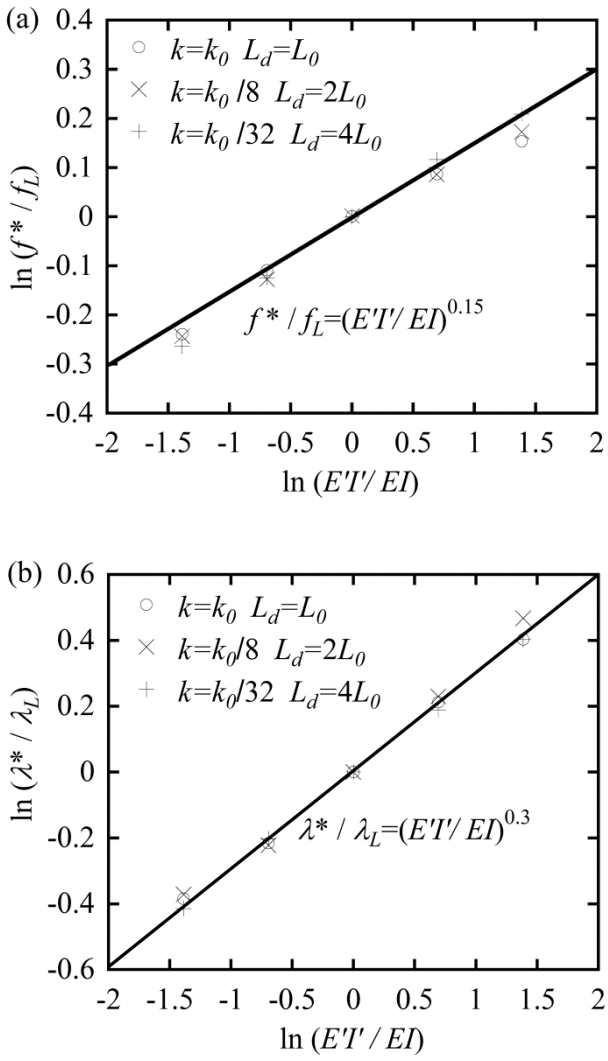

Figure 3.11 Effect of the bending rigidity *EI* on the critical frequency f^* (a) and the associated wave length λ^* (b) of localized vibration.

Obviously, Eqs. (3-3) and (3-4) hold for the basic case. Now, the four constants *a*, *b*, *c* and *d* can be determined by the slops of $\ln\left(f_L / f_0\right)$ versus $\ln\left(L_0 / L_d\right)$ in Figure 3.9 (a), $\ln\left(f_L / f_0\right)$ versus $\ln\left(k / k_0\right)$ in Figure 3.9 (b), $\ln\left(\lambda_L / \lambda_0\right)$ versus $\ln\left(k / k_0\right)$ in Figure 3.10 (a), and $\ln\left(\lambda_L / \lambda_0\right)$ versus $\ln\left(L_d / L_0\right)$ in Figure 3.10 (b) respectively. The fitted equations are expressed as

$$\frac{f_L}{f_0} = \left(\frac{L_0}{L_d}\right)^{1.04} \left(\frac{k}{k_0}\right)^{0.34} \tag{3-5}$$

and

$$\frac{\lambda_L}{\lambda_0}=\left(\frac{L_d}{L_0}\right)^{0.14}\left(\frac{k_0}{k}\right)^{0.32} \tag{3-6}$$

From Figure 3.9 and Figure 3.10, it is found that the fitted equations (3-5) and (3-6) can well represent the data from numerical simulations. It is verified that the two empirical equations are valid within a reasonable range of spring constant (k from $k_0/64$ to k_0) and spacing (L_d from L_0 nm to $12L_0$) of cross linkers provided the wave length λ_L not shorter than $10L_d$.

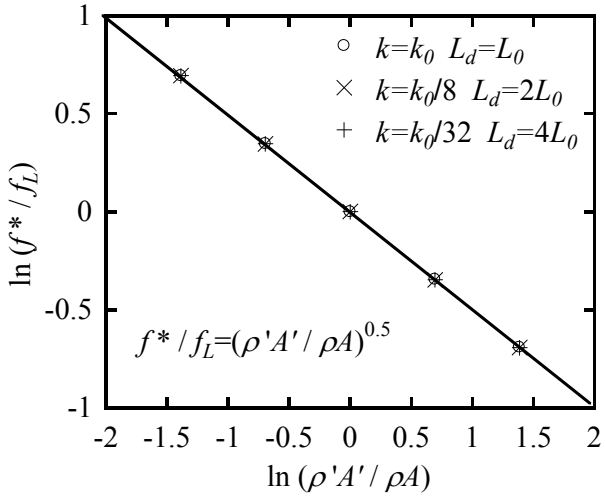

Figure 3.12 Effect of ρA on the critical frequency f^* of localized vibration.

For all cases discussed above, EI of 9.034×10^{-24} Nm^2 (Jin and Ru, 2013) and ρA of 2.06×10^{-12} kg/m (Tounsi et al., 2010) were used for microtubules. As the mechanical parameters of microtubule reported in the literature show relatively high deviation (Felgner et al., 1997), in what follows, we examine the influence of the uncertainty of microtubule parameters on the critical frequency and the associated wave length of localized vibration. For this end, let us consider a range of the microtubule parameters with $E'I'$ from $0.25EI$ to $4EI$ and $\rho'A'$ from $0.25\rho'A'$ to $4\rho'A'$. The obtained critical frequency f^* and the associated wave length λ^* are shown in Figure 3.11 and Figure 3.12 respectively.

Both the critical frequency and the associated wave length of localized vibration are affected by the variation of bending rigidly EI of microtubules. However, the influence of EI on the critical frequency and the associated wave length is insensitive

to the chosen values of k and L_d as shown in Figure 3.11. The wave length of localized vibration increases with increasing value of EI, which is consistent with localized buckling (Jin and Ru, 2013). This result is reasonable because if the bending rigidity of microtubule is much higher than cross linkers, the constraint due to the cross linkers could be ignored and vibration could be not localized.

The value of ρA of microtubules only influences the critical frequency but does not much affect the wave length of localized vibration. In addition, the effect of ρA on localized vibration is also insensitive to the specific values of k and L_d as shown in Figure 3.12. The critical frequency is proportional to the square of ρA, which is similar to the effect of ρA in the classic elastic foundation model Eq. (3-2). It is also found that the effects of ρA and EI are not coupled. Two empirical equations are proposed to best fit the numerical results in Figure 3.11 and Figure 3.12 as

$$f^* / f_L = \left(\rho' A' / \rho A\right)^{0.5} \left(E'I' / EI\right)^{0.15} \tag{3-7}$$

$$\lambda^* / \lambda_L = \left(E'I' / EI\right)^{0.3} \tag{3-8}$$

It is noted that the predicted critical frequency and associated wave length by Eqs. (3-7) and (3-8) plotted in Figure 3.11 and Figure 3.12 as solid lines can well represent the simulation results.

3.3.3. Comparison with experiments

Despite comprehensive studies on microtubule vibration, the comparison between theoretical results and experiments is rare, probably because direct measurement of natural vibration frequency of microtubule *in vivo* is still difficult if not impossible. However, some experimental observations, e.g. Fig. 3 on page 20 of ref. (Marrari et al., 2003), Fig. 2,3 on pages 1099 and 1100 of ref. (Mandato and Bement, 2003), Fig 2, 3 on page 735 of ref. (Brangwynne et al., 2006), indicated that vibration modes are insensitive to microtubule length and clearly localized with wave lengths around 1-4 microns. These observed localized vibration modes are in direct contradiction with those predicted by the classic elastic foundation model, but in reasonable agreement with localized vibration waves of 0.5-3 microns simulated by the present 3D randomly distributed cross linker model.

3.4. Conclusions

A numerical micro-mechanics model is proposed to investigate free vibration of a microtubule surrounded by randomly distributed discrete cross linkers. The present model shows that transverse vibration modes associated with the lowest frequencies are always localized, in sharp contrast to the single-wave mode spreading through the entire microtubule predicted by the widely used classic elastic foundation model. In particular, the lowest frequencies of localized modes are typically at least 50% lower than the minimum classic frequency predicted by the classic elastic foundation model, and the former could be even one order of magnitude lower than the latter for shorter microtubules of only a few microns in length. Different from the vibration modes given by the classic elastic foundation model whose wave lengths decrease with frequency, the deflected length of localized modes predicted by the present model increases with frequency and approaches the entire microtubule when frequency approaches the minimum classic frequency. Based on our numerical simulations, some empirical relations are proposed for the critical (lowest) frequency and the associated wave length of localized modes. The comparison between our simulations and some known experimental observations shows that the localized vibration predicted by the present model and the proposed empirical equations are consistent with a number of available experimental observations. It is hoped that the present work could offer new insights into the understanding of microtubule vibration in living cells.

4. Splitting of microtubule under compressive force

4.1. Introduction

The microtubule (MT) is one of the most important cytoskeletal elements in eukaryotic cells(Boal, 2002). Microtubules are formed by polymerization of α/β tubulin dimers into slender protofilaments, which assemble into hollow tubules. Microtubules are highly dynamic, and "dynamic instability" is referred to switch between polymerization and depolymerization phases at the plus end of a microtubule (Karp, 2009) where microtubule grows and shrinks more rapidly and more extensively than the other (minus) end. The phenomena of "dynamic instability" is essential for the mitosis, cell motility, intracellular transport and many other cell behaviors (Gliksman et al., 1993). It has been widely recognized that a "cap" at the plus end, composed of a few layers of strongly bonded GTP dimers (heterodimer formed by an alpha and a beta tubulin molecule carries two GTP molecules), is essential to prevent microtubules from depolymerization. Actually, loss of the "cap" will certainly lead to depolymerization of microtubules, called "catastrophe" (Mitchison and Kirschner, 1984) characterized by splitting of protofilaments, a phenomenon somewhat similar to splitting of unidirectional fiber-composites or carbon nanotube ropes under axial mechanical compression (Chai et al., 1981, Kachanov, 1988, Ru, 2004), see Figure 4.1 According to existing literature (Mitchison and Kirschner, 1984, Hyman et al., 1992), the loss of the cap is usually considered as a result of hydrolysis of the GTP dimers to unstable GDP dimers at the plus end, a chemical process essential for "dynamic instability".

Microtubules are known to play a key role in maintaining cell shape by bearing compressive forces. In view of the weaker lateral bonding between adjacent protofilaments, it is of greater interest to examine whether a mechanically compressed microtubule, capped by a few layers of GTP dimers at its plus end, could split prior to its overall buckling. In spite of extensive research on continuum modeling of buckling and bending (Wang et al., 2006, Li et al., 2006, Yi et al., 2008) and molecular dynamics or thermodynamics simulation of microtubules (Molodtsov et al., 2005a, VanBuren et al., 2005), mechanical compression driven splitting of microtubules has remained absent in the literature. In the present study, for microtubule capped by a few layers of GTP dimers at its plus end, we shall study compression-driven

protofilament splitting either at middle of a microtubule as shown in Figure 4.1 (a), or at the plus end of a microtubule as shown in Figure 4.1 (b). We are only interested in splitting which happens prior to overall buckling of the compressed microtubule under increasing axial mechanical compression (buckling is shown in Figure 4.1 (c), which has been studied comprehensively in the literature, see e.g. (Odde et al., 1999)). This study could give new insight into the role of mechanical compression in dynamic instability and splitting of capped microtubules, a relevant topic which has not yet been studied in the existing literature.

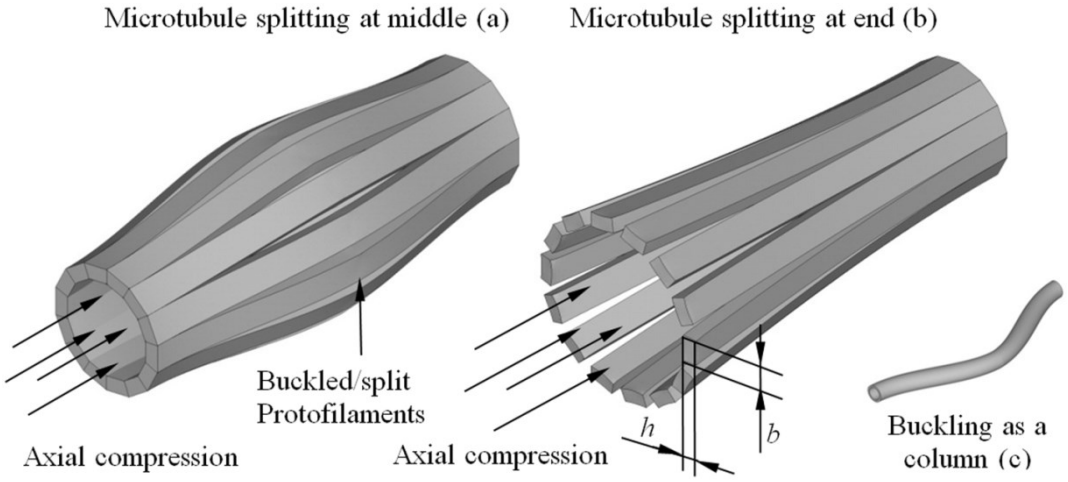

Figure 4.1 Three possible failure modes of a microtubule under axial compression with the minus end anchored in centrosomes (Howard and Hyman, 2003): (a) splitting at the middle, (b) splitting at the plus end, and (c) buckling as a column.

4.2. Modelling

4.2.1. Elastic energy of protofilament in unbuckled and buckled configurations

The measured bending rigidity of microtubules and geometrical parameters of protofilaments can be used to estimate bending rigidity of an individual protofilament. From available data on microtubule and protofilaments (Mickey and Howard, 1995, VanBuren et al., 2005), it is assumed here that protofilament has a rectangular cross section with width b=5.15 (Mickey and Howard, 1995) nm and thickness h , see Figure 4.1 (b). The measured Young's modulus of microtubule fall in the range of 0.5 GPa to 2 GPa (Li et al., 2006), so E=1 GPa is used in the present study. It is also known that a bending strain energy of about 2.8 k_BT /dimer is stored in straight protofilaments which have a natural radius of curvature of R=21 nm (VanBuren et al.,

2005). Since the bending strain energy stored in a beam with rectangular cross section can be calculated based on cross section geometry. The thickness of protofilaments is estimated as 1.84 nm, which is less than the equivalent thickness of microtubule of 2.7 nm (Sirenko et al., 1996), but very close to the effective bending thickness of 1.6 nm (de Pablo et al., 2003) as expected. Then the cross-sectional area $A_{\mathrm{p}} = 9.48\times10^{-18}$ m^2 and the second moment of cross section $I_{\mathrm{p}} = 2.67\times10^{-36}$ m^4 (Mickey and Howard, 1995) of protofilaments can be obtained.

The lateral binding free energy between adjacent protofilaments plays an important role in splitting of a microtubule. The binding free energy between strongly bonded protofilaments composed of GTP dimers is measured as -3.2 to -5.7 k_BT /dimer (VanBuren et al., 2002) for $T = 310\mathrm{K}$, which correspond to -1.6×10^{-12} to -2.8×10^{-12} J/m by assuming that the length of a dimer is about 8.1 nm (Hunyadi et al., 2007). The average value of the upper and lower limits, -2.3×10^{-12} J/m, will be used, which is reasonably close to the simulation results -2.7×10^{-12} J/m (Sept et al., 2003). Thus the adhesion energy of GTP protofilaments $\gamma_{\mathrm{T}} = 2.3\times10^{-12}$ J/m will be used, which represents the external work required to separate two adjacent GTP protofilament of unit length.

On the other hand, reliable data for the lateral adhesion energy between weakly bonded protofilaments composed of GDP dimers (γ_{D}) is still not available, and controversial data have been reported in the existing literature(Nogales et al., 1999, Wang and Nogales, 2005, Molodtsov et al., 2005a), although it is commonly believed that the adhesion energy between GDP protofilaments (γ_{D}) is lower than the adhesion energy between GTP protofilaments (γ_{T}) (Nogales et al., 1999, Wang and Nogales, 2005). As will be shown below, the present model can offer a method to estimate the binding energy γ_{D} between weakly bonded protofilaments composed of GDP dimers.

A microtubule under axial mechanical compression may collapse through three possible modes: protofilament splitting at middle, or protofilament splitting from the plus end, or overall buckling as an elastic column, see Figure 4.1 (a), (b) and (c) respectively. In order to derive the criteria to prevent protofilament splitting of a microtubule, energy expressions for a buckled/unbuckled protofilament is to be

derived. Under axial compression, elastic energy of an unbuckled straight protofilament $U_{\mathrm{D1}}(L)$, of length L composed of GDP dimers (with a natural radius of curvature R), is given as

$$U_{\mathrm{D1}}(L)=\frac{EA_{\mathrm{p}}L\varepsilon^2}{2}+\frac{EI_{\mathrm{p}}L}{2R^2} \tag{4-1}$$

where ε is the applied axial compressive strain, L is the length of protofilament. The first and second terms in Eq. (4-1) are axially compressed strain energy and bending strain energy, respectively. As stated before, the natural radius of curvature R is about 21 nm (Hawkins et al., 2010).

Inside cells, since mechanical compression on microtubules is usually created by cell's membrane, strain-loaded (rather than stress-loaded) compression is more relevant for microtubules. Thus, when a protofilament of length L is debonded and buckled from the compressed microtubule with a deflection $w(x)$, see Figure 4.2, the excess axial strain, defined by (ε - $\varepsilon_{\mathrm{cr}}$), where $\varepsilon_{\mathrm{cr}}$ is the critical axial strain for buckling of a single protofilament under the given (such as doubly-clamped or cantilever) end conditions, is released and the released length is related to the amplitude of buckling deflection by(Chai et al., 1981, Kachanov, 1988, Ru, 2004)

$$(\varepsilon-\varepsilon_{\mathrm{cr}})L=\int_0^L\frac{1}{2}\left(\frac{dw}{dx}\right)^2dx \tag{4-2}$$

It should be stated that, since the present work studies splitting prior to buckling of a microtubule, the applied axial compressive strain ε is comparable to the critical strain for overall buckling of the entire microtubule as a whole and then is much (more than two orders of magnitude) larger than the critical strain for buckling of a single protofilament $\varepsilon_{\mathrm{cr}}$, and therefore LHS of (4-2) is assumed to be positive. Subsequently, the elastic strain energy $U_{\mathrm{D2}}(L)$ of a buckled protofilament of length L is given by

$$U_{\mathrm{D2}}(L)=\frac{EA_{\mathrm{p}}L}{2}\varepsilon_{\mathrm{cr}}^2+\int_0^L\frac{EI_{\mathrm{p}}}{2}\left[\left(\frac{1}{R}\right)-\left(\frac{d^2w}{dx^2}\right)\right]^2dx \tag{4-3}$$

On the other hand, for a naturally straight protofilament composed of GTP dimers, the elastic strain energies at the unbuckled and the buckled states, $U_{\mathrm{T1}}(L)$ and $U_{\mathrm{T2}}(L)$, are given by

$$U_{\mathrm{T1}}(L)=\frac{EA_{\mathrm{p}}L\varepsilon^2}{2} \tag{4-4}$$

and

$$U_{\mathrm{T2}}(L)=\frac{EA_{\mathrm{p}}L}{2}\varepsilon_{\mathrm{cr}}^2+\int_0^L\frac{EI_{\mathrm{p}}}{2}\left(\frac{d^2w}{dx^2}\right)^2dx \tag{4-5}$$

respectively. Obviously, Eqs.(4-1, 4-3) reduce to Eqs.(4-4, 4-5) when the natural curvature disappears and then *R* is infinite.

4.2.2. Protofilament splitting criteria under compressive force

Now, let us first discuss protofilament splitting at middle of a capped compressed microtubule. In this case, the doubly clamped end condition is relevant for buckled protofilament due to the cap at the plus end and the other end anchored in centrosomes(Howard and Hyman, 2003). Then unbuckled configuration (C1) and buckled configuration (C2) of a single protofilament of length *L* are shown in Figure 4.2, where the deflection *w*(*x*) under the doubly clamped end condition can be given as (Brush and Almroth, 1975)

$$w(x)=\frac{1}{2}w_0\left(1-\cos\frac{2\pi x}{L}\right) \tag{4-6}$$

and the critical strain for buckling of a single protofilament as a doubly-clamped column is (Brush and Almroth, 1975)

$$\varepsilon_{\mathrm{cr}}=\varepsilon_{\mathrm{cr1}}=\frac{\pi^2}{3}\left(\frac{h}{L}\right)^2 \tag{4-7}$$

In this study, splitting condition will be derived based on energy consideration. Since the mechanical compression is strain-loaded, the axial force does not do work during splitting or buckling of protofilaments. As a result, the splitting condition can be

derived based on a comparison of energy between the split and the un-split states. Thus, because the adhesion energy between weakly bonded protofilaments composed of GDP dimers $\gamma_{\mathrm{D}}L$ resists splitting, splitting cannot occur if the adhesion energy $\gamma_{\mathrm{D}}L$ is larger than the difference in elastic strain energy between the unbuckled and the buckled configurations. Therefore the condition to prevent splitting from middle of a capped microtubule is

$$\Delta U = U_{\mathrm{D1}}\left(L\right) - U_{\mathrm{D2}}\left(L\right) < \gamma_{\mathrm{D}}L \tag{4-8}$$

On using Eqs. (4-1), (4-2), (4-3), (4-6) and (4-7), the criterion to prevent splitting at middle of a capped microtubule can be rewritten as

$$\Delta U = \frac{EA_{\mathrm{p}}L}{2}\left(\varepsilon - \varepsilon_{\mathrm{cr1}}\right)^2 < \gamma_{\mathrm{D}}L \tag{4-9}$$

Since the derived criterion (4-9) does not contain *R*, the stored strain energy of protofilaments composed of GDP dimers has no influence on splitting at middle of a microtubule. This is simply due to the fact that the buckling deflection under the doubly clamped end condition has equal but opposite effects on the curvature change near the two ends and at the middle of the protofilament and thus they exactly cancel out each other, as shown in Figure 4.2.

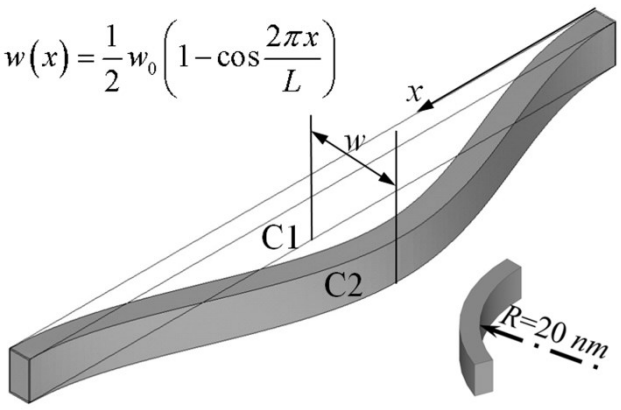

Figure 4.2. Configurations of a split (C2) or un-split (C1) protofilament (with doubly clamped end condition) for splitting of a microtubule at the middle.

For protofilament splitting at the plus end of a microtubule, the clamped-free end condition is relevant since the other end is anchored in centrosomes(Howard and

Hyman, 2003). Due to the existence of the cap composed of a few layers of GTP dimer at the plus end, the split protofilament consists of two sections, one short section composed of GTP dimers at the plus end and the other major section composed of GDP dimers, as shown in Figure 4.3, where the deflection under clamped-free end condition is given as (Brush and Almroth, 1975)

$$w = w_0\left(1-\cos\frac{\pi x}{2L}\right) \tag{4-10}$$

and the critical strain for compressed buckling of a single protofilament as a cantilever elastic column is (Brush and Almroth, 1975)

$$\varepsilon_{cr} = \varepsilon_{cr2} = \frac{\pi^2}{48}\left(\frac{h}{L}\right)^2 \tag{4-11}$$

Here it is stated that the buckling deflection (4-11) used here can also be replaced by another simple approximation $w(x)=w_0x^2$. Our numerical analysis confirmed that such an alternative choice of buckling deflection will not cause any meaningful difference.

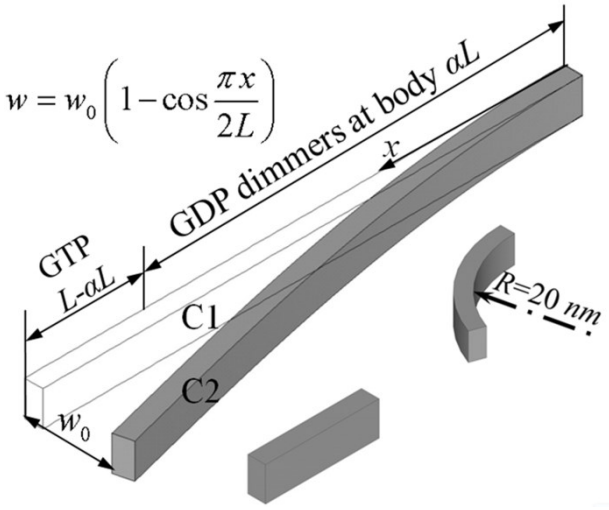

Figure 4.3. Configurations of a split (C2) or un-split (C1) protofilament for splitting at the plus end of a microtubule.

Similar to splitting from middle, under strain-loaded compression, the splitting from unbuckled configuration (C1) to buckled configuration (C2) must overcome the adhesion energy barrier, which is determined by γ_D for the major GDP dimer part of the protofilament and γ_T for the short GTP dimer part at the split plus end. For the

protofilament of length L, let that the major GDP dimer section be of length αL while the short GTP dimer section at the split end be of length $(1-\alpha)L$, see Figure 4.2, where α is between 0 to 1 but close to 1. Thus, the criterion to prevent protofilament splitting at the plus end of a capped microtubule can be derived as

$$\Delta U = U_{\mathrm{D1}}(\alpha L) + U_{\mathrm{T1}}(L-\alpha L) - U_{\mathrm{D2}}(\alpha L) - U_{\mathrm{T2}}^{*}(L-\alpha L) < \gamma_{\mathrm{D}}\alpha L + \gamma_{\mathrm{T}}(L-\alpha L) \qquad (4\text{-}12)$$

where it should be stated that since the integral interval in $U_{\mathrm{T2}}^{*}(L-\alpha L)$ locates at the split end, it can be expressed as

$$U_{\mathrm{T2}}^{*}(L-\alpha L) = \frac{EA_{\mathrm{p}}(L-\alpha L)}{2}\varepsilon_{\mathrm{cr}}^{2} + \int_{\alpha L}^{L}\frac{EI_{\mathrm{p}}}{2}\left(\frac{d^{2}w}{dx^{2}}\right)^{2}dx \qquad (4\text{-}13)$$

Similar to (4-9), condition (4-12) can be rewritten as

$$\Delta U = \frac{EA_{\mathrm{p}}L}{2}\left[\left(\varepsilon-\varepsilon_{\mathrm{cr2}}\right)^{2} + \frac{\pi^{2}h^{2}\sin(\alpha\pi/2)}{3\pi^{2}RL}\sqrt{\varepsilon-\varepsilon_{\mathrm{cr2}}}\right] < \gamma_{\mathrm{D}}\alpha L + \gamma_{\mathrm{T}}(1-\alpha)L \qquad (4\text{-}14)$$

Different from splitting at middle of a microtubule in which the natural curvature of protofilaments does not make any difference, the natural curvature of GDP protofilaments promotes splitting at the plus end of a microtubule, as to be showed below.

4.2.3. Protofilament splitting versus column buckling of a microtubule

The goal of the present study is to examine whether protofilament splitting at middle or the plus end of a compressed microtubule would happen prior to overall buckling of the microtubule. Here it should be clarified that, L defined in previous sections is the length of the split protofilament, which is not necessarily the entire length of the compressed microtubule if partial splitting of protofilaments over only a section of the microtubule is considered. However, since our goal is to find the condition to prevent splitting prior to buckling of the microtubule, and buckling of the entire microtubule will definitely happen prior to buckling of any section of the microtubule, it is sufficient for our purpose to consider splitting of protofilaments of length L prior to buckling of a microtubule of the same length L. For this reason, we shall assume that L is the common length of both the split protofilament and the microtubule. The

critical strain for buckling of the entire microtubule of length L (both strain-loaded or stress-loaded) is given by (Ugural and Fenster, 2003)

$$\varepsilon_{\mathrm{mcr}} = n\frac{\pi^2 I_{\mathrm{m}}}{L^2 A_{\mathrm{m}}} \tag{4-15}$$

where I_{m} and A_{m} are the second moment $0.85\times10^{-32}m^4$ (measured bending rigidity(Venier et al., 1994) over Young's modulus of microtubule of 1 GPa (Li et al., 2006)) and area of the cross-section $1.23\times10^{-16}m^2$ of a microtubule with 13 protofilaments, and the constant n is decided by the end conditions of the microtubule. For example, n=4 for doubly clamped ends, n=1 for simply support ends, or n=0.25 for clamped-free (cantilever) ends. In view of the diversity of end conditions that microtubules may actually experience in *vivo*, the geometrical average value n=1 will be used in the present analysis, which corresponds to simply-supported ends. The competition between splitting at the middle and buckling can be analyzed by combining Eqs. (4-9) and (4-15), while the competition between splitting at the plus end and buckling can be analyzed by combining Eqs. (4-14) and (4-15). Then the required adhesion energy between GDP protofilaments γ_{D}, to prevent splitting at middle of a microtubule prior to its overall buckling, can be given as

$$\gamma_D > \frac{EA_{\mathrm{p}}}{2}\left(\varepsilon_{\mathrm{mcr}} - \varepsilon_{\mathrm{cr1}}\right)^2 \tag{4-16}$$

Similarly, the required adhesion energy (γ_{D}) to prevent splitting at the plus end of a microtubule prior to its overall buckling can be given as

$$\gamma_{\mathrm{D}} > \frac{EA_{\mathrm{p}}}{2\alpha}\left[\left(\varepsilon_{\mathrm{mcr}} - \varepsilon_{\mathrm{cr2}}\right)^2 + \frac{\sin(\alpha\pi/2)h^2}{3RL}\sqrt{\varepsilon_{\mathrm{mcr}} - \varepsilon_{\mathrm{cr2}}}\right] - \gamma_{\mathrm{T}}\frac{(1-\alpha)}{\alpha} \tag{4-17}$$

where $\varepsilon_{\mathrm{mcr}}$, $\varepsilon_{\mathrm{cr1}}$ and $\varepsilon_{\mathrm{cr2}}$ on RHS of (4-16) and (4-17) all depend on the length L of microtubule/protofilaments. Thus, condition (4-16) or (4-17) can be used to determine a critical value of γ_{D} provided all other parameters are given. In particular, because $\varepsilon_{\mathrm{mcr}} >> (\varepsilon_{\mathrm{cr1}}, \varepsilon_{\mathrm{cr2}})$, our numerical results confirmed that neglecting $(\varepsilon_{\mathrm{cr1}}, \varepsilon_{\mathrm{cr2}})$ in (4-17) and (4-18) will not cause any meaningful inaccuracy.

4.3. Results and discussion

4.3.1. Required adhesion energy of GDP protofilaments against splitting from middle of a microtubule

It is noted from Eqs. (4-15) and (4-7) that the required adhesion energy (γ_D) between GDP protofilaments given in (4-16), which ensures that splitting at the middle of a microtubule will not occur prior to buckling of the microtubule, decreases with the length L of microtubule. Thus, based on Eqs. (4-15), (4-7) and (4-16), the required lowest adhesion energy γ_D is plotted in Figure 4.4 as a function of the length L of microtubules composed of 13 protofilaments with the uncertainty of the Young's modulus E (0.5-2 GPa). In this case, γ_T and the stored bending strain energy in GDP protofilaments does not influence the results. Since reliable data for the adhesion energy γ_D is not yet available in the literature, the present result (4-16) offers a method to estimate the adhesion energy γ_D in terms of the microtubule length. For example, to prevent splitting at middle of microtubules of length not shorter than 0.2 micron, it is seen from Figure 4.4 that the adhesion energy (γ_D) of microtubules of 13 protofilaments should be not lower than about $\gamma_D = 0.6\times10^{-12}$ J/m, which is about one fourth of adhesion energy between GTP protofilaments $\gamma_T = 2.3\times10^{-12}$ J/m (VanBuren et al., 2002). Therefore the present model could offer a lower limit of the adhesion energy between GDP protofilaments (γ_D). In particular, it could suggest from Figure 4.4 that compression-driven splitting from middle of a microtubule is possible only for short microtubules but prohibited for microtubules of length longer than a few hundreds of nanometers.

4.3.2. Required layers of GTP cap against end splitting of microtubule

The required adhesion energy (γ_D) to prevent splitting at the plus end of a microtubule can be calculated using (4-17) as a function of the microtubule length L and α (the latter represents portion of GDP dimers in the protofilaments). Since loss of a cap at the plus end will certainly lead to dynamic instability or splitting of a microtubule at the plus end (Mitchison and Kirschner, 1984), the present work will focus on compression-driven splitting of a capped microtubule protected by at least

one layer of GTP dimers at its plus end. If m GTP layers exist at the plus end of a microtubule, the variable α in Eq. (4-17) is given by

$$\alpha = 1 - \frac{m \times L_{\mathrm{m}}}{L} \tag{4-18}$$

where L_{m} is the length of a single GTP dimer of 8.1 nm(Hunyadi et al., 2007), and L is the length of microtubule. Therefore, for a given number of GTP dimer layers at the plus end, the present result (4-17) allows us to determine the minimum adhesion energy γ_{D} to prevent splitting at the plus end if the length of microtubule is given, or to determine the minimum length of the microtubule to prevent splitting at the plus end prior to buckling if the adhesion energy γ_{D} is given. For m equals 1, 2 or 4, the required lower limit of adhesion energy γ_{D} to prevent splitting at the plus end is plotted in Figure 4.5 as a function of the length L with the assumed E=1 GPa and $\gamma_{\mathrm{T}} = 2.3 \times 10^{-12}$ J/m.

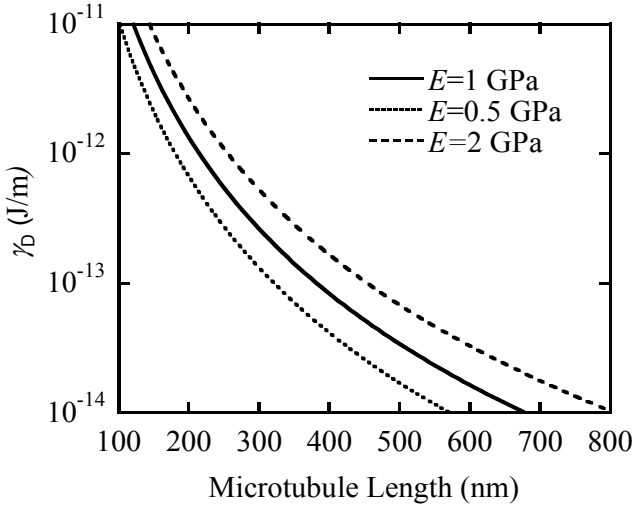

Figure 4.4. Required lowest limit of the adhesion energy between GDP dimers (γ_{D}) to prevent splitting at the middle prior to buckling of a compressed microtubule with Young's modulus varying from 0.5 to 2 GPa.

First of all, it is seen from Figure 4.5 that for microtubules of length shorter than 150 nm, no matter how many GTP layers exist at the plus end, the required adhesion energy between GDP dimers γ_{D}, to prevent splitting prior to buckling, must be

higher than the adhesion energy between GTP dimers, $\gamma_T = 2.3\times10^{-12}$ J/m, which is impossible. Thus for microtubules shorter than 150 nm, splitting of a capped microtubule will happen at the plus end prior to overall buckling of the microtubule under high mechanical compression. If the uncertainty of the Young's modulus (0.5-2 GPa) and adhesion energy between protofilaments (1.7×10^{-12} to 3.0×10^{-12} J/m) are taken into account, this length, below which compression-driven splitting at the plus end will happen prior to overall buckling, is roughly between 125 ~180 nm.

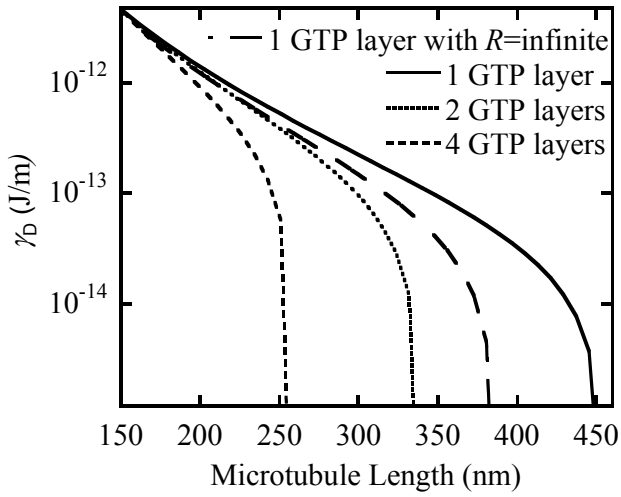

Figure 4.5. Required lowest limit of the adhesion energy between GDP dimers (γ_D) to prevent splitting at the plus end prior to buckling of a compressed microtubule capped by 1, 2 or 4 layers of GTP dimers at the plus end (with R=21 nm) - also included here is the 1-layer case with neglected stored strain energy (R=infinite). These results are obtained based on E=1 GPa and $\gamma_T = 2.3\times10^{-12}$ J/m.

Here, the present model confirms that, with no mechanical compression, stored bending strain energy alone cannot drive splitting at the plus end of a microtubule capped by just one single layer of GTP dimers even when the adhesion energy of GDT protofilaments is completely ignored (i.e. even when γ_D =0). In this case, actually, the released bending strain energy of a deflected GDP protofilament of length L can be estimated from (4-1), (4-3) and (4-10) as $(w_0\pi EI_p)/(2RL)$, where w_0 represents its maximum end deflection. For splitting of the microtubule capped by one single layer of GTP dimers, this released bending strain energy must be bigger than the adhesion energy barrier ($8.1\text{ nm}\times\gamma_T$). Using the data adopted ($W=EI_p/(2R^2)$=3.0

$\times 10^{-12}$ J/m and $\gamma_T = 2.3 \times 10^{-12}$ J/m), it turns out that the released bending strain energy can be larger than the adhesion energy barrier ($8.1\ \text{nm} \times \gamma_T$) only when the end deflection w_0 is larger than about $4\ \text{nm} \times L/R$, which is at least a few nanometer large even when the splitting length L is only a few GDP dimers. In other words, because splitting must begin from zero end-deflection, the adhesion energy barrier offered by even one single layer of GTP cap is sufficient to prevent splitting at the plus end, in spite of huge stored bending strain energy of a long microtubule. This conclusion does not rely on the relation (4-3).

Furthermore, Figure 4.5 indicates that there exists a critical length of microtubules beyond which splitting from the plus end prior to buckling is prohibited even with vanishing adhesion energy γ_D . Such a critical length decreases with increasing number of GTP layers at the plus end. For example, it is seen from Figure 4.5 that the critical length is about 450 nm, 330 nm or 250 nm for 1, 2 or 4 GTP layers at the plus end, respectively. In other words, for microtubules with 1, 2 or 4 GTP dimer layers at the plus end and longer than the above-mentioned respective critical length, splitting at the end will not happen prior to overall buckling of microtubule under mechanical compression, and therefore mechanical compression alone cannot cause splitting and dynamic instability of microtubules. In particular, this conclusion is independent of the specific value of adhesion energy between GDP protofilaments γ_D . If the uncertainty of the Young's modulus (0.5-2 GPa) and adhesion energy between protofilaments (1.7×10^{-12} to 3.0×10^{-12} J/m) are taken into account, the critical length beyond which splitting from the plus end is prohibited even with vanishing adhesion energy γ_D are 300 nm~750 nm for one layer case, 236 nm~526 nm for two layers case, and 180 nm~380 nm for four layers case.

To clearly illustrate this critical length, let us assume that γ_D =0 and the microtubule is capped by *m* layers of GTP dimers. For splitting at the plus end, it can be verified from (4-2) and (4-10) that the end deflection $w_0 = 4L\sqrt{\varepsilon}/\pi$, where ε is the applied axial compressive strain. The critical axial strain for splitting at the plus end is determined by the condition when the sum of released axial compressive strain energy $(EA_p\varepsilon^2 L)/2$ and released bending strain energy $2EI_p\sqrt{\varepsilon}/R$ is equal to the adhesion

energy barrier $8.1\ \text{nm}\times\gamma_{\text{T}}\times m$. Substitution of the applied axial strain ε=ε_{mcr} (the latter is given by (4-15)), we obtain a simple estimate for the dependence of the critical length on the layer number m

$$m \approx \left(\frac{2\pi EI_{\text{p}}}{RL_{\text{d}}\gamma_{\text{T}}}\sqrt{\frac{I_{\text{m}}}{A_{\text{m}}}}\right)\left(\frac{1}{L}\right)+\left(\frac{\pi^4 EA_{\text{p}}I_{\text{m}}^2}{2A_{\text{m}}^2 L_m\gamma_{\text{T}}}\right)\left(\frac{1}{L}\right)^3 \tag{4-19}$$

For example, for m=1, 2 or 4 with E=1 GPa and $\gamma_{\text{T}} = 2.3\times10^{-12}$ J/m, the critical length estimated by (4-19) is 454 nm, 339 nm and 259 nm, in agreement with accurate numerical results indicated in Figure 4.5. The estimated intervals of the critical length mentioned before can also be verified using this equation (4-19).

To illustrate the effect of stored strain energy on splitting, also included in Figure 4.5 is the required adhesion energy (γ_{D}) to prevent splitting at the plus end of a microtubule capped by 1 GTP layer with ignored stored strain energy of protofilaments (R=infinite). Comparison between the 1-layer curves for R=21nm and R=infinite in Figure 4.5 indicates that stored strain energy of GDP protofilaments does offer a driving force for splitting at the plus end, in agreement with some literatures (Mitchison and Kirschner, 1984, Hyman et al., 1992), while the stored strain energy of GDP protofilaments does not affect the splitting from middle of a microtubule as stated previously.

Finally, it is stated that if the microtubule is compressed by a constant axial stress rather than a constant axial strain, the major part of the present analysis remains essentially unchanged provided the released axial compressed strain energy (see the first terms on RHS of (4-14)) is now replaced by the external work of the constant axial force ($EA_{\text{p}}\varepsilon$) on the end axial displacement of the split protofilament given by

$$\left(EA_p\varepsilon\right)\frac{1}{2}\int_0^L\left(\frac{\partial w}{\partial x}\right)^2 dx \tag{4-20}$$

For strain-loaded splitting, on using the amplitude relation (4-2), it is readily seen that the released axial strain energy can be written in a form similar, but different by a factor of two, to the external work (4-20) for stress-loaded splitting. Therefore, although the present amplitude relation (4-2) no longer holds for stress-loaded

splitting, the adhesion energy between GTP and GDP protofilaments still offer sufficient energy barrier to prevent the onset of stress-loaded splitting provided the condition obtained in the present study against strain-loaded splitting is met. Therefore, the condition obtained in the present study against splitting is expected to ensure a sufficient energy barrier against the onset of stress-loaded splitting of microtubules.

4.4. Conclusions

A micro-mechanics model is proposed to study splitting of an axially compressed capped microtubule prior to its overall buckling. Explicit criteria are derived to prevent splitting prior to buckling, which depend on the microtubule length, the adhesion energy between protofilaments and the number of GTP dimer layers of the cap at the plus end. With a cap at the plus end, the required lowest adhesion energy to prevent splitting at the middle of a microtubule decreases with microtubule length, this offers a method to estimate the adhesion energy between GDP protofilaments in terms of the length of microtubules. Our basic conclusion is that compression-driven splitting can happen prior to buckling only for very short capped microtubules but not for longer capped microtubules (typically longer than a few hundreds of nanometers). For microtubules shorter than 125 nm~180 nm (depending on specific values of Young's modulus and adhesion energy between protofilaments), for example, compression-driven splitting will happen prior to buckling even in the presence of a few layers of GTP dimer layers at the plus end. In the other hand, for given number of GTP dimer layers at the plus end, a critical length exists beyond which splitting at the plus end is prohibited even with vanishingly small adhesion energy between GDP protofilaments. In particular, for microtubules of length longer than 0.3~0.75 micron (depending on specific values of Young's modulus and adhesion energy between protofilaments), even one single layer of GTP dimers is sufficient to prevent compression-driven splitting, in agreement with the known observation that a single layer of GTP dimer at the plus end is sufficient to prevent depolymerization phase in dynamic instability of microtubules of practical length (Caplow and Shanks, 1996).

5. Pulling force provided by microtubule splitting

5.1. Introduction

Microtubules with high stiffness and strength compose the skeleton of biological cells. However the function of microtubules *in vivo* is far beyond maintaining the shape of cells: polymeric properties of microtubule are also functional in many cellular activities (Boal, 2002). During the depolymerization of microtubule, a force on order of a few pNs which is comparable to the force generated by some typical motor proteins can be used to position chromosomes and membrane organelles (Hendricks et al., 2012, Asbury et al., 2006). The force is related to a kind of biopolymer named protofilament, typically 13/14 of which are circumferentially assembled in parallel to form a microtubule. The force is generated by the previously stored bending strain energy in these unstable protofilaments with a tendency to splay outward from the microtubule lattice. During the splitting of microtubule, some microtubule associated cellular structure, such as Dam1 ring, could serve as an energy-efficient coupler to generate a pulling force to drive chromosome motion (Grishchuk et al., 2008, Cheeseman and Desai, 2008). The Dam1 ring exhibits lateral mobility that could track the splitting end with the shortening of microtubules (Westermann et al., 2006). It is observed that the splitting of microtubule drives a Dam1-coated bead to move around 3 microns, which is comparable to chromosome displacement *in vivo* (Asbury et al., 2006). In another hand, the depolymerization phase characterized by splitting of microtubules can be suppressed by a tensile force applied on the Dam1 ring (Akiyoshi et al., 2010, Franck et al., 2007). The strong connection between polymeric properties of microtubule and external mechanical force suggest the significance of understanding biomechanical behaviors of microtubules.

Many biomechanical researches were performed to study interacting between mechanical force and depolymerization (splitting) at the end of microtubule (Jánosi et al., 2002, Molodtsov et al., 2005a, Vichare et al., 2013, Inoué and Salmon, 1995, Dogterom et al., 2005, Westermann et al., 2006, Jin and Ru, 2012). Some of studies only illustrated the mechanism of how a pulling force is generated by splaying of protofilament associated with microtubule depolymerization without quantitative analysis (Jánosi et al., 2002, Inoué and Salmon, 1995, Dogterom et al., 2005,

Westermann et al., 2006). An analytical model was developed to predict the pulling force provided by protofilament splaying by modelling protofilaments as elastic beams (Vichare et al., 2013). In Vichare's model, the adhesive energy between protofilaments, which is the energy consumption for unit length of splitting propagation, was assumed as a constant and independent of the deflection of protofilament. Such idealization might introduce certain error if the interaction between protofilaments is not limited to an infinitesimal distance. To better model the protofilaments interaction, Molodtsov et al. proposed a more accurate model based on numerical simulations (Molodtsov et al., 2005b, Molodtsov et al., 2005a). In Molodtsov's model a non-monotonic potential energy as a function of protofilament deflection was introduced to characterize the interaction between protofilaments. However due to intrinsic limitations of numerical simulation, it rendered a less clear picture to physically explain the correlation between biomechanical properties of microtubule and pulling force generation due to microtubule splitting. Most importantly, previous studies were focusing on calculating the force produced by protofilament splaying without verifying whether such force can be provided during spontaneous splitting propagation of microtubule rather or only achievable in a specific configuration/moment. It is crucial to address this issue because the pulling force must be continuously generated given the fact that a microtubule depolymerizes at a rate as high as 27 dimers per second to drive the chromosome separation at the speed around 1 μm/min (Hiraoka et al., 1984). Thus it is desirable to develop an analytical biomechanics model to investigate the pulling force generation by protofilament splaying during the spontaneous and continuous microtubule splitting.

In the present study we first derive expressions for bending strain energy in a protofilament and potential energy between protofilaments based on a continuum elastic beam model and a cohesive zone model respectively. Then the total energy of protofilament and cohesive zone after and before splitting propagation of microtubule is compared to obtain a criterion for the spontaneous splitting propagation. Under the assumption that the Dam1 ring attached to protofilament keeps a constant radius, the force generated by microtubule splitting is then calculated. Based on derived splitting propagation criterion and calculated pulling force, how a microtubule *in vivo* provides pulling force during spontaneous splitting propagation is explained. Finally, our analytical predictions are compared with some known experiments.

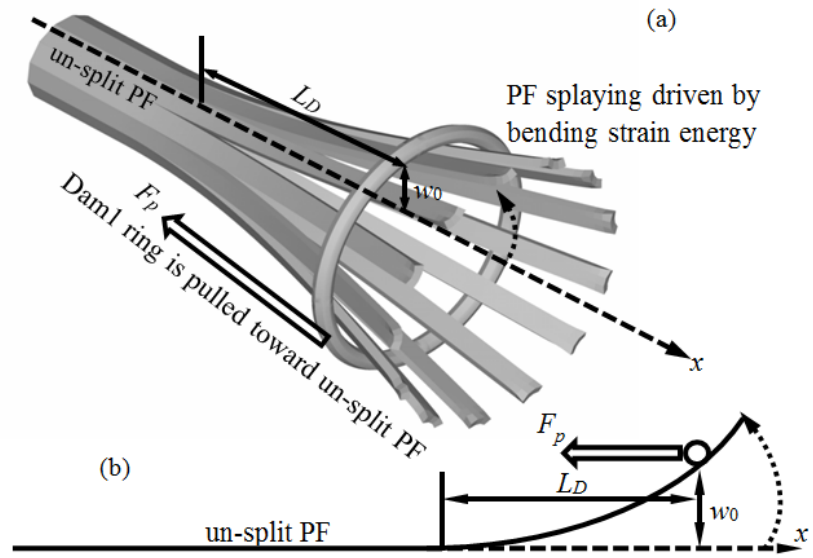

Figure 5.1 Coupled Dam1 ring is pulled by the splitting of a microtubule. (a) a three dimensional illustration with deflection magnitude w_0 and splitting length L_D defined, (b) a simplified model with one protofilament (short for PF in figure) due to symmetrical splaying of other protofilaments with respect to microtubule axis.

5.2. Beam-Cohesive zone model for protofilament

5.2.1. Deflection pattern of protofilament

During continuous force generation with microtubule shortening, the "cap" composed GTP dimers with straight shape and strong adhesion is already lost from the end of microtubule, thus in present study protofilaments purely composed of GDP dimers are modeled as naturally curved elastic beams with radius of curvature R (Hawkins et al., 2010). With propagation of microtubule splitting, the Dam1 ring coupled at the end of microtubule will be pulled by the splaying of protofilaments towards the un-split part of microtubule, see Figure 5.1 (a) for a three dimensional illustration. We assume that all protofilaments behave similarly with respect to the axis of microtubule, as a result only one protofilament is included in our model. The deflection (w) of a protofilament vanishes at the end of splitting propagation and reaches w_0 at x=L_D, where the deflection magnitude w_0 equals to the gap from outer radius of microtubule to the inner radius of Dam1 ring, see Figure 5.1 (b) for an in-plane illustration in view from circumferential direction of microtubule. The L_D is then defined as the splitting length of microtubule. The pulling force is generated only by splaying of protofilament from

x=0 to x=L_D, while the un-split part with x<0 and the x> L_D part exceeding the Dam1 ring have no contribution to the force generation. We propose following function form for the deflection of protofilament from x=0 to x=L_D:

$$w = w_0 \left(\frac{x}{L_D} \right)^2 \tag{5-1}$$

which satisfies the end conditions that the deflection and rotation angle equal to zero at x=0. Actually the deflection form of protofilament should not have very higher order polynomial terms because it will curved into a circle with constant radius of curvature (third order derivative is zero) if detached from microtubule (Elie-Caille et al., 2007). It was also indicated in previous study that by using such a parabolic deflection form, the energy method can predict the critical buckling force with error as low as 1.3% compared with the exact solution (Ugural and Fenster, 2003). A study for microtubule splitting under compression also verified that choosing different forms of protofilament deflection will not lead to a meaningful inconsistency in results (Jin and Ru, 2012). Thus it is contended that the parabolic deflection form in Eq. (5-1) is a reasonable choice.

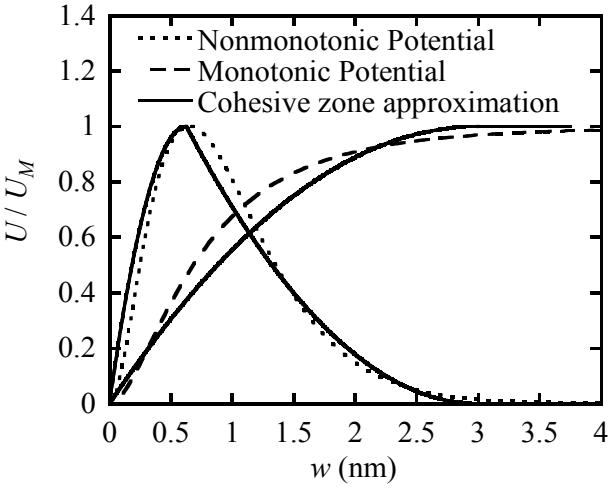

Figure 5.2 Normalized potential energy per unit length U / U_M versus protofilament deflection w from previous models (dash lines) and present cohesive zone model (solid lines).

The elastic strain energy Π_D of a protofilament within splitting length L_D is

$$\Pi_D = \int_0^{L_D} \frac{EI}{2}\left[\left(\frac{1}{R}\right)-\left(\frac{d^2w}{dx^2}\right)\right]^2 dx \tag{5-2}$$

where R is the radius of curve of a protofilament free of external load. By inserting Eq. (5-1) into Eq. (5-2), we derived the expression for Π_D as

$$\Pi_D\left(w_0, L_D\right) = EI\left(\frac{L_D}{2R^2}-\frac{2w_0}{RL_D}+\frac{2w_0^2}{L_D^3}\right) \tag{5-3}$$

5.2.2. Potential energy of cohesive zone at splitting propagation end

The splitting of microtubule is also influenced by interaction between adjacent protofilaments, which was commonly modeled by a potential energy function. One choice is the monotonic Lennard-Jones or Morse potential which assumes that only adhesion exist between adjacent protofilaments (Hunyadi and Jánosi, 2007). Non-monotonic potential energy may also be used as a combination of initial stage and post stage characterized by potentials with opposite effects (Molodtsov et al., 2005a, Molodtsov et al., 2005b, Jiang et al., 2002). In the initial stage, adhesive potential energy offers a resistance force to prevent the deflection of protofilaments until the deflection reaches the maximum adhesive separation r_0. For the post stage with deflection larger than r_0, the potential energy provide a repulsive force incorporated with the bending strain energy to facilitate further deflection of protofilament. The repulsive force will vanish as the deflection reaches maximum repulsive separation r_1 because after that the energy in cohesive zone keeps a constant, see Eq. (5-4). The post repulsive stage was proved to play an important role in propagation of splitting and splaying of protofilament (Molodtsov et al., 2005a), however were ignored in previous linear elastic models (Jin and Ru, 2012, Vichare et al., 2013). In present study, we introduce a cohesive zone model which could capture the feature of both types of previously proposed potential energy functions as

$$U\left(w\right) = \begin{cases} U_M\left[2w/r_0-\left(w/r_0\right)^2\right] & r_0 > w > 0 \\ U_M + U_P\left[\left(1-\dfrac{w-r_0}{r_1-r_0}\right)^2-1\right] & r_1 > w > r_0 \\ U_M - U_P & w \geq r_1 \end{cases} \tag{5-4}$$

where U_M is the energy increase per unit length in the initial stage (the energy barrier from w=0 to w=0.7 nm shown in Figure 5.2) and U_P is the potential energy drop in the second stage per unit length, see w=0.7 nm to w= 3 nm in Figure 5.2. If U_P =0, the potential energy in Eq. (5-4) degenerates to a monotonic potential energy. From a comparison in Figure 5.2, it is noticed that the present model can well represent the potential energy forms adopted in previous research (Molodtsov et al., 2005b, Molodtsov et al., 2005a). The derivative of Eq. (5-4) with respect to w gives

$$-U'(w)=\begin{cases}-2U_M / r_0\left(1-w/r_0\right) & r_0 > w > 0 \\ \dfrac{2U_P}{r_1-r_0}\left(1-\dfrac{w-r_0}{r_1-r_0}\right) & r_1 > w > r_0 \\ 0 & w \geq r_1\end{cases} \tag{5-5}$$

where $-U'(w)$ is force per unit length pushing the protofilament toward the positive direction of deflection w. It is verified from Eq. (5-5) that the potential energy provides adhesive force (negative) in the initial stage ($r_0 > w > 0$) and repelling force (positive) in the post stage $r_1 > w > r_0$.

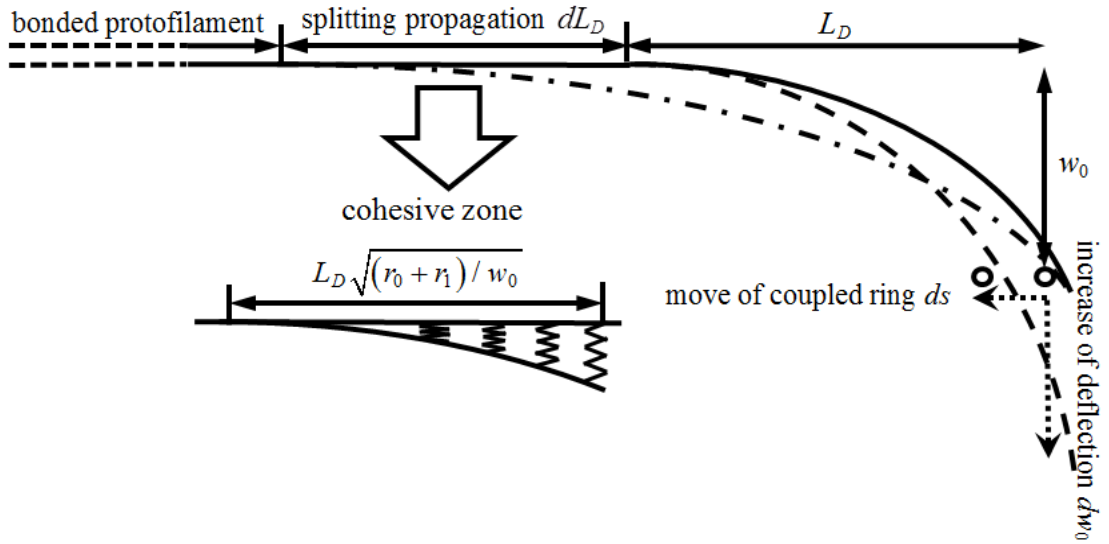

Figure 5.3 Splitting propagation (from solid line to dash dot line) and outward splaying of protofilament (from solid line to dash line). The move of Dam1 ring ds could be induced by increase of deflection dw_0.

By integrating Eq. (5-4) through L_D, the total energy of cohesive zone within splitting length (x=0 ~ L_D) is expressed as

$$\begin{aligned}\Pi_C\left(w_0, L_D\right) = & \int_0^{L_D\sqrt{r_0/w_0}} U_M\left[2w/r_0 - \left(w/r_0\right)^2\right]dx \\ & + \int_{L_D\sqrt{r_0/w_0}}^{L_D\sqrt{r_1/w_0}} U_M + U_P\left[\left(1-\frac{w-r_0}{r_1-r_0}\right)^2 - 1\right]dx \\ & + \int_{L_D\sqrt{r_0/w_0}}^{L_D} U_M - U_P dx\end{aligned} \tag{5-6}$$

By substituting w from Eq.(5-1) into Eq. (5-6), the $\Pi_C\left(w_0, L_D\right)$ is integrated as

$$\begin{aligned}\Pi_C\left(w_0, L_D\right) = & \left(U_M - U_P\right)L_D - \frac{8}{15}\sqrt{\frac{r_0}{w_0}}U_M L_D \\ & + \left[\frac{8r_1^2}{15\left(r_1-r_0\right)^2}\sqrt{\frac{r_1}{w_0}} - \frac{r_0\left(20r_1-12r_0\right)}{15\left(r_1-r_0\right)^2}\sqrt{\frac{r_0}{w_0}}\right]U_P L_D\end{aligned} \tag{5-7}$$

According to the potential energy given by previous models (Molodtsov et al., 2005b, Molodtsov et al., 2005a, Jiang et al., 2002) w_0 is about 20 times of r_0 and r_1 is about 6 times of r_0, then the Eq. (5-7) can be approximately simplified as

$$\Pi_C\left(w_0, L_D\right) \approx \left(U_M - U_P\right)L_D + \frac{8}{15}\left(\sqrt{\frac{r_1}{w_0}}U_P - \sqrt{\frac{r_0}{w_0}}U_M\right)L_D \tag{5-8}$$

It is noticed from Eq. (5-8) that if both r_0 and r_1 are much smaller than w_0, the second term will vanish and the cohesive zone model will degenerated to a surface energy model adopted by previous studies (Jin and Ru, 2012, Vichare et al., 2013), in which the energy between protofilaments is a Heaviside step function of w with magnitude of $U_M - U_P$.

5.2.3. Splitting propagation criterion

Now let us derive a criterion for spontaneous splitting propagation by considering both the bending strain energy of protofilament and the potential energy at cohesive zone. The Dam1 ring is assumed to be static during splitting propagation so that w_0 keeps a constant. The propagation of splitting may occur spontaneously only if the total energy after propagation is smaller than the total energy before propagation. It is assumed that the splitting propagate toward the un-split part by dL_D with position of Dam1 ring fixed as shown in Figure 5.3. The total energy before propagation Π_0 is

composed of an un-split part (zero deflection) of length dL_D (note: the previously stored bending strain energy is not zero for un-split part because protofilaments are naturally curved) and a split part with maximum deflection w_0 of length L_D, which is expressed as

$$\Pi_0 = \Pi_C\left(w_0, L_D\right) + \Pi_D\left(w_0, L_D\right) + \Pi_C\left(0, dL_D\right) + \Pi_D\left(0, dL_D\right) \tag{5-9}$$

The total energy after propagation Π_1 is expressed as

$$\begin{aligned}\Pi_1 &= \Pi_C\left(w_0, L_D + dL_D\right) + \Pi_D\left(w_0, L_D + dL_D\right) \\ &= \Pi_C\left(w_0, L_D\right) + \left.\frac{\partial \Pi_C\left(w_0, L_D\right)}{\partial L_D}\right|_{w_0} dL_D + \Pi_D\left(w_0, L_D\right) + \left.\frac{\partial \Pi_D\left(w_0, L_D\right)}{\partial L_D}\right|_{w_0} dL_D\end{aligned} \tag{5-10}$$

The criterion for spontaneous propagation of splitting is

$$\Pi_0 - \Pi_1 > 0 \tag{5-11}$$

by substituting Eq. (5-9) and (5-10) into inequation. (5-11), we have

$$\Pi_D\left(0, dL_D\right) + \Pi_C\left(0, dL_D\right) - \left.\frac{\partial\left[\Pi_C\left(w_0, L_D\right) + \Pi_D\left(w_0, L_D\right)\right]}{\partial L_D}\right|_{w_0} dL_D > 0 \tag{5-12}$$

The first term in Eq. (5-12) with constant zero deflection is calculated from Eq. (5-3) by setting $w_0 = 0$ and the energy in cohesive zone without deflection is zero, which gives the second term $\Pi_C\left(0, dL_D\right)$=0. By substituting Eq. (5-3) and (5-8) to replace $\Pi_D\left(w_0, L_D\right)$ and $\Pi_C\left(w_0, L_D\right)$ in Eq. (5-12), we obtain the criterion for spontaneous propagation as

$$\left(\frac{w_0 R}{L_D^2}\right)^2 - \frac{1}{3}\left(\frac{w_0 R}{L_D^2}\right) + \frac{U_P}{U_C}\left(\frac{1}{12} - \frac{2}{45}\sqrt{\frac{r_1}{w_0}}\right) - \frac{U_M}{U_C}\left(\frac{1}{12} - \frac{2}{45}\sqrt{\frac{r_0}{w_0}}\right) > 0 \tag{5-13}$$

where $U_C = EI / 2R^2$ is the previously stored bending strain energy in a protofilament per unit length.

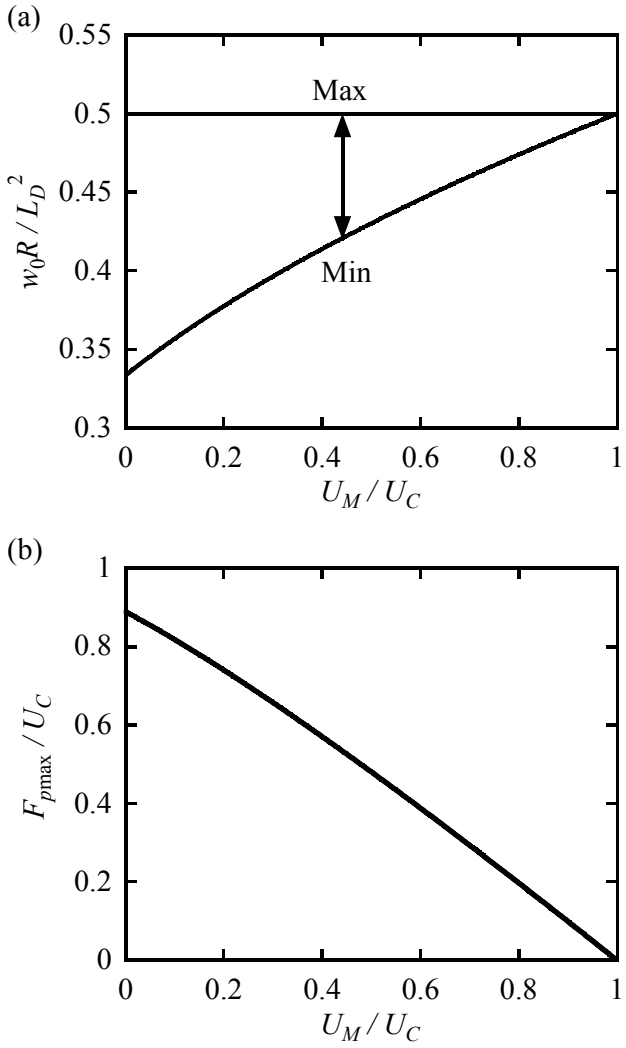

Figure 5.4 For monotonic potential in cohesive zone with $r_0/w_0 = 0$: (a) the range of w_0R/L_D^2 to provide non-negative pulling force during spontaneous splitting propagation versus U_M/U_C. (b) normalized maximum pulling force $F_{p\max}/U_C$ during spontaneous splitting propagation versus U_M/U_C.

5.2.4. Force produced by protofilament deflection

In this section we offer an expression of force produced by splaying of protofilament with given splitting length L_D. As shown in Figure 5.3, with the diameter of Dam1 ring being a constant, the simple geometrical relationship between the deflection increase (dw_0) and subsequently induced displacement of Dam1 ring toward the un-split protofilament (ds) can be expressed as following:

$$dw_0 = \left.\frac{dw}{dx}\right|_{x=L_D} ds = \frac{2w_0}{L_D} ds \tag{5-14}$$

With the splitting length L_D fixed, total mechanical work done to pull the Dam1 ring by ds is the total energy decrease due to the increase of deflection dw_0, which is expressed as

$$F_p ds = -\left.\frac{\partial\left[\Pi_C\left(w_0, L_D\right) + \Pi_D\left(w_0, L_D\right)\right]}{\partial w_0}\right|_{L_D} dw_0 \tag{5-15}$$

where F_p is the pulling force stimulated by protofilament splaying. The Eq. (5-15) can be further simplified by substituting Eqs. (5-3), (5-6) and (5-14) to replace Π_D, Π_C and dw_0, which gives

$$\left(\frac{F_p}{U_C}\right) = -16\left(\frac{w_0 R}{L_D^2}\right)^2 + 8\left(\frac{w_0 R}{L_D^2}\right) + \frac{8}{15}\left(\sqrt{\frac{r_1}{w_0}}\frac{U_P}{U_C} - \sqrt{\frac{r_0}{w_0}}\frac{U_M}{U_C}\right) \tag{5-16}$$

5.3. Results and discussion

5.3.1. Pulling force provided by protofilament during steady splitting

Both Eq (5-13) and Eq. (5-16) should be taken into account to predict the pulling force generated during spontaneous splitting of microtubule. Here we start from the simplest case that the cohesive zone is constituted by a monotonic potential energy (U_P =0) with r_0 and $r_1 << w_0$. To provide pulling force larger than zero, following two conditions simplified from Eqs. (5-13) and (5-16) must be satisfied

$$\begin{cases} \left(\frac{w_0 R}{L_D^2}\right)^2 - \frac{1}{3}\left(\frac{w_0 R}{L_D^2}\right) - \frac{1}{12}\frac{U_M}{U_C} > 0 \\ \left(\frac{F_p}{U_C}\right) = -16\left(\frac{w_0 R}{L_D^2}\right)^2 + 8\left(\frac{w_0 R}{L_D^2}\right) > 0 \end{cases} \tag{5-17}$$

The second condition requires $L_D > \sqrt{2w_0 R}$ and the maximum pulling force $F_p = U_C$ (previously stored bending strain energy is completely utilized to provide pulling

force) is reached as $L_D = \sqrt{4w_0R}$. The second condition alone cannot promise the spontaneous propagation of microtubule unless the first condition in Eq. (5-17) is also satisfied. If the previously stored bending strain energy in protofilaments per unit length U_C is much larger than the adhesive energy per unit length U_M to prevent splitting of protofilaments, i. e., U_M / U_C=0, the first condition gives $L_D < \sqrt{3w_0R}$ with the third term in the first condition vanished. Subsequently the inequation (5-17) yields the range of L_D as $\sqrt{2w_0R} < L_D < \sqrt{3w_0R}$ and the maximum pulling force $F_{p\max} = 0.9U_C$ is reached when $L_D = \sqrt{3w_0R}$, which suggests that with negligible adhesive energy U_M, most of previously stored bending strain energy U_C could be utilized to provide a pulling force to move Dam1 ring. Here maximum pulling force $F_{p\max}$ is defined as the achievable maximum force within the range of splitting length L_D in which the splitting of microtubule could spontaneously propagate. However if $U_M / U_C \geq 1$, the first condition of (5-17) yields that $L_D < \sqrt{2w_0R}$ which is against $L_D > \sqrt{2w_0R}$ required by the second condition which implies that a pulling force cannot be generated during the spontaneous splitting of microtubule. The normalized maximum pulling force $F_{p\max} / U_C$ and range of w_0R / L_D^2 satisfying inequation (5-17) versus the ratio of U_M / U_C from 0 to 1 are plotted in Figure 5.4 (a) and (b). It is verified that at U_M / U_C=1, the maximum and minimum values of w_0R / L_D^2 coincides in Figure 5.4 (a), which suggests that if $U_M / U_C \geq 1$, a microtubule with arbitrary splitting length fails to provide pulling force during spontaneous splitting.

If r_0 is comparable with w_0 and the potential energy is still monotonic, criteria (5-13) and (5-16) are simplified as

$$\begin{cases} \left(\dfrac{w_0R}{L_D^2}\right)^2 - \dfrac{1}{3}\left(\dfrac{w_0R}{L_D^2}\right) - \dfrac{U_M}{U_C}\left(\dfrac{1}{12} - \dfrac{2}{45}\sqrt{\dfrac{r_0}{w_0}}\right) > 0 \\ \left(\dfrac{F_p}{U_C}\right) = -16\left(\dfrac{w_0R}{L_D^2}\right)^2 + 8\left(\dfrac{w_0R}{L_D^2}\right) - \dfrac{8}{15}\dfrac{U_M}{U_C}\sqrt{\dfrac{r_0}{w_0}} > 0 \end{cases} \tag{5-18}$$

The relationship between range of w_0R / L_D^2 and U_M / U_C is given in Figure 5.5 for

different ratios of r_0 to w_0. It is found that for r_0 / w_0=0.1 the range of $w_0 R / L_D^2$ and $F_{p\max} / U_C$ is almost as same as results of r_0 / w_0=0 presented in Figure 5.4 (a) and (b). With r_0 / w_0=1, the range of $w_0 R / L_D^2$ for spontaneous splitting propagation decreases by about 20%. However $F_{p\max}$ still reaches 0.9 U_C when U_M / U_C=0.

Now we further investigate the case with a non-monotonic cohesive. In this case criteria (5-13) and (5-16) shall be applied to give the range of L_D and normalized maximum pulling force $F_{p\max} / U_C$. Typical values of r_0 / w_0 as 0.05 and r_1 / w_0 as 0.3 (Molodtsov et al., 2005b, Molodtsov et al., 2005a, Jiang et al., 2002) are adopted to investigate the influence of U_P. The range of $w_0 R / L_D^2$ versus U_M / U_C is plotted in Figure 5.6 (a) and the normalized maximum pulling force $F_{p\max} / U_C$ versus U_M / U_C is plotted in Figure 5.6 (b). For U_P / U_M=0.4, the $F_{p\max} / U_C$ decreases with the increase of U_M / U_C and vanishes as $U_M / U_C \approx 2$, which indicates that with the assistance of repulsion between protofilaments in the cohesive zone, a pulling force with spontaneous splitting propagation could be generated even if the previously stored bending strain energy U_C is only a half of the energy barrier U_M which blocks the protofilament deflection. This results is in contrast with what we obtained by using monotonic potential in last section which requires $U_C > U_M$ to provide a pulling force. For U_P / U_M=0.8, a pulling force could be provided even when U_M / U_C as large as 5, see Figure 5.6. If U_P / U_M increases to 1, the maximum of pulling force is reached at U_M / U_C=6, which suggests that the pulling force is mainly driven by the repulsion between protofilament due to the potential energy drop U_P rather than the previously stored bending strain energy in protofilaments U_C. However previous studies have theoretically and experimentally demonstrated that the previous stored bending strain energy U_C plays decisive role to cause microtubule splitting (Hyman et al., 1992, Desai et al., 1999, Elie-Caille et al., 2007, Xiao et al., 2006), thus it is assumed that U_P / U_M should not be larger than 0.8.

5.3.2. Comparison with experiments

In this section we compare our analytical predictions with available experiments. The inner radius of Dam1 ring is measured as about 35 nm (Miranda et al., 2005, Westermann et al., 2005) which could slide along the un-split microtubule with outer diameter around 24 nm but too small to pass over the frayed end around 50 nm (Mandelkow et al., 1991). Thus the w_0 as the difference between the inter radius of Dam1 ring and outer radius of microtubule is about of 5.5 nm. The radius of curvature of naturally curved protofilaments is around 21 nm, which gives previously stored bending strain energy U_C as 2.1 ~ 4.2 K_BT per dimer (VanBuren et al., 2005, VanBuren et al., 2002, Caplow and Shanks, 1996). The potential energy barrier blocking protofilament deflection per unit length U_M is measured as 2 ~ 5.7 K_BT per dimer (VanBuren et al., 2002, VanBuren et al., 2005, Sept et al., 2003, Caplow and Shanks, 1996), which gives the ratio of U_M to U_C varying from 0.5 to 2.6. Typical values of r_0 / w_0=0.05 and r_1 / w_0=0.3 adopted in previous studies are used for the further comparison (Molodtsov et al., 2005b, Molodtsov et al., 2005a, Jiang et al., 2002).

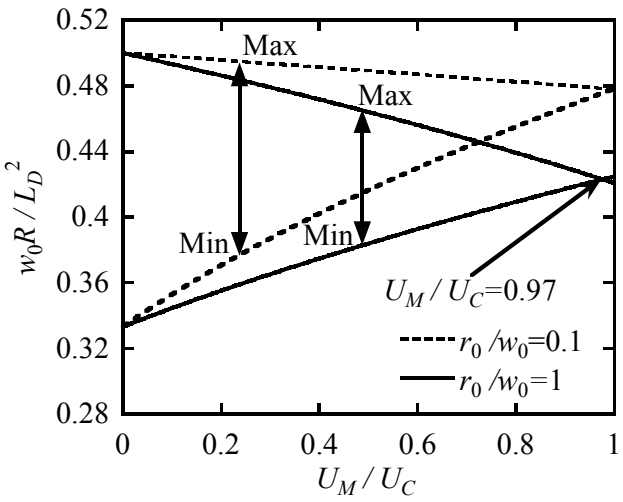

Figure 5.5 The range of w_0R / L_D^2 to provide non-negative pulling force during spontaneous splitting propagation versus U_M / U_C for monotonic potential in cohesive zone with r_0 / w_0=0.1 and 1.

By taking the measured parameters given above for the monotonic potential case (U_P

=0), we can get L_D=1.41$\sqrt{w_0 R}$ ~ 1.52$\sqrt{w_0 R}$ or 15.2 nm ~16.3 nm and the maximum force provided by a single protofilament as 0.46U_C or 0.5 ~ 1 pN (depending on the value used for U_C within measured range) for U_M / U_C = 0.5. Thus the maximum net pulling force of a microtubule composed of 13 protofilaments is about 6.5 ~ 13 pN. If $U_M / U_C \geq 1$, i. e., the potential energy barrier is equal to or larger than previously stored bending strain energy, microtubules are not able to provide pulling force during spontaneous splitting propagation.

For the non-monotonic potential case with U_P=0.4U_C, we get the similar L_D=15.2 nm ~ 16.9 nm but much larger maximum net pulling force about 9.4 ~ 18.9 pN (depending on the value used for U_C within measured range) for U_M / U_C = 0.5. If U_M / U_C exceeds 1.6, microtubules are not able to provide the maximum pulling force of during spontaneous splitting propagation.

For the non-monotonic potential case with U_P=0.8U_C, we get L_D=15.1 nm ~17.6 nm and maximum net pulling force of microtubule as 11.8 ~ 23.8 pN (depending on the value used for U_C within measured range) for U_M / U_C = 0.5. In this case, even if U_M / U_C reaches 2.6, microtubules could still provide the maximum net pulling force within the range of 6.82 ~ 13.8 pN.

The predicted splitting length agrees with the commonly accepted assumption that splitting is strongly localized at frayed microtubule end, i. e., the rest part of microtubule away from the end keeps intact with straight protofilaments perfectly bonded together. In particular, some experimental observations, e. g., figures 2 and 3 in ref. (Müller-Reichert et al., 1998) and figures 4 ~ 7 in ref. (Chrétien et al., 1995), show that the length of a protofilament from zero deflection to deflection 5.5 nm (w_0) at frayed microtubule end is about 10 ~ 30 nm, which is comparable with predicted splitting length L_D around 15 ~ 18 nm by our analytical model.

Some previous experiments measured that the pulling force provided by splitting of a microtubule is about 0.5 ~ 3 pN (Asbury et al., 2006) and 5 pN (Grishchuk et al., 2008), which is lower than the theoretical predicted maximum pulling force 7 ~ 24 pN by present analytical model. It should be noted that the latter is actually the theoretical

upper limit of the pulling force for two reasons. First, the maximum force $F_{p\max}$ is achieved when $\Pi_0 - \Pi_1 = 0$ in Eq. (5-11). Physically, the difference between Π_0 and Π_1 is the driving force to stimulate protofilament propagation. The spontaneous splitting propagation actually requires $\Pi_0 - \Pi_1 > 0$, which requires the actual pulling force lower than $F_{p\max}$. Second, the present analytical model ignores the water resistance and some other forms of energy dissipation which might reduce the pulling force generated *in vivo*. Thus the predicted maximum force in present study is a good estimation to the upper limit of the pulling force generated *in vivo*.

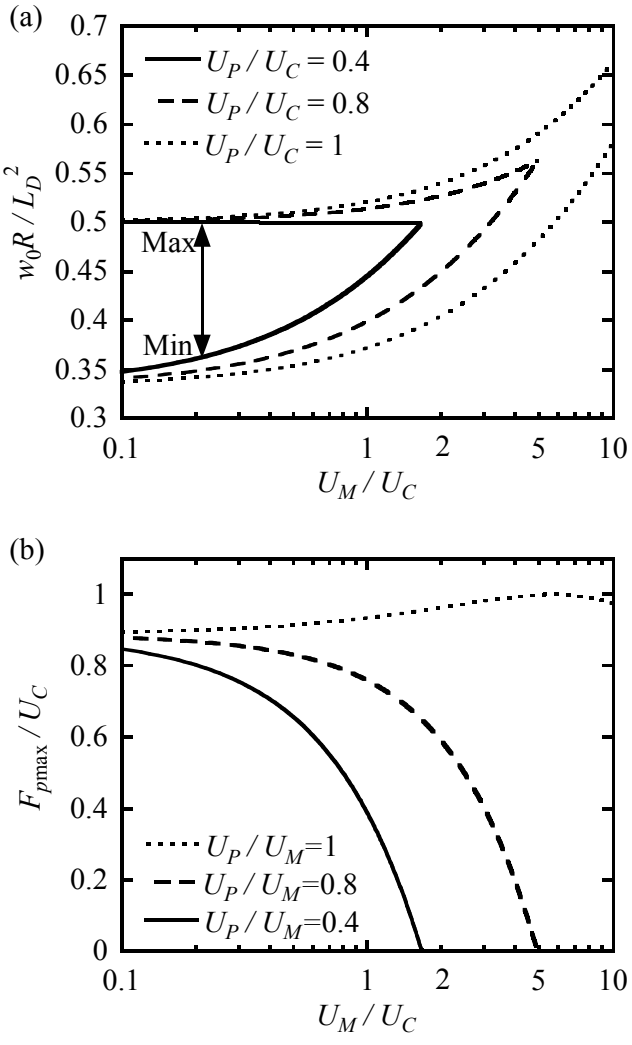

Figure 5.6 For non-monotonic potential with r_0/w_0 =0.05 and r_1/w_0 =0.3: (a) the range of w_0R/L_D^2 to provide non-negative pulling force during spontaneous splitting propagation versus U_M/U_C. (b) Normalized maximum pulling force $F_{p\max}/U_C$ during spontaneous splitting propagation versus U_M/U_C.

5.4. Conclusions

In the present study we developed a new mechanics model to investigate an important biological function of microtubules *in vivo*: generating pulling force during spontaneous microtubule splitting to move the coupled Dam1 ring at frayed end. Due to symmetrical distribution and similar mechanical behaviors of 13 protofilaments with respect to the axis of microtubule, only one protofilament is included and modeled as an elastic beam to represent other protofilaments. The interaction between adjacent protofilaments is characterized by a cohesive zone model with adhesive and repulsive stages. By comparing the total energy before and after propagation of splitting, we derived a criterion for spontaneous splitting propagation in a microtubule. For given splitting length, an explicit expression of generated pulling force is derived based on the total energy decrease with the Dam1 movement caused by splaying of protofilaments. The maximum pulling force is then predicted based on the range of splitting length satisfying the spontaneous splitting propagation criterion. The predicted maximum pulling force by the present model is 7 ~ 24 pN, which offers an upper limit to the experimentally measured force 0.5 ~ 5 pN. The observed splitting length around 10 ~ 30 nm from experiments is also comparable with the predicted splitting length 15 ~ 18 nm by the present model.

6. Concluding remarks and future works

6.1. Conclusions

New analytical and finite element models have been developed in this thesis to investigate mechanical behaviors of an individual microtubule in living cells. Major conclusions achieved in this thesis are summarized below:

(1) By modeling a microtubule as an elastic beam and surrounding cross linkers as randomly distributed discrete springs, we performed numerical simulations for microtubule buckling. Our model predicts that, depending on mechanical properties and interval of the cross linkers, microtubules *in vivo* could buckle under an axial compressive force between 14 ~ 340 pN with highly localized buckling mode of wavelength 0.6 ~ 2.9 microns, which is in reasonable agreement with observed localized buckling wave length of 1 ~ 3 microns and measured buckling force around 100 pN (Gittes et al., 1993, Li, 2008, Brangwynne et al., 2006). It is stressed that such localized buckling mode and the associated buckling force cannot be explained by the existing models.

(2) By modeling a microtubule as an elastic beam and surrounding cross linkers as randomly distributed discrete springs, we performed numerical simulations for microtubule vibration. The predicted lowest frequencies (14 MHz ~ 204 MHz, depending on mechanical properties and interval of the cross linkers) are at least 50% lower than the values predicted by the existing elastic foundation mode and thus in much better agreement with experimentally measured resonance frequency 8 MHz (Cifra et al., 2011). In addition, in contrast with the existing elastic foundation model which predicts wave lengths spreading through the entire microtubule, the wave length of localized vibration predicted by the present model is around 0.5 ~ 3 microns and consistent with the values of 1 ~ 4 microns observed from experiments (Marrari et al., 2003, Mandato and Bement, 2003, Brangwynne et al., 2006).

(3) By using elastic beam model for protofilament and adhesive energy to quantify the energy consumption of splitting propagation, we explored splitting of microtubule driven by axial compression. Our analytical model shows that for

microtubules shorter than 150 nm, compression-driven splitting could occur even with a very strong "cap" composed of stable and strongly bonded GTP dimers at the tip of microtubule. On the other hand, for microtubules of length longer than 450 nm, even the weakest "cap" composed of a single layer of GTP dimers is sufficient to prevent compression-driven splitting prior to overall buckling of the compressed microtubule, in agreement with the well-known observation that a single layer of GTP dimers at microtubule end is sufficient to prevent depolymerization of microtubule longer than a micron (Caplow and Shanks, 1996).

(4) By using elastic beam model for protofilament and cohesive zone model to characterize interaction between adjacent protofilaments, we analytically predict the maximum force generated by spontaneous splitting of microtubule. The maximum pulling force predicted by the present model is found to be around 7 ~ 24 pN associated with splitting length around 15 ~ 18 nm, which reasonably agrees with the experimental values of pulling force around 0.5 ~ 5 pN (Asbury et al., 2006, Grishchuk et al., 2008) and splitting length of 10 ~ 30 nm (Müller-Reichert et al., 1998, Chrétien et al., 1995).

The theoretical models and numerical simulations achieved in this thesis contribute new ideas and insights into the study of microtubule mechanics, and some results predicted by the present models provide plausible explanations for some important experimental phenomena of microtubules *in vivo* which have not been well explained by existing models. It is hoped that the present study has the potential to stimulate further research interest in mechanical modeling of microtubules.

6.2. **Recommended future works**

We would suggest two research topics for future work:

1). A micromechanics model for inhomogeneous microtubule composed of both GDP and GTP dimers

In chapter 5 we studied splitting of a microtubule purely composed of unstable GDP dimers. It is also desirable to develop a more sophisticated model with protofilaments containing both unstable GDP dimers and stable GTP dimers. The modified model can be used to study whether splitting of microtubule can be driven by some other

mechanical loadings than an axial compression. In addition, recently it has been found that GTP dimers can concentrate not only at the tip of microtubule but also at some other locations of microtubule body (Kueh and Mitchison, 2009, Dimitrov et al., 2008). The modified model could also be applied to study effects of these GTP remnants, such as rescuing microtubules from depolymerization (spontaneous splitting).

2). Critical curvature of microtubule failure under bending and indentation

Buckling as a cylinder shell instead of a beam is also an important failure mode for microtubule. It is well known from experiments that the mean radius of curvature of a bent microtubule which could cause microtubule failure is about 1.2 rad / mm (Odde et al., 1999). However critical radius of curvature of a bent microtubule for microtubule buckling as a cylinder shell is predicated theoretically as 0.03 rad / mm (Yi et al., 2008), which is much smaller than the above-mentioned experimental value. Such remarkable discrepancy might be attributed to the inappropriate constitutive model adopted for buckling analysis of microtubules. It is well recognized that a microtubule could be stable either as a cylinder or as a two dimensional flat sheet when it is fully unfolded (Chrétien et al., 1995). A recent study suggested that indentation response of microtubules from experiments are better matched by simulations with both cylinder and sheet as stable configurations (Wu et al., 2012). Existence of two stable configurations might affect critical radius of curvature and other mechanical behaviors of microtubule; however none of existing continuum shell models for microtubule could capture this important feature.

Reference

AKIYOSHI, B., SARANGAPANI, K. K., POWERS, A. F., NELSON, C. R., REICHOW, S. L., ARELLANO-SANTOYO, H., GONEN, T., RANISH, J. A., ASBURY, C. L. & BIGGINS, S. 2010. Tension directly stabilizes reconstituted kinetochore-microtubule attachments. *Nature,* 468**,** 576-579.

ALBERTS, B., BRAY, D., LEWIS, J., RAFF, M., ROBERTS, K. & WATSON, J. 1994. *Molecular Biology of the Cell,* London, Garland Publishing.

ALLEN, K. B., SASOGLU, F. M. & LAYTON, B. E. 2008. Cytoskeleton-Membrane Interactions in Neuronal Growth Cones: A Finite Analysis Study. *Journal of biomechanical engineering,* 131**,** 021006-021006.

ASBURY, C. L., GESTAUT, D. R., POWERS, A. F., FRANCK, A. D. & DAVIS, T. N. 2006. The Dam1 kinetochore complex harnesses microtubule dynamics to produce force and movement. *Proceedings of the National Academy of Sciences,* 103**,** 9873-9878.

BATHE, M., HEUSSINGER, C., CLAAESSENS, M. M. A. E., BAUSCH, A. R. & FREY, E. 2008. Cytoskeletal bundle mechanics. *Biophysical journal,* 94**,** 2955-2964.

BEHRENS, S., WU, J., HABICHT, W. & UNGER, E. 2004. Silver Nanoparticle and Nanowire Formation by Microtubule Templates. *Chemistry of Materials,* 16**,** 3085-3090.

BOAL, D. 2002. *Mechanics of the Cell*, Cambridge Univ Pr.

BRANGWYNNE, C. P., MACKINTOSH, F. C., KUMAR, S., GEISSE, N. A., TALBOT, J., MAHADEVAN, L., PARKER, K. K., INGBER, D. E. & WEITZ, D. A. 2006. Microtubules can bear enhanced compressive loads in living cells because of lateral reinforcement. *Journal of Cell Biology,* 173**,** 733-741.

BRODLAND, G. W. & GORDON, R. 1990. INTERMEDIATE FILAMENTS MAY PREVENT BUCKLING OF COMPRESSIVELY LOADED MICROTUBULES. *Journal of Biomechanical Engineering-Transactions of the Asme,* 112**,** 319-321.

BRUSH, D. O. & ALMROTH, B. O. 1975. *Buckling of bars, plates, and shells*, McGraw-Hill Washington DC.

CANADAS, P., LAURENT, V. M., ODDOU, C., ISABEY, D. & WENDLING, S. 2002. A cellular tensegrity model to analyse the structural viscoelasticity of the cytoskeleton. *Journal of theoretical biology,* 218**,** 155-173.

CAPLOW, M. & SHANKS, J. 1996. Evidence that a single monolayer tubulin-GTP cap is both necessary and sufficient to stabilize microtubules. *Molecular Biology of the Cell,* 7**,** 663-675.

CARTER, N. J. & CROSS, R. A. 2005. Mechanics of the kinesin step. *Nature,* 435**,** 308-312.

CHAI, H., BABCOCK, C. & KNAUSS, W. 1981. One dimensional modelling of failure in laminated plates by delamination buckling. *International Journal of Solids and Structures,* 17**,** 1069-1083.

CHEESEMAN, I. M. & DESAI, A. 2008. Molecular architecture of the kinetochore-microtubule interface. *Nat Rev Mol Cell Biol,* 9**,** 33-46.

CHRÉTIEN, D., FULLER, S. D. & KARSENTI, E. 1995. Structure of growing microtubule ends: two-dimensional sheets close into tubes at variable rates. *The Journal of Cell Biology,* 129**,** 1311-1328.

CIFRA, M., FIELDS, J. Z. & FARHADI, A. 2011. Electromagnetic cellular interactions. *Progress in Biophysics and Molecular Biology,* 105**,** 223-246.

CIFRA, M., POKORNÝ, J., HAVELKA, D. & KUČERA, O. 2010. Electric field generated by axial longitudinal vibration modes of microtubule. *Biosystems,* 100**,** 122-131.

DANESHMAND, F. 2012. Microtubule circumferential vibrations in cytosol. *Proceedings of the Institution of Mechanical Engineers, Part H: Journal of Engineering in Medicine,* 226**,** 589-599.

DE PABLO, P. J., SCHAAP, I. A. T., MACKINTOSH, F. C. & SCHMIDT, C. F. 2003. Deformation and collapse of microtubules on the nanometer scale. *Physical review letters,* 91**,** 98101.

DESAI, A., VERMA, S., MITCHISON, T. J. & WALCZAK, C. E. 1999. Kin I Kinesins Are Microtubule-Destabilizing Enzymes. *Cell,* 96**,** 69-78.

DIMITROV, A., QUESNOIT, M., MOUTEL, S., CANTALOUBE, I., POÜS, C. & PEREZ, F. 2008. Detection of GTP-Tubulin Conformation in Vivo Reveals a Role for GTP Remnants in Microtubule Rescues. *Science,* 322**,** 1353-1356.

DOGTEROM, M., KERSSEMAKERS, J. W. J., ROMET-LEMONNE, G. & JANSON, M. E. 2005. Force generation by dynamic microtubules. *Current Opinion in Cell Biology,* 17**,** 67-74.

ELBAUM, M., FYGENSON, D. K. & LIBCHABER, A. 1996. Buckling microtubules in vesicles. *Physical Review Letters,* 76**,** 4078-4081.

ELIE-CAILLE, C., SEVERIN, F., HELENIUS, J., HOWARD, J., MULLER, D. J. & HYMAN, A. A. 2007. Straight GDP-Tubulin Protofilaments Form in the Presence of Taxol. *Current Biology,* 17**,** 1765-1770.

ENEMARK, S., DERIU, M. A., SONCINI, M. & REDAELLI, A. 2008. Mechanical Model of the Tubulin Dimer Based on Molecular Dynamics Simulations. *Journal of biomechanical engineering,* 130**,** 041008-041008.

FAIVRE-MOSKALENKO, C. & DOGTEROM, M. 2002. Dynamics of microtubule asters in microfabricated chambers: the role of catastrophes. *Proceedings of the National Academy of Sciences,* 99**,** 16788.

FELGNER, H., FRANK, R., BIERNAT, J., MANDELKOW, E. M., MANDELKOW, E., LUDIN, B., MATUS, A. & SCHLIWA, M. 1997. Domains of neuronal microtubule-associated proteins and flexural rigidity of microtubules. *Journal of Cell Biology,* 138**,** 1067-1075.

FRANCK, A. D., POWERS, A. F., GESTAUT, D. R., GONEN, T., DAVIS, T. N. & ASBURY, C. L. 2007. Tension applied through the Dam1 complex promotes microtubule elongation providing a direct mechanism for length control in mitosis. *Nat Cell Biol,* 9**,** 832-837.

GAO, Y. & AN, L. 2010. A nonlocal elastic anisotropic shell model for microtubule

buckling behaviors in cytoplasm. *Physica E: Low-dimensional Systems and Nanostructures,* 42**,** 2406-2415.

GHAVANLOO, E., DANESHMAND, F. & AMABILI, M. 2010. Vibration analysis of a single microtubule surrounded by cytoplasm. *Physica E: Low-dimensional Systems and Nanostructures,* 43**,** 192-198.

GITTES, F., MICKEY, B., NETTLETON, J. & HOWARD, J. 1993. FLEXURAL RIGIDITY OF MICROTUBULES AND ACTIN-FILAMENTS MEASURED FROM THERMAL FLUCTUATIONS IN SHAPE. *Journal of Cell Biology,* 120**,** 923-934.

GLIKSMAN, N., SKIBBENS, R. & SALMON, E. 1993. How the transition frequencies of microtubule dynamic instability (nucleation, catastrophe, and rescue) regulate microtubule dynamics in interphase and mitosis: analysis using a Monte Carlo computer simulation. *Molecular biology of the cell,* 4**,** 1035.

GRIFFITH, L. M. & POLLARD, T. D. 1978. EVIDENCE FOR ACTIN FILAMENT MICROTUBULE INTERACTION MEDIATED BY MICROTUBULE-ASSOCIATED PROTEINS. *Journal of Cell Biology,* 78**,** 958-965.

GRILL, S. W. & HYMAN, A. A. 2005. Spindle Positioning by Cortical Pulling Forces. *Developmental Cell,* 8**,** 461-465.

GRISHCHUK, E. L., EFREMOV, A. K., VOLKOV, V. A., SPIRIDONOV, I. S., GUDIMCHUK, N., WESTERMANN, S., DRUBIN, D., BARNES, G., MCINTOSH, J. R. & ATAULLAKHANOV, F. I. 2008. The Dam1 ring binds microtubules strongly enough to be a processive as well as energy-efficient coupler for chromosome motion. *Proceedings of the National Academy of Sciences of the United States of America,* 105**,** 15423-15428.

GUCK, J., SCHINKINGER, S., LINCOLN, B., WOTTAWAH, F., EBERT, S., ROMEYKE, M., LENZ, D., ERICKSON, H. M., ANANTHAKRISHNAN, R., MITCHELL, D., KÄS, J., ULVICK, S. & BILBY, C. 2005. Optical Deformability as an Inherent Cell Marker for Testing Malignant Transformation and Metastatic Competence. *Biophysical journal,* 88**,** 3689-3698.

GUPTON, S. L., SALMON, W. C. & WATERMAN-STORER, C. M. 2002. Converging Populations of F-Actin Promote Breakage of Associated Microtubules to Spatially Regulate Microtubule Turnover in Migrating Cells. *Current Biology,* 12**,** 1891-1899.

HAWKINS, T., MIRIGIAN, M., SELCUK YASAR, M. & ROSS, J. L. 2010. Mechanics of microtubules. *Journal of biomechanics,* 43**,** 23-30.

HENDRICKS, ADAM G., LAZARUS, JACOB E., PERLSON, E., GARDNER, MELISSA K., ODDE, DAVID J., GOLDMAN, YALE E. & HOLZBAUR, ERIKA L. F. 2012. Dynein Tethers and Stabilizes Dynamic Microtubule Plus Ends. *Current Biology,* 22**,** 632-637.

HIRAOKA, Y., TODA, T. & YANAGIDA, M. 1984. The NDA3 gene of fission yeast encodes β-tubulin: A cold-sensitive nda3 mutation reversibly blocks spindle formation and chromosome movement in mitosis. *Cell,* 39**,** 349-358.

HIROKAWA, N. 1998. Kinesin and Dynein Superfamily Proteins and the Mechanism

of Organelle Transport. *Science,* 279**,** 519-526.

HÖÖG, J. L., HUISMAN, S. M., SEBÖ-LEMKE, Z., SANDBLAD, L., MCINTOSH, J. R., ANTONY, C. & BRUNNER, D. 2011. Electron tomography reveals a flared morphology on growing microtubule ends. *Journal of Cell Science,* 124**,** 693-698.

HOWARD, J. 2001. *Mechanics of motor proteins and the cytoskeleton,* Sunderland, USA: Sinauer Associates, Inc.

HOWARD, J. & HYMAN, A. 2003. Dynamics and mechanics of the microtubule plus end. *Nature,* 422**,** 753-758.

HUNT, G. W., WADEE, M. K. & SHIACOLAS, N. 1993. Localized Elasticae for the Strut on the Linear Foundation. *Journal of Applied Mechanics,* 60**,** 1033-1038.

HUNYADI, V., CHR¨¦TIEN, D., FLYVBJERG, H. & JANOSI, I. 2007. Why is the microtubule lattice helical? *Biology of the Cell,* 99**,** 117-128.

HUNYADI, V. & JÁNOSI, I. M. 2007. Metastability of Microtubules Induced by Competing Internal Forces. *Biophysical Journal,* 92**,** 3092-3097.

HYMAN, A., SALSER, S., DRECHSEL, D., UNWIN, N. & MITCHISON, T. 1992. Role of GTP hydrolysis in microtubule dynamics: information from a slowly hydrolyzable analogue, GMPCPP. *Molecular biology of the cell,* 3**,** 1155.

INOUÉ, S. & SALMON, E. D. 1995. Force Generation by Microtubule Assembly/Disassembly in Mitosis and Related Movements. *Molecular Biology of the Cell,* 6**,** 1619-1640.

JÁNOSI, I. M., CHRÉTIEN, D. & FLYVBJERG, H. 2002. Structural Microtubule Cap: Stability, Catastrophe, Rescue, andThird State. *Biophysical Journal,* 83**,** 1317-1330.

JI, X. Y. & FENG, X. Q. 2011. Coarse-grained mechanochemical model for simulating the dynamic behavior of microtubules. *Physical Review E,* 84.

JIANG, H. Q. & ZHANG, J. P. 2008. Mechanics of Microtubule Buckling Supported by Cytoplasm. *Journal of Applied Mechanics-Transactions of the Asme,* 75**,** 061019.

JIANG, L., GAO, Y., MAO, F., LIU, Z. & LAI, L. 2002. Potential of mean force for protein–protein interaction studies. *Proteins: Structure, Function, and Bioinformatics,* 46**,** 190-196.

JIN, M. Z. & RU, C. Q. 2012. Compressed microtubules: Splitting or buckling. *Journal of Applied Physics,* 111**,** 064701.

JIN, M. Z. & RU, C. Q. 2013. Localized buckling of a microtubule surrounded by randomly distributed cross linkers. *Physical Review E,* 88**,** 012701.

KACHANOV, L. M. 1988. *Delamination buckling of composite materials*, Springer.

KARP, G. 2009. *Cell and molecular biology: concepts and experiments*, Wiley.

KELLY, R. B. 1990. Microtubules, membrane traffic, and cell organization. *Cell,* 61**,** 5-7.

KIKUMOTO, M., KURACHI, M., TOSA, V. & TASHIRO, H. 2006. Flexural Rigidity of Individual Microtubules Measured by a Buckling Force with

Optical Traps. *Biophysical Journal,* 90**,** 1687-1696.

KIMURA, K. & KIMURA, A. 2011. Intracellular organelles mediate cytoplasmic pulling force for centrosome centration in the Caenorhabditis elegans early embryo. *Proceedings of the National Academy of Sciences,* 108**,** 137-142.

KORB, T., SCHLÜTER, K., ENNS, A., SPIEGEL, H.-U., SENNINGER, N., NICOLSON, G. L. & HAIER, J. 2004. Integrity of actin fibers and microtubules influences metastatic tumor cell adhesion. *Experimental Cell Research,* 299**,** 236-247.

KUEH, H. Y. & MITCHISON, T. J. 2009. Structural Plasticity in Actin and Tubulin Polymer Dynamics. *Science,* 325**,** 960-963.

KURACHI, M., HOSHI, M. & TASHIRO, H. 1995. Buckling of a single microtubule by optical trapping forces: Direct measurement of microtubule rigidity. *Cell Motility and the Cytoskeleton,* 30**,** 221-228.

LEE, A. A., KARLON, W. J., GRAHAM, D. A., DELA CRUZ, S. & RATCLIFFE, A. 2001. Fluid Shear Stress-Induced Alignment of Cultured Vascular Smooth Muscle Cells. *Journal of biomechanical engineering,* 124**,** 37-43.

LEE, S. H. & WAAS, A. M. 1996. Initial post-buckling behavior of a finite beam on an elastic foundation. *International Journal of Non-Linear Mechanics,* 31**,** 313-328.

LI, C., RU, C. Q. & MIODUCHOWSKI, A. 2006. Length-dependence of flexural rigidity as a result of anisotropic elastic properties of microtubules. *Biochemical and Biophysical Research Communications,* 349**,** 1145-1150.

LI, T. 2008. A mechanics model of microtubule buckling in living cells. *Journal of biomechanics,* 41**,** 1722-1729.

MANDATO, C. A. & BEMENT, W. M. 2003. Actomyosin Transports Microtubules and Microtubules Control Actomyosin Recruitment during Xenopus Oocyte Wound Healing. *Current Biology,* 13**,** 1096-1105.

MANDELKOW, E. M., MANDELKOW, E. & MILLIGAN, R. A. 1991. Microtubule dynamics and microtubule caps: a time-resolved cryo-electron microscopy study. *The Journal of Cell Biology,* 114**,** 977-991.

MARRARI, Y., CLARKE, E. J., ROUVIÈRE, C. & HOULISTON, E. 2003. Analysis of microtubule movement on isolated Xenopus egg cortices provides evidence that the cortical rotation involves dynein as well as Kinesin Related Proteins and is regulated by local microtubule polymerisation. *Developmental Biology,* 257**,** 55-70.

MEHRBOD, M. & MOFRAD, M. R. K. 2011. On the Significance of Microtubule Flexural Behavior in Cytoskeletal Mechanics. *PloS one,* 6**,** e25627.

MICKEY, B. & HOWARD, J. 1995. Rigidity of microtubules is increased by stabilizing agents. *The Journal of cell biology,* 130**,** 909.

MIRANDA, J. J. L., DE WULF, P., SORGER, P. K. & HARRISON, S. C. 2005. The yeast DASH complex forms closed rings on microtubules. *Nature Structural & Molecular Biology,* 12**,** 138-143.

MITCHISON, T. & KIRSCHNER, M. 1984. Dynamic instability of microtubule growth. *Nature,* 312**,** 237-242.

MOLODTSOV, M. I., ERMAKOVA, E. A., SHNOL, E. E., GRISHCHUK, E. L., MCINTOSH, J. R. & ATAULLAKHANOV, F. I. 2005a. A molecular-mechanical model of the microtubule. *Biophysical Journal,* 88**,** 3167-3179.

MOLODTSOV, M. I., GRISHCHUK, E. L., EFREMOV, A. K., MCINTOSH, J. R. & ATAULLAKHANOV, F. I. 2005b. Force production by depolymerizing microtubules: A theoretical study. *Proceedings of the National Academy of Sciences of the United States of America,* 102**,** 4353-4358.

MÜLLER-REICHERT, T., CHRÉTIEN, D., SEVERIN, F. & HYMAN, A. A. 1998. Structural changes at microtubule ends accompanying GTP hydrolysis: Information from a slowly hydrolyzable analogue of GTP, guanylyl (α,β)methylenediphosphonate. *Proceedings of the National Academy of Sciences,* 95**,** 3661-3666.

NOGALES, E., WHITTAKER, M., MILLIGAN, R. & DOWNING, K. 1999. High-resolution model of the microtubule. *Cell,* 96**,** 79-88.

OCHALEK, T., NORDT, F. J., TULLBERG, K. & BURGER, M. M. 1988. Correlation between cell deformability and metastatic potential in B16-F1 melanoma cell variants. *Cancer Research,* 48**,** 5124-5128.

ODDE, D. J., MA, L., BRIGGS, A. H., DEMARCO, A. & KIRSCHNER, M. W. 1999. Microtubule bending and breaking in living fibroblast cells. *Journal of Cell Science,* 112**,** 3283-3288.

PAMPALONI, F., LATTANZI, G., JONÁŠ, A., SURREY, T., FREY, E. & FLORIN, E.-L. 2006. Thermal fluctuations of grafted microtubules provide evidence of a length-dependent persistence length. *Proceedings of the National Academy of Sciences,* 103**,** 10248-10253.

PETER, S. J. & MOFRAD, M. R. K. 2012. Computational Modeling of Axonal Microtubule Bundles under Tension. *Biophysical journal,* 102**,** 749-757.

POKORNÝ, J. 2004. Excitation of vibrations in microtubules in living cells. *Bioelectrochemistry,* 63**,** 321-326.

POKORNÝ, J., VEDRUCCIO, C., CIFRA, M. & KUČERA, O. 2011. Cancer physics: diagnostics based on damped cellular elastoelectrical vibrations in microtubules. *European Biophysics Journal,* 40**,** 747-759.

PORTET, S., TUSZYŃSKI, J. A., HOGUE, C. W. V. & DIXON, J. M. 2005. Elastic vibrations in seamless microtubules. *European Biophysics Journal,* 34**,** 912-920.

RAI, ARPAN K., RAI, A., RAMAIYA, AVIN J., JHA, R. & MALLIK, R. 2013. Molecular Adaptations Allow Dynein to Generate Large Collective Forces inside Cells. *Cell,* 152**,** 172-182.

RANJITH, P. & KUMAR, P. B. S. 2002. Dynamics of Folding in Semiflexible Filaments. *Physical Review Letters,* 89**,** 018302.

RU, C. Q. 2004. Elastic models for carbon nanotubes. *Encyclopedia of nanoscience and nanotechnology,* 2**,** 731-744.

SEPT, D., BAKER, N. & MCCAMMON, J. 2003. The physical basis of microtubule structure and stability. *Protein Science,* 12**,** 2257-2261.

SHEN, H. S. 2011. Nonlinear vibration of microtubules in living cells. *Current*

Applied Physics, 11**,** 812-821.

SIRENKO, Y. M., STROSCIO, M. A. & KIM, K. W. 1996. Elastic vibrations of microtubules in a fluid. *Physical Review E,* 53**,** 1003-1010.

STAMENOVIĆ, D. & COUGHLIN, M. F. 1999. A Quantitative Model of Cellular Elasticity Based on Tensegrity. *Journal of biomechanical engineering,* 122**,** 39-43.

SUBRA, S. 2007. Biomechanics and biophysics of cancer cells. *Acta Materialia,* 55**,** 3989-4014.

SVITKINA, T. M., VERKHOVSKY, A. B. & BORISY, G. G. 1996. Plectin sidearms mediate interaction of intermediate filaments with microtubules and other components of the cytoskeleton. *Journal of Cell Biology,* 135**,** 991-1007.

TIMOSHENKO, S., YOUNG, D. H. & WEAVER, W. J. 1974. *Vibration problems in engineering*, John Wiley & Sons.

TOUNSI, A., HEIRECHE, H., BENHASSAINI, H. & MISSOURI, M. 2010. Vibration and length-dependent flexural rigidity of protein microtubules using higher order shear deformation theory. *Journal of theoretical biology,* 266**,** 250-255.

UGURAL, A. C. & FENSTER, S. K. 2003. *Advanced strength and applied elasticity*, Prentice Hall.

VANBUREN, V., CASSIMERIS, L. & ODDE, D. J. 2005. Mechanochemical Model of Microtubule Structure and Self-Assembly Kinetics. *Biophysical Journal,* 89**,** 2911-2926.

VANBUREN, V., ODDE, D. J. & CASSIMERIS, L. 2002. Estimates of lateral and longitudinal bond energies within the microtubule lattice. *Proceedings of the National Academy of Sciences,* 99**,** 6035-6040.

VENIER, P., MAGGS, A. C., CARLIER, M. F. & PANTALONI, D. 1994. Analysis of microtubule rigidity using hydrodynamic flow and thermal fluctuations. *Journal of Biological Chemistry,* 269**,** 13353.

VICHARE, S., JAIN, I., INAMDAR, M. M. & PADINHATEERI, R. 2013. Forces due to curving protofilaments in microtubules. *Physical Review E,* 88**,** 062708.

VITRE, B., COQUELLE, F. M., HEICHETTE, C., GARNIER, C., CHRETIEN, D. & ARNAL, I. 2008. EB1 regulates microtubule dynamics and tubulin sheet closure in vitro. *Nat Cell Biol,* 10**,** 415-421.

WANG, C., LI, C. & ADHIKARI, S. 2009. Dynamic behaviors of microtubules in cytosol. *J. Biomech.,* 42**,** 1270-1274.

WANG, C. Y., RU, C. Q. & MIODUCHOWSKI, A. 2006. Orthotropic elastic shell model for buckling of microtubules. *Physical Review E,* 74**,** 052901.

WANG, H. & NOGALES, E. 2005. Nucleotide-dependent bending flexibility of tubulin regulates microtubule assembly. *Nature,* 435**,** 911-915.

WANG, N., NARUSE, K., STAMENOVIC, D., FREDBERG, J. J., MIJAILOVICH, S. M., TORIC-NORRELYKKE, I. M., POLTE, T., MANNIX, R. & INGBER, D. E. 2001. Mechanical behavior in living cells consistent with the tensegrity model. *Proceedings of the National Academy of Sciences of the United States*

of America, 98**,** 7765-7770.

WESTERMANN, S., AVILA-SAKAR, A., WANG, H. W., NIEDERSTRASSER, H., WONG, J., DRUBIN, D. G., NOGALES, E. & BARNES, G. 2005. Formation of a dynamic kinetochore-microtubule interface through assembly of the Dam1 ring complex. *Molecular Cell,* 17**,** 277-290.

WESTERMANN, S., WANG, H.-W., AVILA-SAKAR, A., DRUBIN, D. G., NOGALES, E. & BARNES, G. 2006. The Dam1 kinetochore ring complex moves processively on depolymerizing microtubule ends. *Nature,* 440**,** 565-569.

WU, Z., NOGALES, E. & XING, J. 2012. Comparative studies of microtubule mechanics with two competing models suggest functional roles of alternative tubulin lateral interactions. *Biophysical Journal,* 102**,** 2687-2696.

XIANG, P. & LIEW, K. M. 2012. Free vibration analysis of microtubules based on an atomistic-continuum model. *Journal of Sound and Vibration,* 331**,** 213-230.

XIAO, H., VERDIER-PINARD, P., FERNANDEZ-FUENTES, N., BURD, B., ANGELETTI, R., FISER, A., HORWITZ, S. B. & ORR, G. A. 2006. Insights into the mechanism of microtubule stabilization by Taxol. *Proceedings of the National Academy of Sciences,* 103**,** 10166-10173.

YI, L. J., CHANG, T. C. & RU, C. Q. 2008. Buckling of microtubules under bending and torsion. *Journal of Applied Physics,* 103.

ZEVERDEJANI, M. K. & BENI, Y. T. 2013. The nano scale vibration of protein microtubules based on modified strain gradient theory. *Current Applied Physics,* 13**,** 1566-1576.

Appendix A

Finite element analysis for buckling of microtubule (referred from Abaqus Help documents):

The buckling pattern and critical buckling force of microtubule are simulated based on structural static equilibrium with inertial and damping effects ignored. The overall equilibrium equations for the microtubule are:

$$[K][u]=[f] \tag{A-1}$$

where $[K]$ is the structure stiffens matrix assembled by the stiffness matrix of microtubule modeled by beam elements and the stiffness matrix of cross linkers modeled by spring elements; $[u]$ is the nodal displacement vector and $[f]$ is the total load vector. In present case, $[f]$ is the vector of applied axial compressive force at the end of microtubule.

The effects of large deformation are also included in present finite element simulation. The large deformation computations can be achieved by using a few basic physical variables (motion and deformation) and the corresponding configurations. The applied compressive loading acting on the microtubule make it move from one position to another. This motion can be defined by comparing a vector in the "deformed" and "un-deformed" configurations. The the position vectors in the "deformed" and "un-deformed" state are represented by $\{x\}$ and $\{X\}$ respectively, then the motion (displacement) vector is computed and coupled with Eq. (A-1) to solve the equilibrium of microtubule under axial compressive loading with large deformation.

Appendix B

Finite element analysis for vibration of microtubule (referred from Abaqus Help documents):

The vibration of microtubule is investigated by using linear eigenvalue analysis in finite element method to get natural vibration frequency and corresponding vibration mode. The linear eigenvalue problem in finite element method has the following form:

$$[K][\phi_i] = \lambda_i [M][\phi_i] \tag{B-1}$$

where $[K]$ is the structure stiffness matrix assembled by the stiffness matrix of microtubule modeled by beam elements and stiffness matrix of cross linkers modeled by spring elements; $[\phi_i]$ and λ_i are eigenvector and corresponding eigenvalue to be extracted; $[M]$ is the structure mass matrix assembled based on the density of microtubule and the volume of each beam element; i is the mode number. The frequency and the deflection form of certain mode i can be derived according to extracted eigenvalue λ_i and corresponding eigenvector $[\phi_i]$ respectively. In present study, Block Lanczos algorithm is performed for eigenvalue and eigenvector extraction.